© 2022. Published by The Company of Biologists Ltd | Development (2022) 149, dev200561. doi:10.1242/dev.200561

STEM CELLS AND REGENERATION

TECHNIQUES AND RESOURCES ARTICLE

Rapid and robust directed differentiation of mouse epiblast stem cells into definitive endoderm and forebrain organoids

Daniel Medina-Cano[1,2,‡], Emily K. Corrigan[1,2,*,‡], Rachel A. Glenn[1,2,3,§], Mohammed T. Islam[1,2,§], Yuan Lin[1,2], Juliet Kim[1,2], Hyunwoo Cho[1,2] and Thomas Vierbuchen[1,2,¶]

ABSTRACT

Directed differentiation of pluripotent stem cells (PSCs) is a powerful model system for deconstructing embryonic development. Although mice are the most advanced mammalian model system for genetic studies of embryonic development, state-of-the-art protocols for directed differentiation of mouse PSCs into defined lineages require additional steps and generates target cell types with lower purity than analogous protocols for human PSCs, limiting their application as models for mechanistic studies of development. Here, we examine the potential of mouse epiblast stem cells cultured in media containing Wnt pathway inhibitors as a starting point for directed differentiation. As a proof of concept, we focused our efforts on two specific cell/tissue types that have proven difficult to generate efficiently and reproducibly from mouse embryonic stem cells: definitive endoderm and neural organoids. We present new protocols for rapid generation of nearly pure definitive endoderm and forebrain-patterned neural organoids that model the development of prethalamic and hippocampal neurons. These differentiation models present new possibilities for combining mouse genetic tools with *in vitro* differentiation to characterize molecular and cellular mechanisms of embryonic development.

KEY WORDS: Pluripotent stem cells, Directed differentiation, Definitive endoderm, Neural development, Organoids

INTRODUCTION

Over the last two decades, methods for the directed differentiation of human PSCs (hPSCs) into numerous lineages have been developed and refined. As a result, it is now possible to generate nearly pure populations of multiple specific cell types or 3D multicellular organoids that resemble developing human tissues (Huch et al., 2017; Loh et al., 2016; Tchieu et al., 2017; Yiangou et al., 2018). However, although hPSC-based models for studying development advanced, analogous protocols for mouse PSCs have not yet emerged. Current state-of-the-art protocols for directed differentiation of mouse PSCs tend to be more complex than equivalent hPSC protocols, and they often fail to generate target cell types with high purity. Robust and efficient protocols for directed differentiation of mouse PSCs into defined lineages would be synergistic with *in vivo* studies in mouse and with studies of hPSC-based models of human embryonic development.

A crucial difference between most mouse and human directed differentiation protocols is the starting cell state. hPSCs are generally cultured in the primed pluripotent state, which is roughly equivalent to cells of the pluripotent epiblast around the start of gastrulation [approximately embryonic day (E) 6.5 in mouse] (Rossant and Tam, 2017). In contrast, mouse PSCs are predominantly grown in the naïve pluripotent state [mouse embryonic stem cells (ESCs)], which is equivalent to cells in the inner cell mass of the pre-implantation embryo at ∼E3.5-4.0 (Nichols and Smith, 2012). Like their embryonic equivalents, naïve PSCs must first exit the naïve pluripotent state before they can properly respond to differentiation cues (Morgani et al., 2017; Mulas et al., 2017; Smith, 2017). As a result, mouse naïve PSC directed differentiation protocols must include an additional first step of ∼48 h, during which cells exit the naïve pluripotent state and transition into an early formative and/or later primed pluripotent state that is competent to respond to signals that induce differentiation into specific somatic lineages. The requirement for this additional initial step is problematic because the naïve-to-primed transition is inherently asynchronous, leading to a heterogeneous starting population of formative/primed cells before directed differentiation has commenced (Kalkan et al., 2017; Strawbridge et al., 2020 preprint). The initial naïve-primed conversion step thus represents an impediment to the development of rapid and efficient protocols for directed differentiation that use mouse naïve PSCs as a starting population.

Mouse PSCs can be cultured in a primed pluripotent state, referred to as epiblast stem cells (EpiSCs). EpiSCs share many similarities with hPSCs, including the ability to respond rapidly to differentiation stimuli (Brons et al., 2007; Tesar et al., 2007; Vallier et al., 2009). Protocols that use EpiSCs as a starting point for directed differentiation have been developed, including (but not limited to) robust protocols for generation of oligodendrocyte progenitor cells (OPCs) and neuromesodermal progenitors (Edri et al., 2019; Najm et al., 2011). However, EpiSC-based protocols are not widely used for several reasons: (1) EpiSCs are prone to spontaneous differentiation and thus are more difficult to culture than mouse naïve PSCs or hPSCs; (2) EpiSCs exhibit significant line-to-line variability in their differentiation propensity; and (3) EpiSCs express markers of lineage-primed epiblast cells transiting through the anterior primitive streak (T, FOXA2), which may limit their potential to differentiate into some lineages (Bernemann et al., 2011; Jouneau, 2019; Kojima et al., 2014; Kurek et al., 2015; Rossant and Tam, 2017; Song et al., 2016).

[1]Developmental Biology Program, Sloan Kettering Institute for Cancer Research, New York, NY 10065, USA. [2]Center for Stem Cell Biology, Sloan Kettering Institute for Cancer Research, New York, NY 10065, USA. [3]Cell and Developmental Biology Program, Weill Cornell Graduate School of Medical Sciences, Cornell University, New York, NY 10065, USA.
*Present address: Developmental and Stem Cell Biology Graduate Program, University of California San Francisco, San Francisco, CA 94158, USA.
‡These authors contributed equally to this work
§These authors contributed equally to this work

¶Author for correspondence (vierbuct@mskcc.org)

D.M., 0000-0003-4545-7664; H.C., 0000-0003-3166-585X; T.V., 0000-0002-5690-5680

Handling Editor: James Wells
Received 26 January 2022; Accepted 4 July 2022

Development (2022) 149, dev200561. doi:10.1242/dev.200561

More recently, several groups have demonstrated that inhibition of the canonical Wnt signaling pathway can limit spontaneous differentiation in EpiSC cultures, enabling consistent, long-term maintenance of pluripotent EpiSCs (Kurek et al., 2015; Sumi et al., 2013; Tsakiridis et al., 2014; Wu et al., 2015). Despite this progress, EpiSCs cultured in these conditions (i.e. in the presence of Wnt inhibitors; hereafter referred to as '+WI') are still not commonly used for directed differentiation experiments. Therefore, whether EpiSCs (+WI) have the potential to improve directed differentiation towards multiple lineages *in vitro* remains a significant gap in the field.

Here, we examine the potential of EpiSCs (+WI) as a starting point for *in vitro* directed differentiation studies. We focused on two specific cell populations that have proven difficult to generate reproducibly and efficiently from mouse naïve PSCs: definitive endoderm (DE) and neural organoids. First, we systematically optimized conditions to differentiate EpiSCs into DE, developing a protocol that converts EpiSCs into nearly pure DE in only 40 h. Second, we show that EpiSCs can robustly and reproducibly generate forebrain-patterned neural organoids. In-depth characterization of forebrain-patterned organoids revealed that they undergo polarization into multiple distinct domains of progenitors, including the prethalamic (P3) region of the caudal forebrain (diencephalon), hippocampus and cortical hem, as well as OPCs. The prethalamic progenitors, which give rise primarily to inhibitory (GABAergic) neurons of the thalamic reticular nucleus and the zona incerta, are notable because they have not previously been efficiently generated *in vitro* (Shiraishi et al., 2017; Xiang et al., 2019). Our data suggest that mouse EpiSCs (+WI) could be a powerful platform for directed differentiation studies, enabling direct comparative studies with mouse embryonic development *in vivo* and with hPSC directed differentiation models.

RESULTS

Rationale for using EpiSCs (+WI) as a starting point for directed differentiation experiments

Given the issues associated with using mouse naïve PSCs for directed differentiation, we sought to assess the potential of mouse EpiSCs as a starting point for directed differentiation experiments. We chose to use mouse EpiSCs cultured with Wnt inhibitors (EpiSCs +WI), which had been previously shown to significantly reduce spontaneous differentiation and allow for maintenance of pluripotency over many passages in culture (Kurek et al., 2015; Sumi et al., 2013; Wu et al., 2015). These culture conditions have several features that make them potentially useful for directed differentiation experiments. First, EpiSCs (+WI) are easy for labs that currently work with mouse naïve PSCs to acquire, as naïve PSCs can be converted into stable EpiSC (+WI) lines *in vitro*. Second, there is suggestive data from previous studies indicating that EpiSC culture conditions work well across a variety of genetic backgrounds (including distinct inbred mouse strains) and with both male and female cells (Brons et al., 2007; Tesar et al., 2007). In contrast, culture of naïve PSCs from most inbred mouse strains requires addition of inhibitors of FGF/ERK signaling and GSK3 (2i culture conditions), which impedes *de novo* DNA methyltransferase activity, leading to erosion of parent-of-origin-specific gene regulation (Choi et al., 2017; Czechanski et al., 2014; Yagi et al., 2017; Ying et al., 2008). Finally, given the similarities between EpiSCs (+WI) and hPSCs, we reasoned that it should be possible to adapt strategies developed for hPSC differentiation to EpiSCs (Vallier et al., 2009; Greber et al., 2010).

Derivation and characterization of a panel of ground-state EpiSCs

We derived EpiSCs (+WI) from 12 distinct naïve PSC lines, including lines from several distinct inbred mouse strains: C57Bl/6J (n=5), B6129SF1/J (n=3), DBA/2J (n=1) and PWK/PhJ (n=3) (Czechanski et al., 2014) (Table S4). Briefly, naïve PSCs were converted into epiblast like-cells (EpiLCs) using previously established protocols (Hayashi et al., 2011). Following EpiLC conversion, cells were split onto irradiated mouse embryonic fibroblast feeders and maintained EpiSC media containing a tankyrase inhibitor (NVP-TNKS656) to block canonical Wnt signaling (Shultz et al., 2013). Consistent with previous studies, EpiSCs (+WI) express markers of post-implantation epiblast [OCT4 (POU5F1), SOX2, OTX2, NANOG], do not express markers specifically expressed in naïve pluripotent stem cells (KLF4), and exhibit sparse expression of markers of primed epiblast (FOXA2) and primitive streak (T) (Fig. 1A,B).

To characterize these EpiSC (+WI) lines in greater depth, we measured gene expression by RNA sequencing (RNA-seq; n=12 lines) and mapped accessible chromatin regions across the genome by assay for transposase-accessible chromatin with high-throughput sequencing (ATAC-seq; n=9 lines) (Buenrostro et al., 2015). We observed high expression of primed [*Otx2*, *Oct6* (*Pou3f1*), *Dnmt3b*] and general (*Oct4*, *Sox2*, *Nanog*) pluripotency markers, and low expression of naïve pluripotency markers (*Klf4*, *Tbx3*, *Prdm14*, *Nr5a2*) across all lines, in agreement with results from immunofluorescence staining (Fig. 1B,C). Similarly, genes associated with lineage commitment/lineage priming (*T*, *Foxa2*, *Mixl1*, *Sox17*, *Gata6*, *Cdx2*, *Sox1*) exhibited low to moderate expression across all lines (Fig. 1C). Principal component analysis (PCA) of RNA-seq and ATAC-seq data revealed that pluripotency state (naïve PSCs versus EpiSCs) is the primary driver of gene expression differences between lines, followed by genetic background (PC1; ∼56% and ∼71% of total variance, respectively, Fig. 1D,E). EpiSC lines from the same genetic background had highly correlated profiles of both gene expression and chromatin accessibility.

Next, we compared chromatin accessibility across the genome in our new EpiSC lines to cell populations in the embryo at E6.5 (epiblast, visceral endoderm, primitive streak, and germ layer progenitors) as well as EpiSC lines cultured in the presence (EpiSC-AFX) or absence (EpiSC-AF) of the tankyrase inhibitor XAV939 (Kinoshita et al., 2021; Xiang et al., 2020). PCA of chromatin accessibility profiles revealed that EpiSC lines most closely resemble EpiSC-AF and EpiSC-AFX, followed by *in vivo* epiblast tissue, and are least similar to primitive streak and endoderm/mesoderm (Fig. 1F). Taken together, these data suggest that EpiSCs (+WI) exhibit expected features of primed PSCs and can be stably maintained in an undifferentiated state in culture.

Optimized directed differentiation of EpiSCs into DE

We next sought to test whether EpiSCs (+WI) can be directed to differentiate efficiently into DE. Current protocols for directed differentiation of hPSCs into DE are rapid and efficient, and serve as the foundation for robust protocols for generating progenitors of various endodermal organs (Yiangou et al., 2018). In contrast, protocols for DE differentiation of mouse PSCs require additional steps and give rise to heterogeneous populations of DE and mesodermal cell types (Fig. S1A, Table S1).

hPSC DE differentiation protocols consist of two steps that mimic the signals that sequentially specify DE during gastrulation (Gadue et al., 2006; Loh et al., 2014; Yiangou et al., 2018; Zorn and Wells,

Development (2022) 149, dev200561. doi:10.1242/dev.200561

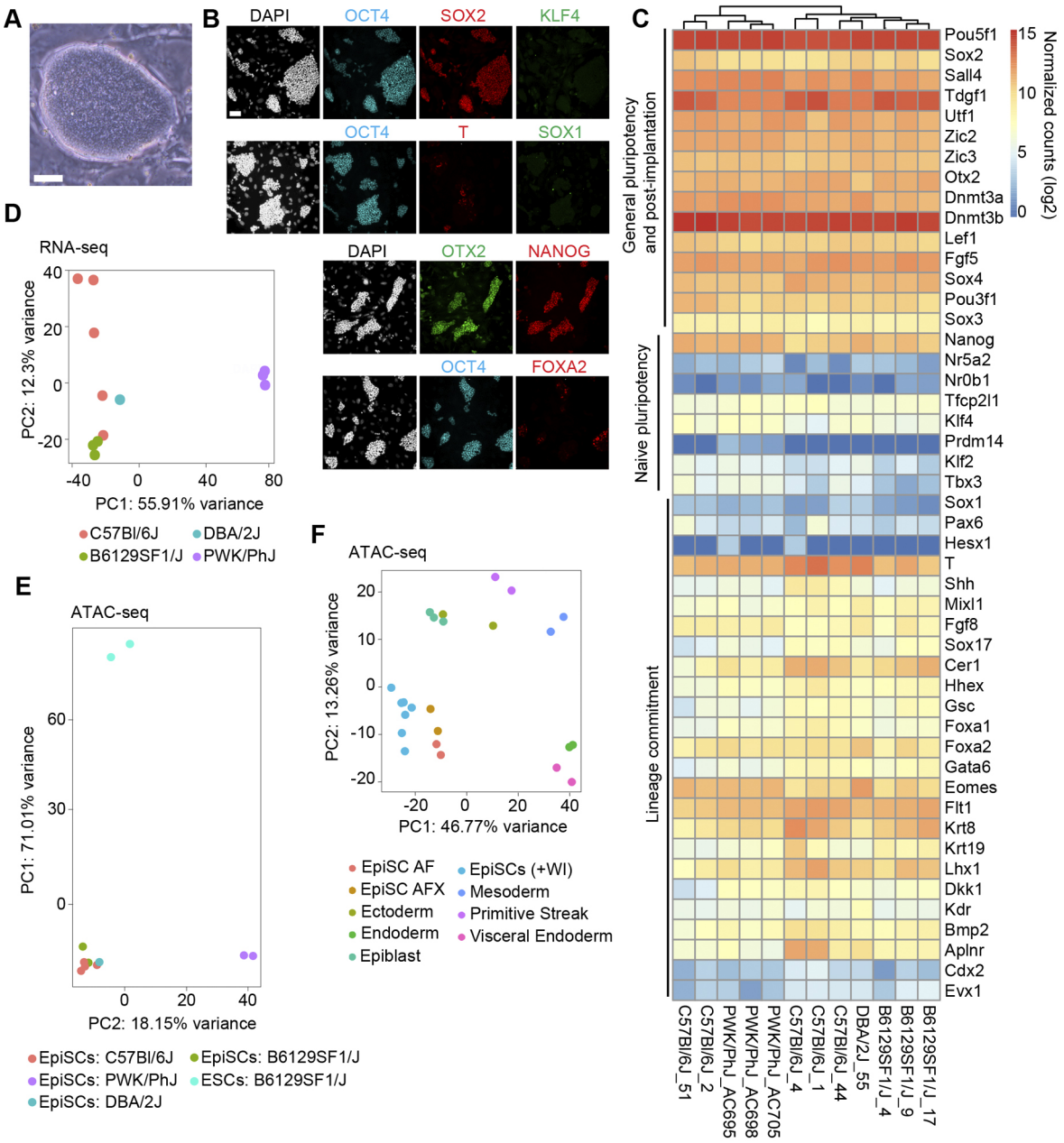

Fig. 1. Derivation and characterization of mouse EpiSCs cultured in primed ground state conditions. (A) Phase-contrast image of an EpiSC (+WI) colony. Scale bar: 50 µm. (B) Immunofluorescence images of EpiSC (+WI) cultures showing markers of general pluripotency (SOX2, OCT4), primed pluripotency (OTX2), naive pluripotency (KFL4, NANOG) and lineage commitment (T, FOXA2, SOX1). Scale bar: 50 µm. (C) Gene expression heatmap of RNA-seq data from EpiSC (+WI) lines (n=12; biological replicates derived from distinct naïve mouse ESC lines) for selected genes associated with pluripotency and lineage commitment. (D) PCA plot of RNA-seq data (biological replicates; C57Bl/6J=5, B6129SF1/J=3, PWK/PhJ=3, DBA/2J=1) for EpiSC (+WI) lines. (E) ATAC-seq data (n=9 biological replicates; C57Bl/6J=3, B6129SF1/J=2, PWK/PhJ=3, DBA/2J=1) for EpiSC (+WI) and ESC lines (n=2; B6129SF1/J). (F) PCA plot of ATAC-seq data for EpiSC (+WI) lines (biological replicates; C57Bl/6J=4, PWK/PhJ=2, DBA/2J=1; all shown as light blue). For comparison, ATAC-seq data from an additional set of EpiSC lines EpiSC-AF (cultured with activin A and FGF2) and EpiSC-AFX (cultured with activin A, FGF2 and the Wnt inhibitor XAV939) (taken from Kinoshita et al., 2021) and from early embryonic lineages *in vivo* (E6.5 epiblast, E6.5 visceral endoderm, E7.5 ectoderm, E7.5 mesoderm, E7.5 endoderm, E7.5 primitive streak (taken from Xiang et al., 2020).

2009). In the first step, Wnt and TGFβ/Nodal signaling promote exit from pluripotency and differentiation into anterior PS-like (aPS) progenitors. In the second step, high TGFβ/Nodal signaling promotes the commitment of aPS progenitors into DE. This general approach has been applied to a variety of hPSC lines and can consistently generate >85% pure DE (Loh et al., 2014). We hypothesized that signaling requirements for mouse DE differentiation from EpiSCs (+WI) would be similar to those of hPSCs, but that it was likely that the timing of each stage and the appropriate concentration of signaling factors would be different for mouse EpiSCs compared with hPSCs (Greber et al., 2010; Vallier et al., 2009)

To determine the optimal timing and concentration of each signal for aPS induction, we applied a gradient of increasing concentrations of CHIR99201 (to activate Wnt signaling via GSK3 inhibition) and activin A (to activate TGFβ/nodal

Development (2022) 149, dev200561. doi:10.1242/dev.200561

signaling) to EpiSCs (DBA/2J) for either 16, 20 or 24 h (see Materials and Methods for further details). After aPS induction, all conditions were shifted to the same DE commitment conditions for an additional 24 h, and DE induction purity (fraction of the total population co-expressing FOXA2 and SOX17) was determined by immunostaining (Fig. 2A, Fig. S1B). Across all conditions, we observed DE purity ranging from 7% to 82%. The highest purity was achieved in conditions with higher activin A and the highest levels of Wnt activation. Exposure to these aPS conditions for 16 h was sufficient to enable DE commitment in the second stage of the protocol, and no further increase in purity was observed in the 20 or 24 h aPS conditions.

Having defined these improved conditions for aPS induction, we next sought to define the optimal conditions for DE commitment of aPS-like cells (Stage 2) (Fig. 2B, Fig. S1C). To promote commitment of aPS-like cells into DE, DE differentiation protocols for hPSCs add a high concentration of activin A for 48 h. Concurrent inhibition of BMP and/or Wnt signaling has also been reported to reduce off-target differentiation of aPS cells into mesodermal lineages (Loh et al., 2014). Based on these data, we tested the effects of activin A concentration, BMP inhibition (LDN-193189), Wnt inhibition (NVP-TNKS656, LGK-974), and the total duration of Stage 2 on DE commitment.

We induced aPS using the optimized conditions from Fig. 2A and examined the effects of different signaling conditions and timing (24, 36, 48 h) on DE commitment. We observed the highest purity of DE differentiation in conditions with the highest levels of activin A (~75% of $SOX17^+$ cells with 100 ng/ml versus ~65% $SOX17^+$ cells with 40 ng/ml; Fig. 2B). Inhibition of BMP signaling markedly increased DE purity across all conditions, whereas Wnt inhibition had minimal effects. DE purity was highest in the 24 h Stage 2 condition, with longer durations leading to a substantial reduction of FOXA2/SOX17-positive DE cells. In the 24 h condition, rare SOX17-negative cells were observed in small clusters of densely packed cells. Most of these off-target cells co-expressed OCT4 and T, were FOXA2 negative and lacked expression of CDX2, which is expressed by paraxial mesoderm cells that are also generated from aPS-like progenitors. These data suggest that the $OCT4^+/T^+/FOXA2^-$ cells are most likely to be lagging aPS-like cells or immature mesodermal cells. However, in the 36 and 48 h conditions, $SOX17^-$ cells could also result from properly specified DE cells that have started to adopt distinct anterior-posterior (A-P) identities that no longer express SOX17, such as anterior or posterior foregut (Li et al., 2018).

These systematic optimization experiments demonstrate that the combination of Wnt activation in the presence of moderate TGFβ/Nodal signaling, followed by TGFβ/Nodal activation and BMP inhibition can generate high purity DE from mouse EpiSCs in ~40 h (Fig. 2C, supplementary Materials and Methods). Application of this protocol to EpiSCs (+WI) cultured in feeder-free conditions gave similar results (Fig. S3B).

To determine the purity of DE generated by our protocol more quantitatively, we used flow cytometry to measure the levels of the surface marker CXCR4 (expressed in endoderm and mesoderm)

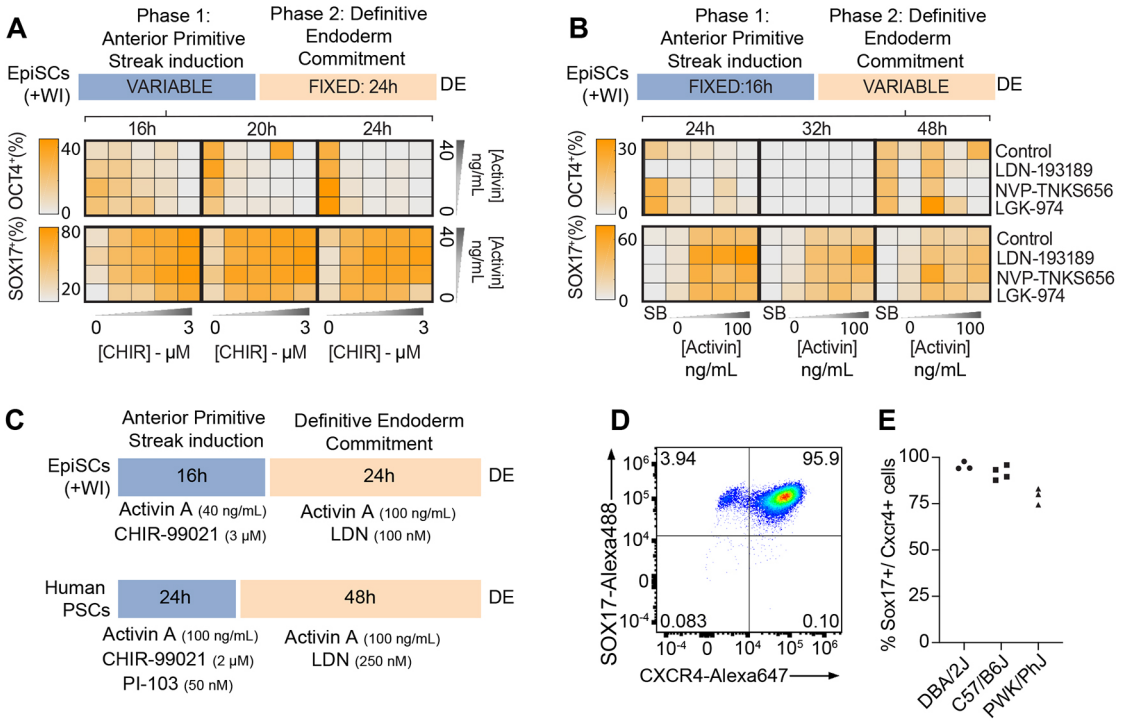

Fig. 2. Systematic optimization of conditions for EpiSC-DE differentiation. (A,B) Results of DE protocol optimization experiments. For each condition, immunofluorescence staining was performed following 40 h of differentiation (end of Stage 2). Immunofluorescence images were quantified using CellProfiler. Markers of DE (FOXA2, SOX17), pluripotency (OCT4) and aPS/mesoderm (T, CDX2) were examined. (A) Summary of results aPS (Stage 1) optimization (n=2 technical replicates). Note that we did not test the effects of <16 h of aPS induction. (B) Summary of results for optimization of DE commitment (Stage 2) (n=2 technical replicates). For Stage 1, the optimal conditions identified in A were used, then cells were switched into the indicated conditions for Stage 2. (C) Diagram of the optimized protocol for differentiation of mouse EpiSCs (+WI) into DE and a current hPSC-to-DE protocol (Loh et al., 2014). (D) FACS quantification of immunostaining for DE markers (SOX17-Alexa Fluor 488 and CXCR4-Alexa Fluor 647) from cells at the endpoint of the optimized DE differentiation protocol. (E) Quantification of DE differentiation purity (SOX17+/CXCR4+ cells) across multiple experiments (technical replicates; C57Bl/6J, n=4; DBA/2J, n=3; PWK/PhJ, n=3).

Development (2022) 149, dev200561. doi:10.1242/dev.200561

and the transcription factor (TF) SOX17 (expressed exclusively in DE) (Fig. 2D). This analysis indicated that the DE purity was ∼95% using the optimized conditions. Next, we used flow cytometry to assess the performance of our DE protocol on two additional EpiSC lines derived from distinct inbred strains of mice. The average DE purity achieved with a C57Bl/6J EpiSC line was similar to the DBA/2J line used for optimization (∼95%), whereas the purity achieved with a PWK/PhJ EpiSC line was slightly lower (∼80%) (Fig. 2E). However, for each line the results were similar between technical replicates from independent experiments (n=3-4 technical replicates/line).

Molecular characterization of mouse EpiSC-derived DE

To further characterize DE generated by our new protocol, we performed RNA-seq and ATAC-seq on DE generated from four independently derived C57Bl/6J EpiSC lines (characterized in Fig. 1C-E). CXCR4^{+} DE was purified with magnetic assisted cell sorting (MACS). EpiSC-derived DE exhibited large-scale transcriptional changes compared with EpiSCs, including upregulation of canonical DE marker genes (*Sox17*, *Foxa2*, *Cxcr4*, *Gata4/6*, *Cer1*) and downregulation of pluripotency-associated genes, including *Oct4* and *Nanog* (Fig. 3A, Fig. S2A-D), consistent with results obtained using immunofluorescence staining (Fig. S2E) (Genga et al., 2019; Nowotschin et al., 2019). There were also widespread changes in chromatin accessibility in DE compared with EpiSCs. PCA of ATAC-seq data indicated that cell type (EpiSCs versus DE) accounted for the majority of variation observed across samples (PC1; 92.5%) (Fig. S2B). Accordingly, we observed significant increases in chromatin accessibility at numerous putative enhancer elements near genes known to be

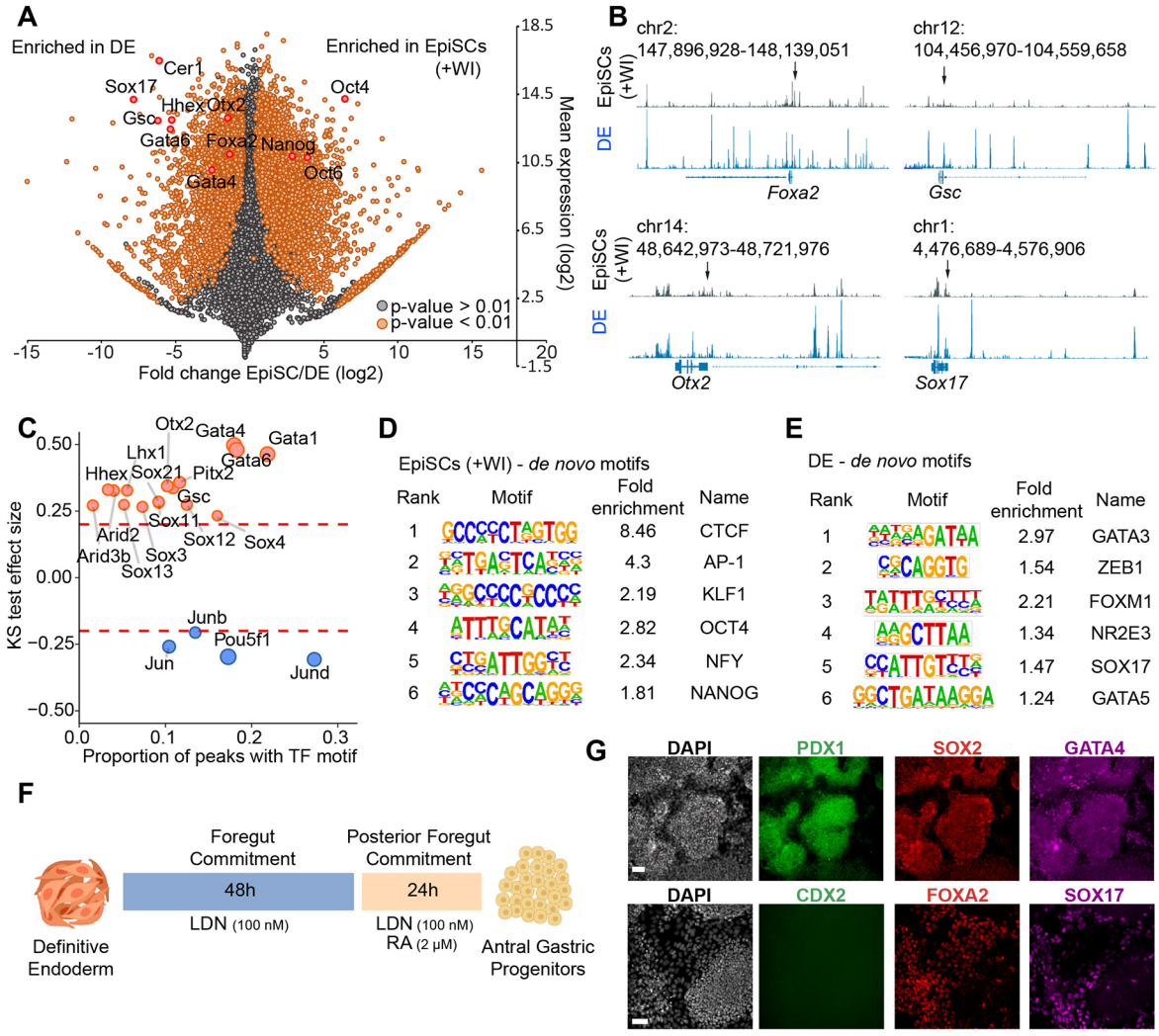

Fig. 3. Genomic characterization of DE derived from EpiSCs (+WI). (A) RNA-seq data from C57Bl/6J EpiSCs (n=5, biological replicates) and C57Bl/6J DE purified by MACS (n=4, biological replicates). Differentially expressed genes between EpiSCs (+WI) and DE are highlighted in orange (P<0.01, Wald test and corrected using the Benjamini–Hochberg method). A set of essential genes for primed pluripotency and DE are further annotated in red. (B) ATAC-seq data from EpiSCs (+WI) (top) or DE (bottom). Gene loci known to play crucial roles in DE development are displayed. Arrows indicate the promoter of each gene. (C) Comparison of TF binding motif enrichment in accessible chromatin regions during the EpiSC (+WI) to DE transition. Peaks with differential chromatin accessibility between stages were compared with identify TF motifs enriched in cis-regulatory elements in each cell state [one-sided Kolmogorov–Smirnov (KS) test]. TF motifs with a KS test effect size ≥0.20 are indicated by dashed lines. (D,E) Results of *de novo* TF motif searches within EpiSCs (+WI) (D) or MACS-sorted DE (E) ATAC-seq peaks. (F) Diagram of the optimized protocol for differentiation of mouse DE into posterior foregut and antral gastric progenitors. (G) Antral gastric progenitors stained with antibodies against markers of posterior foregut (PDX1, SOX2 and GATA4), midgut/hindgut progenitors (CDX2) and DE (FOXA2, SOX17) (n=3 biological replicates). Scale bars: 50 µm.

Development (2022) 149, dev200561. doi:10.1242/dev.200561

essential for DE differentiation (*Foxa2*, *Gsc*, *Otx2*, *Sox17*) (Fig. 3B). Across the genome, regions of hyper-accessible chromatin (peaks identified by ATAC-seq) in DE compared with EpiSCs were enriched for binding motifs for TFs known to play key roles in DE specification (GATA4/6, OTX2, SOX17, GSC). In contrast, ATAC-seq peaks in EpiSCs compared with DE exhibited enrichment for OCT4 and AP-1 (FOS/JUN) binding motifs (Fig. 3C-E). In summary, these genomic data demonstrate that DE exhibits global changes in gene expression and TF binding compared with EpiSCs and has the expected genomic features of bona fide PSC-derived DE.

Finally, we examined whether the DE generated by this protocol can be further patterned into specific populations of organ progenitors. We treated EpiSC-derived DE with conditions that promote posterior foregut patterning and subsequent differentiation into antral gastric progenitors (modified from protocols developed for hPSCs by Broda et al., 2019; McCracken et al., 2014) (Fig. 3F). After 72 h of additional differentiation, we observed a high density of cell clusters expressing markers of antral gastric epithelial progenitors (SOX2, PDX1, GATA4) and lacking expression of markers of midgut/hindgut (CDX2) and DE (FOXA2 and SOX17) (Fig. 3G). These data indicate that EpiSC-derived DE can be further patterned into organ progenitors and demonstrate the value of generating a high-purity population of DE for subsequent stages of differentiation.

Efficient and homogeneous conversion of EpiSCs into forebrain-patterned organoids

The first neural organoid protocols were developed using embryoid bodies (EBs) formed from naïve mouse PSCs (Eiraku et al., 2008; Wataya et al., 2008). Given the success of our efforts to generate DE from EpiSCs (+WI), we next sought to determine whether EpiSCs (+WI) would also be a better starting cell type for generating neural organoids. We chose to focus our attempts on generating dorsal forebrain-patterned organoids, which have the potential to give rise to progenitors of multiple brain regions, including the cerebral cortex, hippocampus and thalamus (Montiel and Aboitiz, 2015).

Following extensive testing, we were able to identify conditions for robust EB formation, neural induction and forebrain patterning of EpiSC-derived EBs (summarized in Fig. 4A,B). Briefly, EpiSCs (+WI) were dissociated into single cells and EBs formed from ∼1000 EpiSCs in neural induction media in AggreWell plates. We found that addition of chroman 1 (ROCK inhibitor) and emricasan (pan-caspase inhibitor), components of the recently reported CEPT cocktail (Chen et al., 2021), help to dramatically reduce cell death during EB formation compared with commonly used ROCK inhibitors (Y-27632 or thiazovivin; Fig. S4A). To promote the generation of forebrain fates (telencephalon, diencephalon), we inhibited Wnt signaling by addition of the porcupine (PORCN) inhibitor LGK-974 for the first 2 days of differentiation (Rifes et al., 2020; Tchieu et al., 2017). Inhibition of FGF signaling (by the FGFR inhibitor PD173074) during this period can promote forebrain patterning, but it is not essential for forebrain specification in this system. After the first 24 h, EBs were removed from AggreWell plates and embedded in Matrigel (based on Qian et al., 2018). Under these conditions, many EpiSCs expressed SOX1 after the first 24 h of EB formation, and nearly all cells in EBs expressed SOX1 after 48 h (Fig. 4C). In contrast, mouse neural organoid protocols that start from naïve PSCs have few SOX1^{+} cells after 72 h in culture (Eiraku et al., 2008).

During early A-P patterning of the neural plate, FGF signaling promotes acquisition of more posterior neural fates, but shortly thereafter promotes telencephalic identity in the anterior-most region of the neural epithelium (∼E8.25) (Garel et al., 2003;

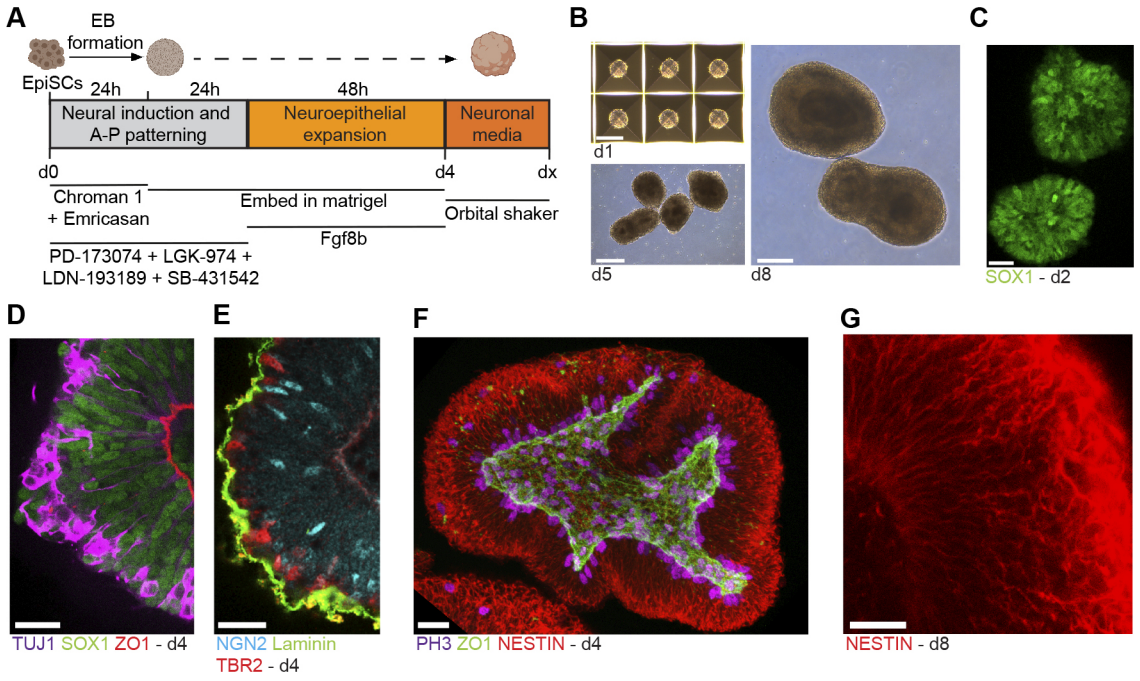

Fig. 4. Generation of forebrain-patterned organoids from mouse EpiSCs. (A) Diagram of the protocol for forebrain-patterned neural organoid generation. (B) Brightfield images of forebrain organoids. (C) Confocal immunofluorescence image of a developing organoid after 48 h (d2). (D,E) Confocal immunofluorescence images of a d4 organoid. (F) *z*-stack reconstruction of a d4 organoid. (G) Confocal immunofluorescence image of a day 8 organoid. Scale bars: 200 µm (B); 25 µm (C-G). For C-G, all organoids were cleared (see Materials and Methods) and imaged *in toto* without sectioning.

Development (2022) 149, dev200561. doi:10.1242/dev.200561

Shimamura and Rubenstein, 1997). Therefore, we hypothesized that addition of FGF8 (FGF8b) after the first 48 h of differentiation would facilitate induction of anterior telencephalic fates and could subsequently promote the proliferation and survival of telencephalic neuroepithelial progenitors (Storm et al., 2006). By 96 h [day (d) 4], EBs formed continuous neuroepithelia, with consistent apicobasal polarity (Fig. 4D,E, Fig. S4B) (Movie 1). Characterization of the complete 3D structure of d4 organoids using tissue clearing revealed mitotic neuroepithelial progenitors at the apical membrane, a central lumen, nestin-expressing cells with characteristic radial-glial morphologies spanning the length of the apical-basal axis of the developing tissue, as well as intermediate/basal progenitors and early-born postmitotic neurons migrating outward towards the basal lamina (Fig. 4D-G). Live-imaging of sparsely labeled radial glial cells in organoids over a 24 h period (d3-d4) revealed interkinetic nuclear migration and cell division behaviors characteristic of radial glial cells in the embryonic brain (Arai and Taverna, 2017; Noctor et al., 2004) (Movie 2). After d4, organoids were removed from Matrigel and switched into maintenance media (N2B27 media with vitamin A, and the neurotrophic factors BDNF and GDNF) in low-adhesion cell culture dishes on an orbital shaker.

Next, we sought to characterize the specific regional identity of progenitors and neuronal populations generated in these organoids. At d4, all organoids expressed PAX6, which is expressed by progenitors in the caudal forebrain (diencephalon) and/or dorsal telencephalon, depending on the exact stage (Puelles et al., 2000). However, PAX6 expression was not homogeneous throughout the organoids, suggesting that not all neuroepithelial progenitors acquire the same regional identity under these conditions (Fig. 5A). By d8, most organoids spontaneously pattern into two opposing domains, which mirror the $Pax6^+$ and $Pax6^-$ regions at d4 (Renner et al., 2017; Takata et al., 2017) (Fig. 5B-G). Surprisingly, one domain contained large numbers of $PAX6^+$ post-mitotic neurons, which occur almost exclusively in the developing prethalamus, generated from the anterior-most domain of the diencephalon (prosomere 3, p3) (Caballero et al., 2014; Manuel et al., 2015) (Fig. 5C). In the other domain, we observed neurons expressing markers of the cerebral cortex, such as TBR1, BCL11B (also known as CTIP2) and BRN2 (POU3F2), as well as RELN, a marker of Cajal–Retzius cells (Fig. 5D-G, Fig. S5). Taken together, these data suggest that organoids generated in these conditions polarize early into distinct domains that represent different A-P identities: the dorsal telencephalon and the anterior diencephalon (prosomere 3). Importantly, these results are reproducible across technical replicates and when starting with distinct EpiSC (+WI) lines (three additional EpiSC lines) (Fig. S5C,D, Table S5).

Characterization of forebrain organoids using single-cell RNA-seq

To gain further insight into the precise cell populations present within forebrain organoids, we generated single-cell (sc)RNA-seq data from d12 organoids (5652 total cells). Reduced-dimensionality visualization using uniform manifold approximation and projection (UMAP) revealed multiple distinct clusters, which we tentatively classified as specific cell types based on their expression of known marker genes. Importantly, nearly all cells within the organoid appeared to be neuroectodermal derivatives, suggesting that neural induction in EBs is highly efficient (Fig. 6, Fig. S6A, Fig. S7).

Consistent with our immunostaining results, we observed clusters that appeared to be immature (cluster 7) and more mature (cluster 8) prethalamic neurons. In the embryo, the prethalamic domain generates multiple distinct types of GABAergic neurons that form the thalamic reticular nucleus and the zona incerta (Puelles et al., 2013). Accordingly, the early prethalamic neuron cluster (cluster 7) was characterized by expression of markers associated with early development of GABAergic neurons (*Ascl1*, *Dlx5*, *Dlx6*, *Gad1*, *Gad2*). The more mature prethalamic neuron cluster (Cluster 8) was characterized by expression of the prethalamic neuron markers (*Pax6*, *Isl1*, *Meis2*, *Mmp16*) (Mandai et al., 2014; Nagalski et al., 2016; Ono et al., 2014; Virolainen et al., 2012) (Fig. 6E). Within cells in this cluster, there was further heterogeneity based on the relative expression levels of *Ptprd* and *Pax6*, which distinguishes the lateral or the medial portions of the developing prethalamus *in vivo* (Guo and Li, 2019; Kim et al., 2020; Li et al., 2020; Sommer et al., 1997; Tuttle et al., 1999). In addition, more mature prethalamic neurons express higher levels of *L1cam* and *Nrcam*, which play a role in the pathfinding of axons from prethalamic neurons that project into the thalamus (Molnar et al., 2012; Quintana-Urzainqui et al., 2020) (Fig. S6B).

We identified one cluster (Cluster 6) that appeared to correspond to the glutamatergic neurons expressing TBR1 and/or BCL11B. However, although expression of TBR1 and BCL11B is often associated with cerebral cortex development, neurons in this cluster instead expressed several markers specific to hippocampal neurons (*Zbtb20*, *Neurod1*, *Prox1*), and lack expression of the telencephalic marker *Foxg1*, which is expressed broadly in the cerebral cortex, but has low expression, or is even absent, in the hippocampus (Hatami et al., 2018) (Fig. 6F). These data suggest that these neurons more closely resemble developing hippocampal neurons than deep layer cortical neurons. The observed similarity in marker profiles between these two cell types is consistent with *in vivo* data showing that the developing neocortex (cerebral cortex) and allocortex (hippocampus and olfactory bulb) have similar expression profiles during embryonic development (Cadwell et al., 2019).

We also observed a cluster of cells (Cluster 3) that resemble cortical hem, and are characterized by expression of RSPO genes, *Wnt8b*, *Wnt9a* and *Bmp7* (Grove et al., 1998; Hasenpusch-Theil et al., 2012) (Fig. S7). The cortical hem is a secondary organizer located next to the developing hippocampus in the dorsomedial region of the developing telencephalon (Vieira et al., 2010). In addition to its role in cortical patterning via secretion of Wnt and BMP, neural progenitors in the cortical hem also generate Cajal–Retzius cells during early stages of telencephalon development (Takiguchi-Hayashi et al., 2004). Accordingly, we observed cells bridging clusters 3 and 6 that co-expressed the Cajal–Retzius cell markers *Trp73* (also known as p73) and *Reln* (reelin) (Hanashima et al., 2007; Simon et al., 2012) (Fig. 6F).

We also used VoxHunt (Fleck et al., 2021) to comprehensively compare our single-cell dataset to gene expression data from the developing embryonic brain (*in situ* hybridization data from the E18 Allen Developing Mouse Brain Atlas; Thompson et al., 2014). This analysis confirmed that the forebrain organoids most closely resemble medial pallium (hippocampus/cortical hem) and prethalamus/p3 (Fig. 6H).

In addition to these neuronal clusters, we also found clusters (clusters 4 and 5) that appear to represent OPCs, characterized by high expression of *Olig1*, *Olig2*, *Pdgfra* and *Dll1* (Fig. 6G, Fig. S7). Among all of the clusters, OPCs appeared to be the only actively proliferating cells within organoids at d12 (Fig. 6D). Immunofluorescence staining for OLIG2 at d12 confirmed the presence of these cells, which were intermingled with $BCL11B^+$ hippocampal neurons, suggesting that the same progenitors that give rise to the hippocampal glutamatergic neurons progress to produce

Development (2022) 149, dev200561. doi:10.1242/dev.200561

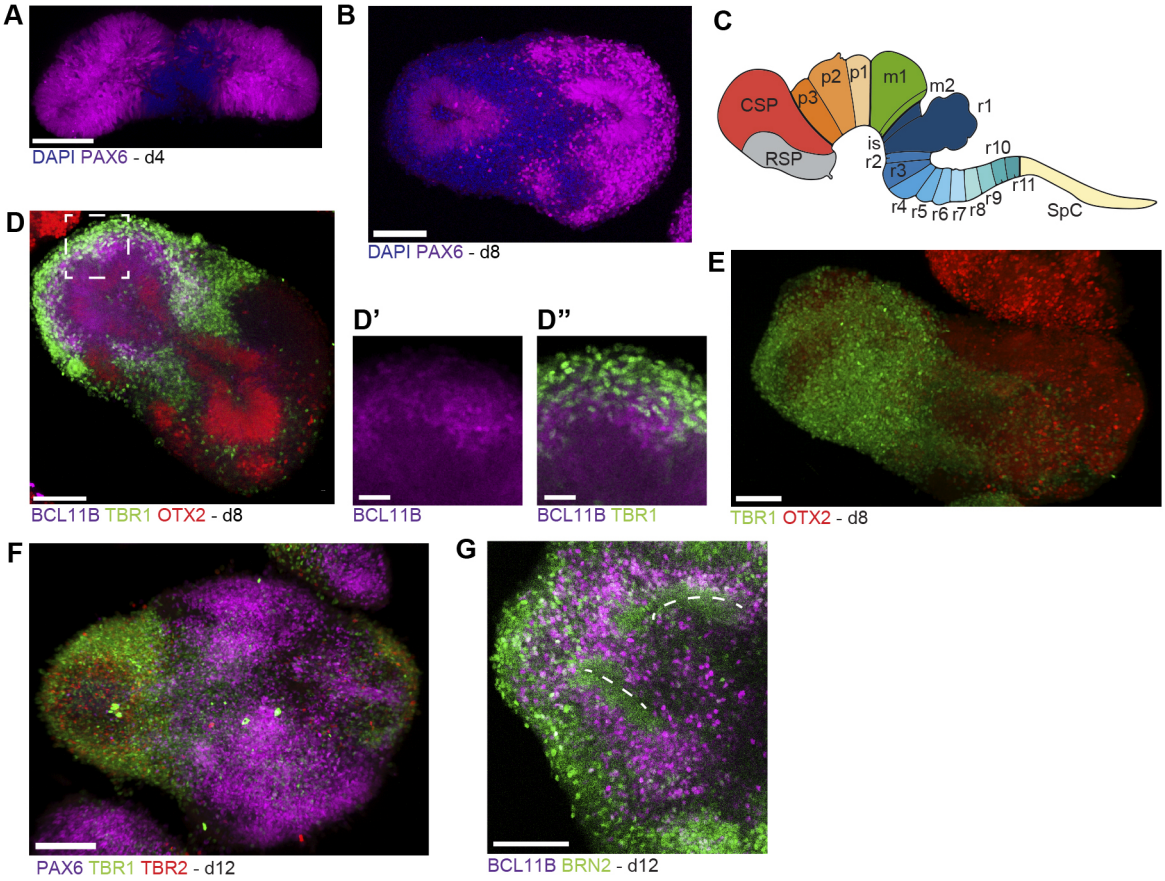

Fig. 5. Characterization of the identity of progenitors and neurons generated in forebrain organoids. (A,B) Confocal immunofluorescence image of organoids at d4 (A) and d8 (B). (C) Diagram of prosomeres in the mouse brain (modified from Puelles et al., 2013). CSP, caudal secondary prosencephalon; is, isthmic organizer; m1, m2, midbrain mesomeres 1 and 2; p1, p2, p3, prosomeres 1-3 of the diencephalon; r1-r11, rhombomeres 1-11; RSP, rostral secondary prosencephalon; SpC, spinal cord. (D-D″) Confocal immunofluorescence images of a d8 organoid (boxed area magnified in D′ and D″), immunostained using antibodies against the deep layer cortical neuron markers TBR1 and BCL11B, and the forebrain neural progenitor marker OTX2. (E-G) Confocal immunofluorescence image (3D projection) of a d8 (E) and d12 (F,G) organoids. Dashed lines in G indicate apical regions of neuroepithelia. Scale bars: 100 µm (A,B,D,E-G); 25 µm (D′,D″).

OPCs (Fig. S5C). This is consistent with prior studies showing that mouse radial glial cells from the dorsal telencephalon give rise to OPCs after birth, and explant studies demonstrating that dorsal telencephalic progenitors from the embryonic brain often generate OPCs when explanted or cultured *in vitro* (Kessaris et al., 2006; Qian et al., 1997; Tekki-Kessaris et al., 2001).

Taken together, these data reveal that our EpiSC-based forebrain organoid protocol can robustly generate organoids containing multiple distinct regions of the developing forebrain, including dorsal, caudo-medial telencephalon (hippocampus and cortical hem) and dorsal anterior diencephalon (prosomere 3, prethalamus). These two domains are adjacent to one another, each bordering the boundary between the telencephalon and diencephalon. Prethalamic domains and hippocampal/cortical hem domains generally formed on opposite poles of organoids, suggesting that organoids undergo spontaneous polarization during early stages of development and develop into distinct domains representing different A-P identities (Takata et al., 2017).

DISCUSSION

Directed differentiation models enable a range of experimental techniques that would be difficult or impossible to perform *in vivo*, including genetic and chemical screens, live imaging, and experimental embryology approaches such as *in vitro* reconstitution (Hadjantonakis et al., 2020; Li et al., 2019; Moris et al., 2020; Schlissel and Li, 2020). Using mouse PSCs for directed differentiation has multiple advantages compared with hPSCs. For example, using mouse PSCs makes it possible to use the extensive genetic tools and resources that have been generated for mice. This includes not only knockout lines, reporter lines and human disease models, but also numerous distinct inbred strains and outbred heterogeneous stocks such as Diversity Outbred mice that can be used for quantitative genetic approaches (Churchill et al., 2012; Skelly et al., 2020). In addition, results from mouse PSC differentiation models can be directly compared with genetically matched tissues from mouse embryos, which allows for rigorous assessments of model validity (Voelkl et al., 2020). Such data represent an important proof of concept for hPSC-based cellular models of development and disease processes, as it will never be possible to perform similar cross-validation experiments in developing human embryos (Kleiman and Engle, 2021).

Despite the advantages of mouse directed differentiation, mouse PSC models are much less frequently used than hPSC-based models. This is likely due in part to the limited availability of mouse PSC directed differentiation protocols that are robust, efficient, generalizable and user-friendly. We found that by

Development (2022) 149, dev200561. doi:10.1242/dev.200561

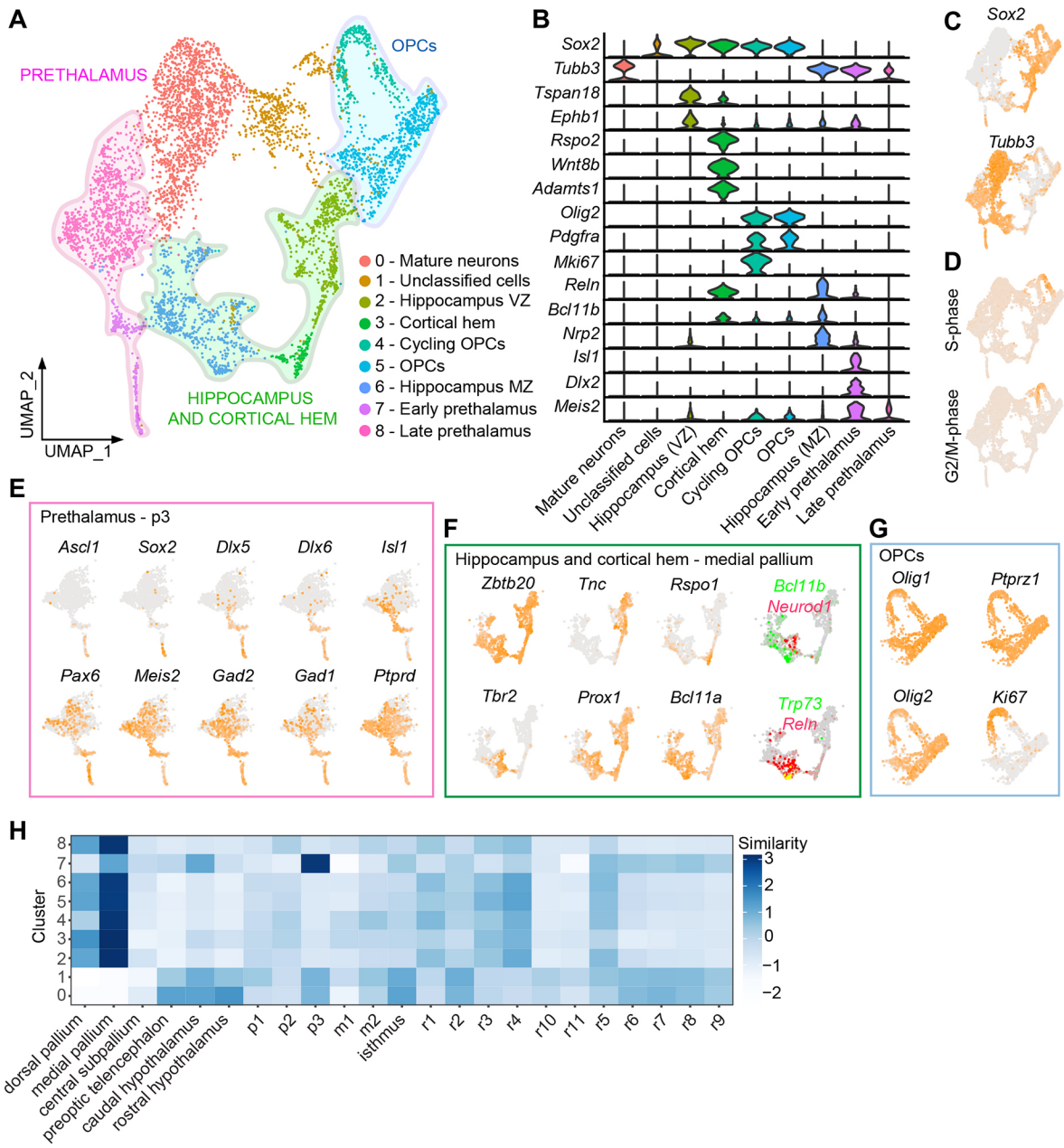

Fig. 6. Characterization of day 12 forebrain organoids using scRNA-seq. (A) UMAP representation of scRNA-seq data from d12 organoids. Three broad classes of cell types are highlighted: OPCs, hippocampus/cortical hem and prethalamus. (B) Violin plots of gene expression levels for representative markers used to identify each cluster in A (see also Table S5). (C) Annotated UMAP highlighting the expression of *Sox2*, a neuronal progenitor marker, and *Tubb3* (also known as *Tuj1*), a pan-neuronal marker. (D) Cell cycle analyses on d12 scRNA-seq data. (E) UMAP representations of cells from putative prethalamic clusters (from A), highlighting expression of known prethalamic markers. (F) UMAP representations of gene expression data from putative hippocampal/cortical hem clusters from A. Expression of *Bcl11b* and *Neurod1*, which delineate the early development of the CA1-2 and CA3 regions of the developing hippocampus, respectively, appear to be mutually exclusive (Simon et al., 2012). (G) UMAP representations of gene expression data from putative OPC clusters from A. (H) VoxHunt analyses on the scRNA-seq dataset, separated by cluster, compared with the E18 developing mouse brain. p1, p2, p3, prosomeres 1-3 of the diencephalon; m1, m2, midbrain mesomeres 1 and 2; r1-r11, rhombomeres 1-11.

using EpiSCs (+WI) it is possible to develop protocols for directed differentiation that are as robust as state-of-the-art hPSC protocols. As naïve PSCs can be converted into EpiSCs (+WI) *in vitro*, our new protocols can be applied to generate DE and neural organoids from pre-existing naïve PSC lines that carry specific genetic modifications, including gene knockouts or fluorescent reporters. These new optimized methods for directed differentiation represent a valuable addition to the experimental toolkit available for studying mouse development and thus should be of substantial interest to the developmental and stem cell biology research communities.

Rapid and efficient generation of DE from EpiSCs

By adapting protocols developed for hPSCs, we demonstrate that EpiSCs (+WI) can be differentiated into DE with high purity (>90%) in only 40 h. Our findings are consistent with previous work showing that EpiSCs and hPSCs respond similarly to most differentiation cues (Greber et al., 2010; Vallier et al., 2009).

Development (2022) 149, dev200561. doi:10.1242/dev.200561

The most significant difference we observe between hPSC and EpiSC differentiation is timing. The optimal timing for EpiSCs is 16 h for aPS induction and 24 h to DE commitment, whereas hPSC protocols use 24 h for aPS induction and 48 h to DE commitment (Loh et al., 2014). These differences are consistent with the faster pace of mouse development compared with human, which has been previously observed when directly comparing mouse and human differentiation protocols (Ebisuya and Briscoe, 2018).

The high-purity DE generated by our protocol will be an ideal starting point for subsequent differentiation into progenitors of a variety of endodermal organs, such as lung, liver, intestinal tissues or organoids (Fowler et al., 2020; Yiangou et al., 2018). As a proof of concept, we demonstrated that EpiSC-derived DE can be further patterned to posterior foregut progenitors and antral gastric progenitors by adapting previously developed protocols for hPSC differentiation (Broda et al., 2019; McCracken et al., 2014). The high purity of DE achieved by this protocol should also facilitate large-scale genetic screens to identify genes that control endoderm commitment (Li et al., 2019).

Improved methods for mouse neural organoid generation

The first neural organoid protocols were developed using naïve mouse PSCs (Eiraku et al., 2008; Wataya et al., 2008). Although these pioneering studies provided the foundation for the subsequent development of protocols to generate neural organoids from hPSCs, the original mouse protocols are now rarely used. This is due, at least in part, to the fact that these protocols were less robust and user-friendly than current hPSC organoid protocols. In addition, most of these early mouse neural organoid protocols pre-date the development of improved methods for consistently generating polarized neuroepithelia in neural organoids (e.g. Matrigel embedding or addition of laminin/Matrigel to the culture media) (Lancaster et al., 2013; Nasu et al., 2012). Therefore, we reasoned that by starting with EpiSCs instead of naïve PSCs, and by implementing improved techniques for organoid generation developed for hPSCs, we would be able to develop an improved protocol for the generation of mouse neural organoids.

Although our initial goal was to generate a mouse organoid model of cerebral cortex development, we instead observed domains of hippocampal and prethalamic progenitors. This suggests that our conditions for A-P patterning must be further modified to generate cerebral cortex, which comes from the most anterior region of the developing neuroectoderm. Previous work with mouse neural organoids found that insulin exerts posteriorizing effects on developing neuroectoderm via activation of FGF signaling, and it is necessary to remove insulin from the media at early stages of neural induction to maintain anterior neuroectoderm patterning (Takata et al., 2017; Wataya et al., 2008). However, this strategy is not readily adaptable to primed PSC organoid models because insulin is required for primed PSC growth and survival, making it difficult to form EBs and perform neural induction in insulin-free conditions. Based on these studies, we added FGFR inhibitors in addition to Wnt inhibitors for the first 2 days to block the posteriorizing influence of FGF signaling. However, FGFR inhibition was not strictly required for forebrain specification if Wnt signaling is sufficiently inhibited. Within forebrain organoids, we observed spontaneous polarization into telencephalic and diencephalic regions (Renner et al., 2017; Takata et al., 2017). Interestingly, for hPSC-based cerebral cortex organoids, inhibition of Wnt signaling (in addition to dual SMAD inhibition for neural induction) is generally sufficient to maintain anterior neuroectodermal identity and specification of cortical fates, even in the presence of high levels of insulin. It will be interesting to explore the mechanisms underlying this apparent difference in A-P patterning between mouse and human.

Methods for the generation of organoids containing diencephalic progenitors have previously been reported (Shiraishi et al., 2017; Xiang et al., 2019). These protocols use a combination of moderate insulin, inhibition of FGF/ERK and activation of BMP signaling (BMP7) to specify diencephalic progenitors of the thalamus and epithalamus (prosomere 2) and pretectum (prosomere 1). In contrast, we find that addition of high levels of FGF8b without exogenous BMP7 induces prethalamic (prosomere 3) fates. This is consistent with the high expression of FGF8b in the dorsal midline of p3 and prethalamic eminence at early stages of diencephalon development (E10.5-E12.5) (Martinez-Ferre and Martinez, 2009). *In vivo*, prethalamic progenitors generate numerous distinct types of inhibitory (GABAergic) neurons that form the thalamic reticular nucleus and the zona incerta (Li et al., 2020). Prethalamic neurons have not been generated efficiently in previous mouse and human thalamic organoids, and thus our forebrain organoid protocol should be useful for studying the development of this complex and understudied brain region.

Mouse forebrain-patterned organoids can complement *in vivo* mouse models of forebrain development as well as neurodevelopmental disorders (Sestan and State, 2018). Our neural organoid model should facilitate direct comparisons between the phenotypes observed *in vivo* in mice with mutations associated with neurodevelopmental disorders, and those observed in analogous mouse organoid models *in vitro*. In contrast, hPSC-based models of neurodevelopmental disorders cannot be conclusively validated *in vivo*, and thus it is difficult to evaluate the relevance of observations made in neural organoid models *in vitro* for developmental pathophysiology *in vivo*. More rigorous assessment of the strengths and limitations of *in vitro* models in mice would help to inform experimental design for hPSC-based modeling of neurodevelopmental disorders. In future studies, it will be interesting to perform in-depth comparisons of developing neural organoids and their analogous cell types *in vivo*, and to compare mouse and human organoid development.

Limitations of the study

Although we were able to develop robust protocols for differentiation of EpiSCs (+WI) into DE and neural organoids, it is possible that EpiSCs (+WI) will not be an ideal starting point for differentiation into all cell types.

For some protocols, EpiLCs or more recently described stable formative stage stem cells might be superior to EpiSCs (+WI) (Hayashi et al., 2011; Kinoshita et al., 2021; Morgani et al., 2018; Yu et al., 2021). Even when cultured with Wnt inhibition, we observe some heterogeneity in EpiSC cultures, marked by expression of anterior primitive streak markers *Foxa2* and *T* (Bernemann et al., 2011; Blauwkamp et al., 2012; Song et al., 2016; Tsakiridis et al., 2014). Additional optimization of EpiSC (+WI) conditions could help to develop conditions that are as robust as hPSCs and further mitigate issues with current culture conditions, such as residual heterogeneity and the need for fibroblast feeder cells. In this study, we exclusively used EpiSCs (+WI) that we derived *in vitro* via conversion of naïve mouse PSCs. Previous work suggests that EpiSCs derived *in vitro* are highly similar to EpiSC lines derived directly from post-implantation epiblast (Kojima et al., 2014), so we would expect cells from both sources to behave similarly, but we have not demonstrated that this is the case. There is an emerging consensus in the hPSC directed differentiation field

Development (2022) 149, dev200561. doi:10.1242/dev.200561

that the initial culture conditions of hPSCs have a significant impact on their ability to differentiate into specific lineages (Cornacchia et al., 2019; Watanabe et al., 2019 preprint). Thus, it is likely that further improvements of EpiSC (+WI) culture will be the best way to generally improve their performance in directed differentiation experiments. The impact of long-term culture on genetic and epigenetic stability of EpiSCs (+WI) has not been characterized in depth (Halliwell et al., 2020). Similarly, the long-term effects of tankyrase inhibition on the genetic and epigenetic stability of EpiSCs remain to be characterized. Several types of Wnt inhibitors have been used for EpiSC culture, and it remains uncertain how different means of inhibiting Wnt activity might change the properties of the resulting EpiSCs (Kurek et al., 2015; Sumi et al., 2013; Wu et al., 2015).

MATERIALS AND METHODS

Summary

Step-by-step protocols for directed differentiation experiments are provided as supplementary Materials and Methods. Detailed information about the reagents used can be found in Table S3.

Mouse ESC culture and conversion to EpiSCs

All mouse ESC lines were maintained on gelatin-coated dishes with irradiated mouse embryonic fibroblast feeder cells using serum/LIF media composed of DMEM (high glucose, GlutaMAX, HEPES), 1% nonessential amino acids, 1% sodium pyruvate, 1% penicillin-streptomycin, 0.1% 2-mercaptoethanol, 10% fetal bovine serum and 1000 units/ml ESGRO LIF. All ESC lines (except lines from B6129SF1/J background) were cultured in serum/LIF media with 2i containing 3 µM CHIR99201 and 1 µM PD0325901. Media was changed daily, and ESCs were passaged upon 70% confluence at a 1:6 ratio using TrypLE. ESC-to-EpiLC conversion was performed as described by Morgani et al. (2018). Briefly, ESCs were lifted using 0.5 µ/µl collagenase IV, centrifuged (200 ***g*** for 3 min at room temperature) and dissociated into a single-cell solution using Accutase. The ESC suspension was plated on fibronectin-coated plates (16.7 µg/ml) at a density of 17,500 cells/cm^2 in N2B27 media supplemented with 12.5 ng/ml heat-stable recombinant human bFGF, 20 ng/ml activin A, and 1% Knockout Serum Replacement (Gibco, 1082028). N2B27 media consists of 50% DMEM-F12, 50% Neurobasal medium, 0.5% N2 supplement, 1% B27 supplement without vitamin A, 2 mM GlutaMAX, 1% penicillin-streptomycin and 0.1% 2-mercaptoethanol. The media was changed after 24 h, and cells were converted to EpiSCs after 48 h. For EpiLC-to-EpiSC conversion, EpiLCs were dissociated into small clumps (approximately three to five cells) with Accutase and plated at a density of ∼50,000-100,000 cells per cm^2 on irradiated mouse fibroblast feeder cells in N2B27 supplemented with 20 ng/ml activin A, 12.5 ng/ml heat-stable bFGF and Wnt inhibitor (175 nM NVP-TNKS656). EpiSC media was changed daily, and cells were passaged every ∼48 h at a 1:6 ratio using 0.5 µ/µl collagenase IV followed by dissociation with Accutase into small clumps of three to five cells. For feeder-free EpiSC culture, EpiSCs growing on feeders were isolated using 0.5 µ/µl collagenase IV and seeded on fibronectin-coated plates (16.7 µg/ml). After the first feeder-free passage, cells were passaged using Accutase only. The EpiSCs were considered as feeder-free after two passages with no visible feeder cell remaining.

DE and antral gastric progenitor differentiation

For DE differentiation, EpiSCs were generally used after approximately four to eight passages in EpiSC conditions. For differentiations, high-quality cultures of EpiSCs were detached using collagenase IV (0.5 µ/µl), washed once with PBS, and then dissociated into a single-cell suspension using Accutase. EpiSCs were plated at a density of 110,000 cells/cm^2 in chemically defined media (CDM) containing 50% IMDM, 50% Ham's F12 Nutrient Mix with GlutaMAX, 1% chemically defined lipid concentrate, 450 µM monothioglycerol, 1% polyvinyl alcohol (w/v), 15 µg/ml Apo-transferrin, 0.5% GlutaMAX, 0.7 µg/ml insulin and supplemented with 20 ng/ml activin A, 12.5 ng/ml heat-stable bFGF, 175 nM NVP-TNKS656, 1% Knockout Serum Replacement, and 2 µM thiazovivin. Plating media was removed 6 h after seeding, cells were washed gently with PBS without calcium or magnesium (PBS-/-) and the media was changed to CDM supplemented with 3 µM CHIR99201 and 40 ng/ml activin A. Sixteen hours after the first media change, cells were washed with PBS-/- and the media was replaced with CDM supplemented with 100 ng/ml activin A and 100 nM LDN-193189. After 24 h (46 total hours after cells were initially seeded), cells were fixed for immunostaining or collected for further analysis. For antral gastric progenitor differentiation, DE cells were kept in CDM with 100 nM LDN-193189 and 2% fetal bovine serum, with a renewal of the media after 24 h. After 48 h, the media was changed to CDM with 100 nM LDN-193189, 2 µM retinoic acid and 2% fetal bovine serum for a further 24 h. After 72 h, cells were fixed for immunostaining.

Immunostaining

For immunostaining of adherent cells (EpiSCs and DE), cells were rinsed twice with PBS-/- and fixed with 4% paraformaldehyde solution for 30 min at room temperature. After fixing, cells were washed twice with PBS-/- and permeabilized with PBS-/- containing 1% Triton X-100 (PBST) for 10 min at room temperature and blocked for 30 min with PBS-/- containing 0.3% Triton X-100 and 5% fetal bovine serum. Primary antibodies were diluted in PBST with 1% fetal bovine serum and incubated overnight at 4°C. Detailed information about the antibodies used can be found in Table S2. Following overnight incubation and three 10 min washes with PBST, cells were incubated with secondary antibodies for 2 h at room temperature. Cells were rinsed with two 10 min washes of PBST before DAPI staining (1 µM) for 15 min at room temperature. Cells were rinsed with PBST and imaged using a Leica Dmi8 microscope.

Quantification of immunofluorescence images

All image quantification was performed using Cell Profiler version 4.2.1 to calculate efficiency of DE differentiations based on FOXA2 and SOX17 expression. DAPI-stained nuclei were identified using the 'Identify Objects' module. To identify nuclei stained with each antibody, segmented nuclei were further analyzed using the 'Identify Objects' module and the 'Relate Objects' Module. These data were then classified as either positive or negative for each marker using the 'Filter Objects' module and overall efficiency was calculated based on percentage of expression for each marker.

Flow cytometry

Following DE differentiation, cells were dissociated in Accutase and washed in FACS buffer consisting of PBS-/-, 20% fetal bovine serum and 0.1% 0.5 M EDTA. CXCR4 antibody conjugated to Alexa Fluor 647 and live/dead zombie UV staining were diluted in FACS buffer at the manufacturer's recommended concentration (Thermo Fisher) and incubated for 15 min at room temperature. Cells were washed and resuspended in FACS buffer with fixation/permeabilization diluent and fixation/permeabilization concentrate for 30 min at room temperature. The cells were then resuspended in permeabilization buffer with SOX17 antibody conjugated to Alexa Fluor 488 at the manufacturer's recommended concentration for an additional 30 min at room temperature. Fixed cells were then analyzed using a Cytek Aurora cell sorter.

Flow cytometry results were analyzed using FlowJo software v10.8 and single-color stainings were used as a negative control for gating purposes.

MACS purification of DE

DE cells were isolated for ATAC-seq and RNA-seq analyses using MACS following the manufacturer's instructions, with slight modifications. Cells were dissociated in Accutase, washed in FACS buffer, counted, and resuspended with rat anti-mouse CD184/CXCR4 Alexa Fluor 647-conjugated antibody at a concentration of 1 µl/10^6 cells and incubated for 1 h at 4°C. Cells were then washed with FACS buffer, centrifuged (200 ***g*** for 3 min at 4°C) and resuspended in a solution composed by 80% FACS buffer and 20% anti-rat IgG MicroBeads (Miltenyi Biotec, 130-048-501). Cells were incubated in the mixture for 15 min at 4°C, then washed and resuspended in 500 µl buffer. The MS column was placed in an OctoMACS

Development (2022) 149, dev200561. doi:10.1242/dev.200561

separator (Miltenyi Biotec, 130-048-501) on the MACS multistand. The cell suspension was added to the column and rinsed three times with buffer. Finally, the column was removed from the separator and the magnetically labeled cells were collected.

RNA extraction for RNA-seq

Phase separation in cells lysed in TRIzol was induced with 50% isopropanol and 0.5% 2-mercaptoethanol and RNA was extracted from the aqueous phase using the MagMAX mirVana Total RNA Isolation Kit (Thermo Fisher, A27828) on a KingFisher Flex Magnetic Particle Processor according to the manufacturer's protocol with 1-2 million cells input. Samples were eluted in 38 µl elution buffer.

Transcriptome sequencing of EpiSC samples

After RiboGreen quantification and quality control using an Agilent BioAnalyzer, 100-500 ng of total RNA with RIN values of 9.5-10 underwent polyA selection and TruSeq library preparation according to instructions provided by Illumina (TruSeq Stranded mRNA LT Kit), with eight cycles of PCR. Samples were barcoded and run on a NovaSeq 6000 in a PE100 run, using the NovaSeq 6000 S4 Reagent Kit (200 Cycles) (Illumina). An average of 36 million paired reads were generated per sample and the percentage of mRNA bases per sample ranged from 84% to 89%.

Transcriptome sequencing of DE samples

After RiboGreen quantification and quality control using an Agilent BioAnalyzer, 2 ng total RNA with RNA integrity numbers ranging from 7.7 to 10 underwent amplification using the SMART-Seq v4 Ultra Low Input RNA Kit, with 12 cycles of amplification. Subsequently, 10 ng of amplified cDNA was used to prepare libraries with the KAPA Hyper Prep Kit using eight cycles of PCR. Samples were barcoded and run on a NovaSeq 6000 in a PE100 run, using the NovaSeq 6000 S4 Reagent Kit (200 Cycles) (Illumina). An average of 39 million paired reads were generated per sample and the percentage of mRNA bases per sample ranged from 83% to 87%.

ATAC-seq

ATAC-seq was performed as previously described (Buenrostro et al., 2015; see also dx.doi.org/10.17504/protocols.io.bv9mn946 at https://www.protocols.io/view/atac-sequencing-protocol-dm6gpwmpplzp/v1) with minor modifications. Briefly, cells were dissociated into single cells, filtered through a Flowmi cell strainer and the nuclei were isolated by incubation with lysis buffer [10 mM Tris-HCl pH 7.4, 10 mM NaCl, 3 mM $MgCl_2$, 0.1% Tween-20, 0.1% NP-40, 0.01% digitonin and 1% bovine serum albumin (BSA)] for 5 min at 4°C; 20,000 and 40,000 nuclei were isolated, and the DNA was tagmented with Tn5 (Illumina) and amplified using NEBNext® High-Fidelity 2X PCR Master Mix (NEB). The number of cycles was estimated by qPCR. DNA tagmentation efficacy was evaluated with a Bioanalyzer 2100 (Agilent Technologies) and the DNA amounts calculated with Qubit. i5 and i7 primer sequences were obtained from Mezger et al. (2018). The resulting DNA libraries were sequenced using the NextSeq550 system (Illumina) and about 25 million reads were obtained per sample in duplicate.

RNA-seq analysis

Resulting fastq files were mapped to their transcripts and quantified using Salmon (Patro et al., 2017) against the genome version mm10. For downstream analyses, Rstudio was used with the packages DESeq2, pcaExplorer and pheatmap (Love et al., 2014; Marini and Binder, 2019). Statistical significance was calculated using a Wald test and corrected using the Benjamini–Hochberg method.

ATAC-seq analysis

The raw fast data were analyzed using BasePair software (https://www.basepairtech.com/) with a pipeline that included the following steps. The raw reads were trimmed using fastp to remove low-quality bases from reads (quality<20) and adapter sequences. The trimmed reads were aligned using Bowtie2 (Langmead and Salzberg, 2012) to UCSC genome assembly mm10. Duplicate reads were removed using Sambamba. Peaks were identified with MACS2 (Gaspar, 2018 preprint) and those overlapping with satellite repeat regions were discarded. For further analyses, a union peak atlas was created from the MACS2 files. Peak intensity for each sample was counted using featureCounts (Liao et al., 2014). HOMER (v4.11) (Heinz et al., 2010) was used for motif analyses. PCA was carried out using the R packages DESeq2 (Love et al., 2014) and pcaExplorer (Marini and Binder, 2019).

For motif enrichment analysis, ATAC-seq peaks in the atlas were associated with TF motifs in the CIS-BP database (Weirauch et al., 2014) using FIMO (Grant et al., 2011) of MEME suite (Bailey et al., 2009), under the *P*-value cutoff of 1e−4. We limited the motif analyses to motifs for 236 TFs that are expressed in EpiSCs or DE (RPKM>5). Normalized counts were obtained using variance-stabilizing transformation in DESeq2. The shift in the cumulative distribution of normalized counts was compared between the subset of the atlas containing the TF motif and the total atlas using a one-sided Kolmogorov–Smirnov test.

Generation of forebrain organoids

For forebrain organoid generation, B6129SF1/J EpiSC colonies were detached using collagenase IV (0.5 µ/µl), washed once with PBS-/-, and then dissociated into a single-cell suspension using Accutase. EpiSCs were then seeded at 1000 cells/microwell in an AggreWell plate in EB formation media containing 50 nM chroman-1, 5 µM emricasan, 400 nM LDN-193189, 10 µM SB-431542, 100 nM PD173074 and 4 nM LGK-974 in N2B27 (B27 without vitamin A) media. After 24 h, the EBs were recovered and transferred to the same media but without chroman-1 and emricasan and embedded in Matrigel as previously described (Qian et al., 2018). Briefly, 66.7 µl of EBs and media were mixed with 100 µl of Matrigel using wide-bore tips. The mix was added to a non-adherent 6-well plate without touching the edges of the well and incubated at 37°C for 30 min. After 30 min, 3 ml of warm media were added on top. At day 2, the media was changed to plain N2B27 (B27 without vitamin A) with 100 ng/ml Fgf8b and kept for 48 h more. Day 4 EBs were recovered from Matrigel using cell recovery solution (Corning) and incubating for 30 min at 4°C. After day 4, the EBs were transferred to a Petri dish and kept in N2B27 (B27 supplement with vitamin A) with BDNF and GDNF while shaking at 65 rpm (Infors HT, Celltron benchtop shaker). For sparse labeling of neuronal progenitor cells with CytoTune EmGFP Sendai fluorescence reporter, 7.5 µl were added to the 2 ml media in the AggreWell plate at d0 and kept until d1. The organoids were then imaged for ∼24 h from d3 to d4.

Immunofluorescence staining of organoids

For organoid staining, the organoids were collected in tubes pre-coated with 1% BSA. The samples were washed twice with PBS-/- and fixed with 4% paraformaldehyde for 45 min at 4°C. Afterwards, they were washed twice with PBS-/- and permeabilized with 0.5% Triton X-100 for 15 min at 4°C. Blocking was performed for 15 min in organoid washing solution (OWS; adapted from Dekkers et al., 2019), consisting of 0.2% Triton X-100, 0.02% SDS and 0.2% BSA in PBS-/-) at 4°C. Next, the samples were incubated in OWS with primary antibodies overnight at 4°C. On the following day, they were washed three times for 2 h each with OWB while shaking, then incubated overnight at 4°C with secondary antibodies and DAPI (1 µM) in OWB. The next day, the organoids were washed three times with OWB for 6 h total while shaking. Finally, the organoids were mounted in DeepClear solution (CelExplorer Labs). The samples were imaged using a confocal Nikon A1RHD25 or Leica SP8 confocal microscope and analyzed with Imaris software. For live imaging, the organoids were embedded in phenol-free Matrigel and imaged using the TrueLive3D Imager system (Luxendo).

scRNA-seq

Multiple organoids were collected and mixed at d12, washed with PBS-/- and dissociated with Accutase until a single-cell suspension was achieved. Then, the sample was washed once again with PBS-/-. The resulting cell suspension was used for 10x scRNA-seq (10x Genomics, Single Cell 3′ Kit v3.1, dual index) following the manufacturer's directions; 326 M reads were obtained. The resulting fastq files were processed with Cell Ranger (10x genomics cloud). CellBender was used to eliminate background reads and

other artifacts (Fleming et al., 2019 preprint), and any cell with more than 10% mitochondrial reads was excluded. The Seurat package (v4) was used for downstream analyses (Hao et al., 2021). Cluster annotation was performed using the cited literature and the Allen Developing Mouse Brain Atlas, stages E15.5 and E18.5. VoxHunt analyses were performed as described by Fleck et al. (2021).

Acknowledgements
This study would not have been possible without the core facilities at MSKCC. We would like to specifically thank Dr Yas Furuta (Mouse Genetics Core facility, MSKCC), Murray Tipping and Vitaly Boyko (Molecular Cytology Core, MSKCC), Dr Richard Koche (Epigenetics Innovation Lab, MSKCC), and members of the Integrated Genomics Operation Core (MSKCC) for their advice and assistance with experiments and data analysis throughout the course of this project. In addition, we would like to thank Dr James Muller (Director of Developmental Biology Program's Microscope Cluster) for assistance with light-sheet microscopy and advance about imaging organoids and Dr Ronan Chaligne (Single Cell Research Initiative, MSKCC) for advice and assistance with single cell RNA-sequencing analysis. We would like to thank Dr Laura Reinholdt and Anne Czechanski (The Jackson Laboratory) for sharing PWK/PhJ ESC lines, Dr Christopher Baker and Dr Candice Byers (The Jackson Laboratory) for sharing C57Bl/6J ESC lines, and Dr Matthias Stadtfeld (Weill Cornell Medical College) for sharing B6129SF1/J ESC lines. We would like to thank our colleagues Dr Anna Katerina Hadjantonakis, Dr Danwei Huangfu, Dr Lorenz Studer, Dr Nan Yang, Dr Matthias Stadtfeld, Dr Eftychia Apostolou, Dr Sophie Morgani, Dr Clayton Schwarz, Dr Gabriele Ciceri, Dr Ryan Walsh, Bess Rosen (Huangfu Lab), Renhe Luo (Huangfu lab), Dapeng Yang (Huangfu Lab) for helpful discussions and advice throughout the course of the study. Figure panels 2C, 3F and 4A were created with BioRender.com. We would like to thank Dr Nan Yang (Mount Sinai), Dr Matthias Stadtfeld, Dr Timothy Cherry for helpful comments on the manuscript.

Competing interests
The authors declare no competing or financial interests.

Author contributions
Conceptualization: D.M.-C., E.K.C., T.V.; Methodology: D.M.-C., E.K.C., R.A.G., M.T.I., J.K., T.V.; Formal analysis: D.M.-C., E.K.C., R.A.G., M.T.I., H.C.; Investigation: D.M.-C., E.K.C., R.A.G., M.T.I., Y.L., J.K., T.V.; Resources: T.V.; Data curation: D.M.-C., E.K.C., T.V.; Writing - original draft: D.M.-C., E.K.C., R.A.G., T.V.; Writing - review & editing: D.M.-C., E.K.C., R.A.G., T.V.; Supervision: T.V.; Project administration: T.V.; Funding acquisition: T.V.

Funding
This study was made possible by financial support from: Startup funding from the Sloan Kettering Institute for Cancer Research (MSKCC) (T.V.) and the Josie Robertson Investigator Program (T.V.), a NARSAD Young Investigator Grant from the Brain & Behavior Research Foundation (28756 to T.V.), Tri-Institutional Stem Cell Initiative (Starr Foundation), and a training award from New York State Stem Cell Science (NYSTEM; contract number C32559GG) and the Center for Stem Cell Biology at MSKCC (D.M.-C.).

Data availability
Source data and processed files are available in the Gene expression Omnibus under the accession numbers GSE189869 (RNA and ATAC-seq datasets) and GSE189870 (scRNA-seq).

Peer review history
The peer review history is available online at https://journals.biologists.com/dev/article-lookup/doi/10.1242/dev.200561.

References
Arai, Y. and Taverna, E. (2017). Neural progenitor cell polarity and cortical development. *Front. Cell Neurosci.* **11**, 384. doi:10.3389/fncel.2017.00384

Bailey, T. L., Boden, M., Buske, F. A., Frith, M., Grant, C. E., Clementi, L., Ren, J., Li, W. W. and Noble, W. S. (2009). MEME SUITE: tools for motif discovery and searching. *Nucleic Acids Res.* **37**, W202-W208. doi:10.1093/nar/gkp335

Bernemann, C., Greber, B., Ko, K., Sterneckert, J., Han, D. W., Arauzo-Bravo, M. J. and Schöler, H. R. (2011). Distinct developmental ground states of epiblast stem cell lines determine different pluripotency features. *Stem Cells* **29**, 1496-1503. doi:10.1002/stem.709

Blauwkamp, T. A., Nigam, S., Ardehali, R., Weissman, I. L. and Nusse, R. (2012). Endogenous Wnt signalling in human embryonic stem cells generates an equilibrium of distinct lineage-specified progenitors. *Nat. Commun.* **3**, 1070. doi:10.1038/ncomms2064

Borowiak, M., Maehr, R., Chen, S., Chen, A. E., Tang, W., Fox, J. L., Schreiber, S. L. and Melton, D. A. (2009). Small molecules efficiently direct endodermal differentiation of mouse and human embryonic stem cells. *Cell Stem Cell* **4**, 348-358. doi:10.1016/j.stem.2009.01.014

Broda, T. R., McCracken, K. W. and Wells, J. M. (2019). Generation of human antral and fundic gastric organoids from pluripotent stem cells. *Nat. Protoc.* **14**, 28-50. doi:10.1038/s41596-018-0080-z

Brons, I. G., Smithers, L. E., Trotter, M. W., Rugg-Gunn, P., Sun, B., de Sousa Lopes, C., Howlett, S. M., Clarkson, S. K., Ahrlund-Richter, A., Pedersen, L. (2007). Derivation of pluripotent epiblast stem cells from mammalian embryos. *Nature* **448**, 191-195. doi:10.1038/nature05950

Buenrostro, J. D., Wu, B., Chang, H. Y. and Greenleaf, W. J. (2015). ATAC-seq: a method for assaying chromatin accessibility genome-wide. *Curr. Protoc. Mol. Biol.* **109**, 21.29.21-21.29.29. doi:10.1002/0471142727.mb2129s109

Caballero, I. M., Manuel, M. N., Molinek, M., Quintana-Urzainqui, I., Mi, D., Shimogori, T. and Price, D. J. (2014). Cell-autonomous repression of Shh by transcription factor Pax6 regulates diencephalic patterning by controlling the central diencephalic organizer. *Cell Rep.* **8**, 1405-1418. doi:10.1016/j.celrep.2014.07.051

Cadwell, C. R., Bhaduri, A., Mostajo-Radji, M. A., Keefe, M. G. and Nowakowski, T. J. (2019). Development and arealization of the cerebral cortex. *Neuron* **103**, 980-1004. doi:10.1016/j.neuron.2019.07.009

Chen, A. E., Borowiak, M., Sherwood, R. I., Kweudjeu, A. and Melton, D. A. (2013). Functional evaluation of ES cell-derived endodermal populations reveals differences between Nodal and Activin A-guided differentiation. *Development* **140**, 675-686. doi:10.1242/dev.085431

Chen, Y., Tristan, C. A., Chen, L., Jovanovic, V. M., Malley, C., Chu, P. H., Ryu, S., Deng, T., Ormanoglu, P., Tao, D. et al. (2021). A versatile polypharmacology platform promotes cytoprotection and viability of human pluripotent and differentiated cells. *Nat. Methods* **18**, 528-541. doi:10.1038/s41592-021-01126-2

Choi, J., Huebner, A. J., Clement, K., Walsh, R. M., Savol, A., Lin, K., Gu, H., Di Stefano, B., Brumbaugh, J., Kim, S. Y. et al. (2017). Prolonged Mek1/2 suppression impairs the developmental potential of embryonic stem cells. *Nature* **548**, 219-223. doi:10.1038/nature23274

Churchill, G. A., Gatti, D. M., Munger, S. C. and Svenson, K. L. (2012). The diversity outbred mouse population. *Mamm. Genome* **23**, 713-718. doi:10.1007/s00335-012-9414-2

Cornacchia, D., Zhang, C., Zimmer, B., Chung, S. Y., Fan, Y., Soliman, M. A., Tchieu, J., Chambers, S. M., Shah, H., Paull, D. et al. (2019). Lipid deprivation induces a stable, naive-to-primed intermediate state of pluripotency in human PSCs. *Cell Stem Cell* **25**, 120-136.e110. doi:10.1016/j.stem.2019.05.001

Czechanski, A., Byers, C., Greenstein, I., Schrode, N., Donahue, L. R., Hadjantonakis, A. K. and Reinholdt, L. G. (2014). Derivation and characterization of mouse embryonic stem cells from permissive and nonpermissive strains. *Nat. Protoc.* **9**, 559-574. doi:10.1038/nprot.2014.030

D'Amour, K. A., Agulnick, A. D., Eliazer, S., Kelly, O. G., Kroon, E. and Baetge, E. E. (2005). Efficient differentiation of human embryonic stem cells to definitive endoderm. *Nat. Biotechnol.* **23**, 1534-1541. doi:10.1038/nbt1163

Dekkers, J. F., Alieva, M., Wellens, L. M., Ariese, H. C. R., Jamieson, P. R., Vonk, A. M., Amatngalim, G. D., Hu, H., Oost, K. C., Snippert, H. J. G. et al. (2019). High-resolution 3D imaging of fixed and cleared organoids. *Nat. Protoc.* **14**, 1756-1771. doi:10.1038/s41596-019-0160-8

Diekmann, U., Wolling, H., Dettmer, R., Niwolik, I., Naujok, O. and Buettner, F. F. R. (2019). Chemically defined and xenogeneic-free differentiation of human pluripotent stem cells into definitive endoderm in 3D culture. *Sci. Rep.* **9**, 996. doi:10.1038/s41598-018-37650-z

Ebisuya, M. and Briscoe, J. (2018). What does time mean in development? *Development* **145**, dev164368. doi:10.1242/dev.164368

Edri, S., Hayward, P., Baillie-Johnson, P., Steventon, B. J. and Martinez Arias, A. (2019). An epiblast stem cell-derived multipotent progenitor population for axial extension. *Development* **146**, dev168187. doi:10.1242/dev.168187

Eiraku, M., Watanabe, K., Matsuo-Takasaki, M., Kawada, M., Yonemura, S., Matsumura, M., Wataya, T., Nishiyama, A., Muguruma, K. and Sasai, Y. (2008). Self-organized formation of polarized cortical tissues from ESCs and its active manipulation by extrinsic signals. *Cell Stem Cell* **3**, 519-532. doi:10.1016/j.stem.2008.09.002

Fleck, J. S., Sanchis-Calleja, F., He, Z., Santel, M., Boyle, M. J., Camp, J. G. and Treutlein, B. (2021). Resolving organoid brain region identities by mapping single-cell genomic data to reference atlases. *Cell Stem Cell* **28**, 1148-1159.e8. doi:10.1016/j.stem.2021.02.015

Fleming, S. J., Marioni, J. C. and Babadi, M. (2019). CellBender remove-background: a deep generative model for unsupervised removal of background noise from scRNA-seq datasets. *bioRxiv*. doi: 10.1101/791699

Fowler, J. L., Ang, L. T. and Loh, K. M. (2020). A critical look: challenges in differentiating human pluripotent stem cells into desired cell types and organoids. *Wiley Interdiscip. Rev. Dev. Biol.* **9**, e368. doi:10.1002/wdev.368

Gadue, P., Huber, T. L., Paddison, P. J. and Keller, G. M. (2006). Wnt and TGF-β signaling are required for the induction of an in vitro model of primitive streak

formation using embryonic stem cells. *Proc. Natl. Acad. Sci. USA* **103**, 16806-16811. doi:10.1073/pnas.0603916103
Garel, S., Huffman, K. J. and Rubenstein, J. L. (2003). Molecular regionalization of the neocortex is disrupted in Fgf8 hypomorphic mutants. *Development* **130**, 1903-1914. doi:10.1242/dev.00416
Gaspar, J. M. (2018). Improved peak-calling with MACS2. *bioRxiv*. doi:10.1101/496521
Genga, R. M. J., Kernfeld, E. M., Parsi, K. M., Parsons, T. J., Ziller, M. J. and Maehr, R. (2019). Single-cell RNA-Sequencing-based CRISPRi screening resolves molecular drivers of early human endoderm development. *Cell Rep.* **27**, 708-718.e10. doi:10.1016/j.celrep.2019.03.076
Grant, C. E., Bailey, T. L. and Noble, W. S. (2011). FIMO: scanning for occurrences of a given motif. *Bioinformatics* **27**, 1017-1018. doi:10.1093/bioinformatics/btr064
Greber, B., Wu, G., Bernemann, C., Joo, J. Y., Han, D. W., Ko, K., Tapia, N., Sabour, D., Sterneckert, J., Tesar, P. et al. (2010). Conserved and divergent roles of FGF signaling in mouse epiblast stem cells and human embryonic stem cells. *Cell Stem Cell* **6**, 215-226. doi:10.1016/j.stem.2010.01.003
Green, M. D., Chen, A., Nostro, M. C., d'Souza, S. L., Schaniel, C., Lemischka, I. R., Gouon-Evans, V., Keller, G. and Snoeck, H. W. (2011). Generation of anterior foregut endoderm from human embryonic and induced pluripotent stem cells. *Nat. Biotechnol.* **29**, 267-272. doi:10.1038/nbt.1788
Grove, E. A., Tole, S., Limon, J., Yip, L. and Ragsdale, C. W. (1998). The hem of the embryonic cerebral cortex is defined by the expression of multiple Wnt genes and is compromised in Gli3-deficient mice. *Development* **125**, 2315-2325. doi:10.1242/dev.125.12.2315
Guo, Q. and Li, J. Y. H. (2019). Defining developmental diversification of diencephalon neurons through single cell gene expression profiling. *Development* **146**. dev174284. doi:10.1242/dev.174284
Hadjantonakis, A. K., Siggia, E. D. and Simunovic, M. (2020). In vitro modeling of early mammalian embryogenesis. *Curr. Opin. Biomed. Eng.* **13**, 134-143. doi:10.1016/j.cobme.2020.02.003
Halliwell, J., Barbaric, I. and Andrews, P. W. (2020). Acquired genetic changes in human pluripotent stem cells: origins and consequences. *Nat. Rev. Mol. Cell Biol.* **21**, 715-728. doi:10.1038/s41580-020-00292-z
Hanashima, C., Fernandes, M., Hebert, J. M. and Fishell, G. (2007). The role of Foxg1 and dorsal midline signaling in the generation of Cajal-Retzius subtypes. *J. Neurosci.* **27**, 11103-11111. doi:10.1523/JNEUROSCI.1066-07.2007
Hao, Y., Hao, S., Andersen-Nissen, E., Mauck, W. M., 3rd, Zheng, S., Butler, A., Lee, M. J., Wilk, A. J., Darby, C., Zager, M. et al. (2021). Integrated analysis of multimodal single-cell data. *Cell* **184**, 3573-3587.e29. doi:10.1016/j.cell.2021.04.048
Hasenpusch-Theil, K., Magnani, D., Amaniti, E. M., Han, L., Armstrong, D. and Theil, T. (2012). Transcriptional analysis of Gli3 mutants identifies Wnt target genes in the developing hippocampus. *Cereb. Cortex* **22**, 2878-2893. doi:10.1093/cercor/bhr365
Hatami, M., Conrad, S., Naghsh, P., Alvarez-Bolado, G. and Skutella, T. (2018). Cell-biological requirements for the generation of dentate gyrus granule neurons. *Front. Cell Neurosci.* **12**, 402. doi:10.3389/fncel.2018.00402
Hayashi, K., Ohta, H., Kurimoto, K., Aramaki, S. and Saitou, M. (2011). Reconstitution of the mouse germ cell specification pathway in culture by pluripotent stem cells. *Cell* **146**, 519-532. doi:10.1016/j.cell.2011.06.052
Heinz, S., Benner, C., Spann, N., Bertolino, E., Lin, Y. C., Laslo, P., Cheng, J. X., Murre, C., Singh, H. and Glass, C. K. (2010). Simple combinations of lineage-determining transcription factors prime cis-regulatory elements required for macrophage and B cell identities. *Mol. Cell* **38**, 576-589. doi:10.1016/j.molcel.2010.05.004
Huch, M., Knoblich, J. A., Lutolf, M. P. and Martinez-Arias, A. (2017). The hope and the hype of organoid research. *Development* **144**, 938-941. doi:10.1242/dev.150201
Jouneau, A. (2019). Heterogeneity in epiblast stem cells. *Adv. Exp. Med. Biol.* **1123**, 5-17. doi:10.1007/978-3-030-11096-3_2
Kalkan, T., Olova, N., Roode, M., Mulas, C., Lee, H. J., Nett, I., Marks, H., Walker, R., Stunnenberg, H. G., Lilley, K. S. et al. (2017). Tracking the embryonic stem cell transition from ground state pluripotency. *Development* **144**, 1221-1234. doi: 10.1242/dev.14271
Kessaris, N., Fogarty, M., Iannarelli, P., Grist, M., Wegner, M. and Richardson, W. D. (2006). Competing waves of oligodendrocytes in the forebrain and postnatal elimination of an embryonic lineage. *Nat. Neurosci.* **9**, 173-179. doi:10.1038/nn1620
Kim, D. W., Washington, P. W., Wang, Z. Q., Lin, S. H., Sun, C., Ismail, B. T., Wang, H., Jiang, L. and Blackshaw, S. (2020). The cellular and molecular landscape of hypothalamic patterning and differentiation from embryonic to late postnatal development. *Nat. Commun.* **11**, 4360. doi:10.1038/s41467-020-18231-z
Kinoshita, M., Barber, M., Mansfield, W., Cui, Y., Spindlow, D., Stirparo, G. G., Dietmann, S., Nichols, J. and Smith, A. (2021). Capture of mouse and human stem cells with features of formative pluripotency. *Cell Stem Cell* **28**, 453-471.e8. doi:10.1016/j.stem.2020.11.005
Kleiman, R. J. and Engle, S. J. (2021). Human inducible pluripotent stem cells: realization of initial promise in drug discovery. *Cell Stem Cell* **28**, 1507-1515. doi:10.1016/j.stem.2021.08.002
Kojima, Y., Kaufman-Francis, K., Studdert, J. B., Steiner, K. A., Power, M. D., Loebel, D. A., Jones, V., Hor, A., de Alencastro, G., Logan, G. J. et al. (2014). The transcriptional and functional properties of mouse epiblast stem cells resemble the anterior primitive streak. *Cell Stem Cell* **14**, 107-120. doi:10.1016/j.stem.2013.09.014
Korostylev, A., Mahaddalkar, P. U., Keminer, O., Hadian, K., Schorpp, K., Gribbon, P. and Lickert, H. (2017). A high-content small molecule screen identifies novel inducers of definitive endoderm. *Mol. Metab.* **6**, 640-650. doi:10.1016/j.molmet.2017.04.009
Kurek, D., Neagu, A., Tastemel, M., Tuysuz, N., Lehmann, J., van de Werken, H. J. G., Philipsen, S., van der Linden, R., Maas, A., van Ijcken, W. F. J. et al. (2015). Endogenous WNT signals mediate BMP-induced and spontaneous differentiation of epiblast stem cells and human embryonic stem cells. *Stem Cell Rep.* **4**, 114-128. doi:10.1016/j.stemcr.2014.11.007
Lancaster, M. A., Renner, M., Martin, C. A., Wenzel, D., Bicknell, L. S., Hurles, M. E., Homfray, T., Penninger, J. M., Jackson, A. P. and Knoblich, J. A. (2013). Cerebral organoids model human brain development and microcephaly. *Nature* **501**, 373-379. doi:10.1038/nature12517
Langmead, B. and Salzberg, S. L. (2012). Fast gapped-read alignment with Bowtie 2. *Nat. Methods* **9**, 357-359. doi:10.1038/nmeth.1923
Li, F., He, Z., Li, Y., Liu, P., Chen, F., Wang, M., Zhu, H., Ding, X., Wangensteen, K. J., Hu, Y. et al. (2011). Combined activin A/LiCl/Noggin treatment improves production of mouse embryonic stem cell-derived definitive endoderm cells. *J. Cell. Biochem.* **112**, 1022-1034. doi:10.1002/jcb.22962
Li, L.-C., Qiu, W. L., Zhang, Y. W., Xu, Z. R., Xiao, Y. N., Hou, C., Lamaoqiezhong, Yu, P., Cheng, X., and Xu, C. R. (2018). Single-cell transcriptomic analyses reveal distinct dorsal/ventral pancreatic programs. *EMBO Rep.* **19**, e46148. doi:10.15252/embr.201846148
Li, Q. V., Dixon, G., Verma, N., Rosen, B. P., Gordillo, M., Luo, R., Xu, C., Wang, Q., Soh, C. L., Yang, D. et al. (2019). Genome-scale screens identify JNK-JUN signaling as a barrier for pluripotency exit and endoderm differentiation. *Nat. Genet.* **51**, 999-1010. doi:10.1038/s41588-019-0408-9
Li, Y., Lopez-Huerta, V. G., Adiconis, X., Levandowski, K., Choi, S., Simmons, S. K., Arias-Garcia, M. A., Guo, B., Yao, A. Y., Blosser, T. R. et al. (2020). Distinct subnetworks of the thalamic reticular nucleus. *Nature* **583**, 819-824. doi:10.1038/s41586-020-2504-5
Liao, Y., Smyth, G. K. and Shi, W. (2014). featureCounts: an efficient general purpose program for assigning sequence reads to genomic features. *Bioinformatics* **30**, 923-930. doi:10.1093/bioinformatics/btt656
Loh, K. M., Ang, L. T., Zhang, J., Kumar, V., Ang, J., Auyeong, J. Q., Lee, K. L., Choo, S. H., Lim, C. Y., Nichane, M. et al. (2014). Efficient endoderm induction from human pluripotent stem cells by logically directing signals controlling lineage bifurcations. *Cell Stem Cell* **14**, 237-252. doi:10.1016/j.stem.2013.12.007
Loh, K. M., Chen, A., Koh, P. W., Deng, T. Z., Sinha, R., Tsai, J. M., Barkal, A. A., Shen, K. Y., Jain, R., Morganti, R. M. et al. (2016). Mapping the pairwise choices leading from pluripotency to human bone, heart, and other mesoderm cell types. *Cell* **166**, 451-467. doi:10.1016/j.cell.2016.06.011
Love, M. I., Huber, W. and Anders, S. (2014). Moderated estimation of fold change and dispersion for RNA-seq data with DESeq2. *Genome Biol.* **15**, 550. doi:10.1186/s13059-014-0550-8
Mandai, K., Reimert, D. V. and Ginty, D. D. (2014). Linx mediates interaxonal interactions and formation of the internal capsule. *Neuron* **83**, 93-103. doi:10.1016/j.neuron.2014.05.020
Manuel, M. N., Mi, D., Mason, J. O. and Price, D. J. (2015). Regulation of cerebral cortical neurogenesis by the Pax6 transcription factor. *Front. Cell Neurosci.* **9**, 70. doi:10.3389/fncel.2015.00070
Marini, F. and Binder, H. (2019). pcaExplorer: an R/Bioconductor package for interacting with RNA-seq principal components. *BMC Bioinform.* **20**, 331. doi:10.1186/s12859-019-2879-1
Martinez-Ferre, A. and Martinez, S. (2009). The development of the thalamic motor learning area is regulated by Fgf8 expression. *J. Neurosci.* **29**, 13389-13400. doi:10.1523/JNEUROSCI.2625-09.2009
McCracken, K. W., Cata, E. M., Crawford, C. M., Sinagoga, K. L., Schumacher, M., Rockich, B. E., Tsai, Y. H., Mayhew, C. N., Spence, J. R., Zavros, Y. et al. (2014). Modelling human development and disease in pluripotent stem-cell-derived gastric organoids. *Nature* **516**, 400-404. doi:10.1038/nature13863
Mezger, A., Klemm, S., Mann, I., Brower, K., Mir, A., Bostick, M., Farmer, A., Fordyce, P., Linnarsson, S. and Greenleaf, W. (2018). High-throughput chromatin accessibility profiling at single-cell resolution. *Nat. Commun.* **9**, 3647. doi:10.1038/s41467-018-05887-x
Mfopou, J. K., Geeraerts, M., Dejene, R., Van Langenhoven, S., Aberkane, A., Van Grunsven, L. A. and Bouwens, L. (2014). Efficient definitive endoderm induction from mouse embryonic stem cell adherent cultures: a rapid screening model for differentiation studies. *Stem Cell Res.* **12**, 166-177. doi:10.1016/j.scr.2013.10.004

Molnar, Z., Garel, S., López-Bendito, G., Maness, P. and Price, D. J. (2012). Mechanisms controlling the guidance of thalamocortical axons through the embryonic forebrain. *Eur. J. Neurosci.* **35**, 1573-1585. doi:10.1111/j.1460-9568.2012.08119.x

Montiel, J. F. and Aboitiz, F. (2015). Pallial patterning and the origin of the isocortex. *Front. Neurosci.* **9**, 377. doi:10.3389/fnins.2015.00377

Morgani, S., Nichols, J. and Hadjantonakis, A. K. (2017). The many faces of pluripotency: in vitro adaptations of a continuum of in vivo states. *BMC Dev. Biol.* **17**, 7. doi:10.1186/s12861-017-0150-4

Morgani, S. M., Metzger, J. J., Nichols, J., Siggia, E. D. and Hadjantonakis, A. K. (2018). Micropattern differentiation of mouse pluripotent stem cells recapitulates embryo regionalized cell fate patterning. *Elife* **7**, e32839. doi:10.7554/eLife.32839

Moris, N., Martinez Arias, A. and Steventon, B. (2020). Experimental embryology of gastrulation: pluripotent stem cells as a new model system. *Curr. Opin. Genet. Dev.* **64**, 78-83. doi:10.1016/j.gde.2020.05.031

Morrison, G. M., Oikonomopoulou, I., Migueles, R. P., Soneji, S., Livigni, A., Enver, T. and Brickman, J. M. (2008). Anterior definitive endoderm from ESCs reveals a role for FGF signaling. *Cell Stem Cell* **3**, 402-415. doi:10.1016/j.stem.2008.07.021

Morrison, G., Scognamiglio, R., Trumpp, A. and Smith, A. (2016). Convergence of cMyc and β-catenin on Tcf7l1 enables endoderm specification. *EMBO J.* **35**, 356-368. doi:10.15252/embj.201592116

Mou, H., Zhao, R., Sherwood, R., Ahfeldt, T., Lapey, A., Wain, J., Sicilian, L., Izvolsky, K., Musunuru, K., Cowan, C. et al. (2012). Generation of multipotent lung and airway progenitors from mouse ESCs and patient-specific cystic fibrosis iPSCs. *Cell Stem Cell* **10**, 385-397. doi:10.1016/j.stem.2012.01.018

Mulas, C., Kalkan, T. and Smith, A. (2017). NODAL secures pluripotency upon embryonic stem cell progression from the ground state. *Stem Cell Rep.* **9**, 77-91. doi:10.1016/j.stemcr.2017.05.033

Nagalski, A., Puelles, L., Dabrowski, M., Wegierski, T., Kuznicki, J. and Wisniewska, M. B. (2016). Molecular anatomy of the thalamic complex and the underlying transcription factors. *Brain Struct. Funct.* **221**, 2493-2510. doi:10.1007/s00429-015-1052-5

Najm, F. J., Zaremba, A., Caprariello, A. V., Nayak, S., Freundt, E. C., Scacheri, P. C., Miller, R. H. and Tesar, P. J. (2011). Rapid and robust generation of functional oligodendrocyte progenitor cells from epiblast stem cells. *Nat. Methods* **8**, 957-962. doi:10.1038/nmeth.1712

Nasu, M., Takata, N., Danjo, T., Sakaguchi, H., Kadoshima, T., Futaki, S., Sekiguchi, K., Eiraku, M. and Sasai, Y. (2012). Robust formation and maintenance of continuous stratified cortical neuroepithelium by laminin-containing matrix in mouse ES cell culture. *PLoS One* **7**, e53024. doi:10.1371/journal.pone.0053024

Nichols, J. and Smith, A. (2012). Pluripotency in the embryo and in culture. *Cold Spring Harb. Perspect. Biol.* **4**, a008128. doi:10.1101/cshperspect.a008128

Noctor, S. C., Martínez-Cerdeño, V., Ivic, L. and Kriegstein, A. R. (2004). Cortical neurons arise in symmetric and asymmetric division zones and migrate through specific phases. *Nat. Neurosci.* **7**, 136-144. doi:10.1038/nn1172

Nowotschin, S., Setty, M., Kuo, Y.-Y., Liu, V., Garg, V., Sharma, R., Simon, C. S., Saiz, N., Gardner, R., Boutet, S. C. et al. (2019). The emergent landscape of the mouse gut endoderm at single-cell resolution. *Nature* **569**, 361-367. doi:10.1038/s41586-019-1127-1

Ono, K., Clavairoly, A., Nomura, T., Gotoh, H., Uno, A., Armant, O., Takebayashi, H., Zhang, Q., Shimamura, K., Itohara, S. et al. (2014). Development of the prethalamus is crucial for thalamocortical projection formation and is regulated by Olig2. *Development* **141**, 2075-2084. doi:10.1242/dev.097790

Ortmann, D., Brown, S., Czechanski, A., Aydin, S., Muraro, D., Huang, Y., Tomaz, R. A., Osnato, A., Canu, G., Wesley, B. T. et al. (2020). Naive pluripotent stem cells exhibit phenotypic variability that is driven by genetic variation. *Cell Stem Cell* **27**, 470-481.e6. doi:10.1016/j.stem.2020.07.019

Patro, R., Duggal, G., Love, M. I., Irizarry, R. A. and Kingsford, C. (2017). Salmon provides fast and bias-aware quantification of transcript expression. *Nat. Methods* **14**, 417-419. doi:10.1038/nmeth.4197

Puelles, L., Kuwana, E., Puelles, E., Bulfone, A., Shimamura, K., Keleher, J., Smiga, S. and Rubenstein, J. L. (2000). Pallial and subpallial derivatives in the embryonic chick and mouse telencephalon, traced by the expression of the genes Dlx-2, Emx-1, Nkx-2.1, Pax-6, and Tbr-1. *J. Comp. Neurol.* **424**, 409-438. doi:10.1002/1096-9861(20000828)424:3<409::AID-CNE3>3.0.CO;2-7

Puelles, L., Harrison, M., Paxinos, G. and Watson, C. (2013). A developmental ontology for the mammalian brain based on the prosomeric model. *Trends Neurosci.* **36**, 570-578. doi:10.1016/j.tins.2013.06.004

Qian, X., Davis, A. A., Goderie, S. K. and Temple, S. (1997). FGF2 concentration regulates the generation of neurons and glia from multipotent cortical stem cells. *Neuron* **18**, 81-93. doi:10.1016/S0896-6273(01)80048-9

Qian, X., Jacob, F., Song, M. M., Nguyen, H. N., Song, H. and Ming, G.-L. (2018). Generation of human brain region-specific organoids using a miniaturized spinning bioreactor. *Nat. Protoc.* **13**, 565-580. doi:10.1038/nprot.2017.152

Quintana-Urzainqui, I., Hernandez-Malmierca, P., Clegg, J. M., Li, Z., Kozic, Z. and Price, D. J. (2020). The role of the diencephalon in the guidance of thalamocortical axons in mice. *Development* **147**. dev184523. doi:10.1242/dev.184523

Renner, M., Lancaster, M. A., Bian, S., Choi, H., Ku, T., Peer, A., Chung, K. and Knoblich, J. A. (2017). Self-organized developmental patterning and differentiation in cerebral organoids. *EMBO J.* **36**, 1316-1329. doi:10.15252/embj.201694700

Rifes, P., Isaksson, M., Rathore, G. S., Aldrin-Kirk, P., Moller, O. K., Barzaghi, G., Lee, J., Egerod, K. L., Rausch, D. M., Parmar, M. et al. (2020). Modeling neural tube development by differentiation of human embryonic stem cells in a microfluidic WNT gradient. *Nat. Biotechnol.* **38**, 1265-1273. doi:10.1038/s41587-020-0525-0

Rossant, J. and Tam, P. P. L. (2017). New insights into early human development: lessons for stem cell derivation and differentiation. *Cell Stem Cell* **20**, 18-28. doi:10.1016/j.stem.2016.12.004

Schlissel, G. and Li, P. (2020). Synthetic developmental biology: understanding through reconstitution. *Annu. Rev. Cell Dev. Biol.* **36**, 339-357. doi:10.1146/annurev-cellbio-020620-090650

Sestan, N. and State, M. W. (2018). Lost in translation: traversing the complex path from genomics to therapeutics in autism spectrum disorder. *Neuron* **100**, 406-423. doi:10.1016/j.neuron.2018.10.015

Sherwood, R. I., Maehr, R., Mazzoni, E. O. and Melton, D. A. (2011). Wnt signaling specifies and patterns intestinal endoderm. *Mech. Dev.* **128**, 387-400. doi:10.1016/j.mod.2011.07.005

Shi, Z. D., Lee, K., Yang, D., Amin, S., Verma, N., Li, Q. V., Zhu, Z., Soh, C. L., Kumar, R., Evans, T. et al. (2017). Genome editing in hPSCs reveals GATA6 haploinsufficiency and a genetic interaction with GATA4 in human pancreatic development. *Cell Stem Cell* **20**, 675-688.e6. doi:10.1016/j.stem.2017.01.001

Shimamura, K. and Rubenstein, J. L. (1997). Inductive interactions direct early regionalization of the mouse forebrain. *Development* **124**, 2709-2718. doi:10.1242/dev.124.14.2709

Shiraishi, A., Muguruma, K. and Sasai, Y. (2017). Generation of thalamic neurons from mouse embryonic stem cells. *Development* **144**, 1211-1220. doi:10.1242/dev.144071

Shultz, M. D., Cheung, A. K., Kirby, C. A., Firestone, B., Fan, J., Chen, C. H.-T., Chen, Z., Chin, D. N., Dipietro, L., Fazal, A. et al. (2013). Identification of NVP-TNKS656: the use of structure-efficiency relationships to generate a highly potent, selective, and orally active tankyrase inhibitor. *J. Med. Chem.* **56**, 6495-6511. doi:10.1021/jm400807n

Simon, R., Brylka, H., Schwegler, H., Venkataramanappa, S., Andratschke, J., Wiegreffe, C., Liu, P., Fuchs, E., Jenkins, N. A., Copeland, N. G. et al. (2012). A dual function of Bcl11b/Ctip2 in hippocampal neurogenesis. *EMBO J.* **31**, 2922-2936. doi:10.1038/emboj.2012.142

Skelly, D. A., Czechanski, A., Byers, C., Aydin, S., Spruce, C., Olivier, C., Choi, K., Gatti, D. M., Raghupathy, N., Keele, G. R. et al. (2020). Mapping the effects of genetic variation on chromatin state and gene expression reveals loci that control ground state pluripotency. *Cell Stem Cell* **27**, 459-469.e8. doi:10.1016/j.stem.2020.07.005

Smith, A. (2017). Formative pluripotency: the executive phase in a developmental continuum. *Development* **144**, 365-373. doi:10.1242/dev.142679

Sommer, L., Rao, M. and Anderson, D. J. (1997). RPTPδ and the novel protein tyrosine phosphatase RPTPΨ are expressed in restricted regions of the developing central nervous system. *Dev. Dyn.* **208**, 48-61. doi:10.1002/(SICI)1097-0177(199701)208:1<48::AID-AJA5>3.0.CO;2-1

Song, L., Chen, J., Peng, G., Tang, K. and Jing, N. (2016). Dynamic heterogeneity of Brachyury in mouse epiblast stem cells mediates distinct response to extrinsic bone morphogenetic protein (BMP) signaling. *J. Biol. Chem.* **291**, 15212-15225. doi:10.1074/jbc.M115.705418

Storm, E. E., Garel, S., Borello, U., Hebert, J. M., Martinez, S., McConnell, S. K., Martin, G. R. and Rubenstein, J. L. (2006). Dose-dependent functions of Fgf8 in regulating telencephalic patterning centers. *Development* **133**, 1831-1844. doi:10.1242/dev.02324

Strawbridge, S. E., Blanchard, G. B., Smith, A., Kugler, H. and Martello, G. (2020). Embryonic stem cells commit to differentiation by symmetric divisions following a variable lag period. *bioRxiv*. doi:10.1101/2020.06.17.157578

Sumi, T., Oki, S., Kitajima, K. and Meno, C. (2013). Epiblast ground state is controlled by canonical Wnt/β-catenin signaling in the postimplantation mouse embryo and epiblast stem cells. *PLoS One* **8**, e63378. doi:10.1371/journal.pone.0063378

Takata, N., Sakakura, E., Eiraku, M., Kasukawa, T. and Sasai, Y. (2017). Self-patterning of rostral-caudal neuroectoderm requires dual role of Fgf signaling for localized Wnt antagonism. *Nat. Commun.* **8**, 1339. doi:10.1038/s41467-017-01105-2

Takiguchi-Hayashi, K., Sekiguchi, M., Ashigaki, S., Takamatsu, M., Hasegawa, H., Suzuki-Migishima, R., Yokoyama, M., Nakanishi, S. and Tanabe, Y. (2004). Generation of reelin-positive marginal zone cells from the caudomedial wall of telencephalic vesicles. *J. Neurosci.* **24**, 2286-2295. doi:10.1523/JNEUROSCI.4671-03.2004

Tchieu, J., Zimmer, B., Fattahi, F., Amin, S., Zeltner, N., Chen, S. and Studer, L. (2017). A modular platform for differentiation of human PSCs into all major

ectodermal lineages. *Cell Stem Cell* **21**, 399-410.e7. doi:10.1016/j.stem.2017.08.015

Tekki-Kessaris, N., Woodruff, R., Hall, A. C., Gaffield, W., Kimura, S., Stiles, C. D., Rowitch, D. H. and Richardson, W. D. (2001). Hedgehog-dependent oligodendrocyte lineage specification in the telencephalon. *Development* **128**, 2545-2554. doi:10.1242/dev.128.13.2545

Tesar, P. J., Chenoweth, J. G., Brook, F. A., Davies, T. J., Evans, E. P., Mack, D. L., Gardner, R. L. and McKay, R. D. (2007). New cell lines from mouse epiblast share defining features with human embryonic stem cells. *Nature* **448**, 196-199. doi:10.1038/nature05972

Thompson, C. L., Ng, L., Menon, V., Martinez, S., Lee, C. K., Glattfelder, K., Sunkin, S. M., Henry, A., Lau, C., Dang, C. et al. (2014). A high-resolution spatiotemporal atlas of gene expression of the developing mouse brain. *Neuron* **83**, 309-323. doi:10.1016/j.neuron.2014.05.033

Tsakiridis, A., Huang, Y., Blin, G., Skylaki, S., Wymeersch, F., Osorno, R., Economou, C., Karagianni, E., Zhao, S., Lowell, S. et al. (2014). Distinct Wnt-driven primitive streak-like populations reflect in vivo lineage precursors. *Development* **141**, 1209-1221. doi:10.1242/dev.101014

Tuttle, R., Nakagawa, Y., Johnson, J. E. and O'Leary, D. D. (1999). Defects in thalamocortical axon pathfinding correlate with altered cell domains in Mash-1-deficient mice. *Development* **126**, 1903-1916. doi:10.1242/dev.126.9.1903

Vallier, L., Touboul, T., Chng, Z., Brimpari, M., Hannan, N., Millan, E., Smithers, L. E., Trotter, M., Rugg-Gunn, P., Weber, A. et al. (2009). Early cell fate decisions of human embryonic stem cells and mouse epiblast stem cells are controlled by the same signalling pathways. *PLoS One* **4**, e6082. doi:10.1371/journal.pone.0006082

Vieira, C., Pombero, A., Garcia-Lopez, R., Gimeno, L., Echevarria, D. and Martinez, S. (2010). Molecular mechanisms controlling brain development: an overview of neuroepithelial secondary organizers. *Int. J. Dev. Biol.* **54**, 7-20. doi:10.1387/ijdb.092853cv

Virolainen, S.-M., Achim, K., Peltopuro, P., Salminen, M. and Partanen, J. (2012). Transcriptional regulatory mechanisms underlying the GABAergic neuron fate in different diencephalic prosomeres. *Development* **139**, 3795-3805. doi:10.1242/dev.075192

Voelkl, B., Altman, N. S., Forsman, A., Forstmeier, W., Gurevitch, J., Jaric, I., Karp, N. A., Kas, M. J., Schielzeth, H., Van de Casteele, T. et al. (2020). Reproducibility of animal research in light of biological variation. *Nat. Rev. Neurosci.* **21**, 384-393. doi:10.1038/s41583-020-0313-3

Watanabe, M., Haney, J. R., Vishlaghi, N., Turcios, F., Buth, J. E., Gu, W., Collier, A. J., Miranda, O. A., Chen, D., Sabri, S. et al. (2019). TGFβ superfamily signaling regulates the state of human stem cell pluripotency and competency to create telencephalic organoids. *bioRxiv*. doi:10.1101/2019.12.13.875773

Wataya, T., Ando, S., Muguruma, K., Ikeda, H., Watanabe, K., Eiraku, M., Kawada, M., Takahashi, J., Hashimoto, N. and Sasai, Y. (2008). Minimization of exogenous signals in ES cell culture induces rostral hypothalamic differentiation. *Proc. Natl. Acad. Sci. USA* **105**, 11796-11801. doi:10.1073/pnas.0803078105

Weirauch, M. T., Yang, A., Albu, M., Cote, A. G., Montenegro-Montero, A., Drewe, P., Najafabadi, H. S., Lambert, S. A., Mann, I., Cook, K. et al. (2014). Determination and inference of eukaryotic transcription factor sequence specificity. *Cell* **158**, 1431-1443. doi:10.1016/j.cell.2014.08.009

Wu, J., Okamura, D., Li, M., Suzuki, K., Luo, C., Ma, L., He, Y., Li, Z., Benner, C., Tamura, I. et al. (2015). An alternative pluripotent state confers interspecies chimaeric competency. *Nature* **521**, 316-321. doi:10.1038/nature14413

Xiang, Y., Tanaka, Y., Cakir, B., Patterson, B., Kim, K.-Y., Sun, P., Kang, Y.-J., Zhong, M., Liu, X., Patra, P. et al. (2019). hESC-derived thalamic organoids form reciprocal projections when fused with cortical organoids. *Cell Stem Cell* **24**, 487-497.e7. doi:10.1016/j.stem.2018.12.015

Xiang, Y., Zhang, Y., Xu, Q., Zhou, C., Liu, B., Du, Z., Zhang, K., Zhang, B., Wang, X., Gayen, S. et al. (2020). Epigenomic analysis of gastrulation identifies a unique chromatin state for primed pluripotency. *Nat. Genet.* **52**, 95-105. doi:10.1038/s41588-019-0545-1

Yagi, M., Kishigami, S., Tanaka, A., Semi, K., Mizutani, E., Wakayama, S., Wakayama, T., Yamamoto, T. and Yamada, Y. (2017). Derivation of ground-state female ES cells maintaining gamete-derived DNA methylation. *Nature* **548**, 224-227. doi:10.1038/nature23286

Yiangou, L., Ross, A. D. B., Goh, K. J. and Vallier, L. (2018). Human pluripotent stem cell-derived endoderm for modeling development and clinical applications. *Cell Stem Cell* **22**, 485-499. doi:10.1016/j.stem.2018.03.016

Ying, Q. L., Wray, J., Nichols, J., Batlle-Morera, L., Doble, B., Woodgett, J., Cohen, P. and Smith, A. (2008). The ground state of embryonic stem cell self-renewal. *Nature* **453**, 519-523. doi:10.1038/nature06968

Yu, L., Wei, Y., Sun, H. X., Mahdi, A. K., Pinzon Arteaga, C. A., Sakurai, M., Schmitz, D. A., Zheng, C., Ballard, E. D., Li, J. et al. (2021). Derivation of intermediate pluripotent stem cells amenable to primordial germ cell specification. *Cell Stem Cell* **28**, 550-567.e12. doi:10.1016/j.stem.2020.11.003

Zorn, A. M. and Wells, J. M. (2009). Vertebrate endoderm development and organ formation. *Annu. Rev. Cell Dev. Biol.* **25**, 221-251. doi:10.1146/annurev.cellbio.042308.113344

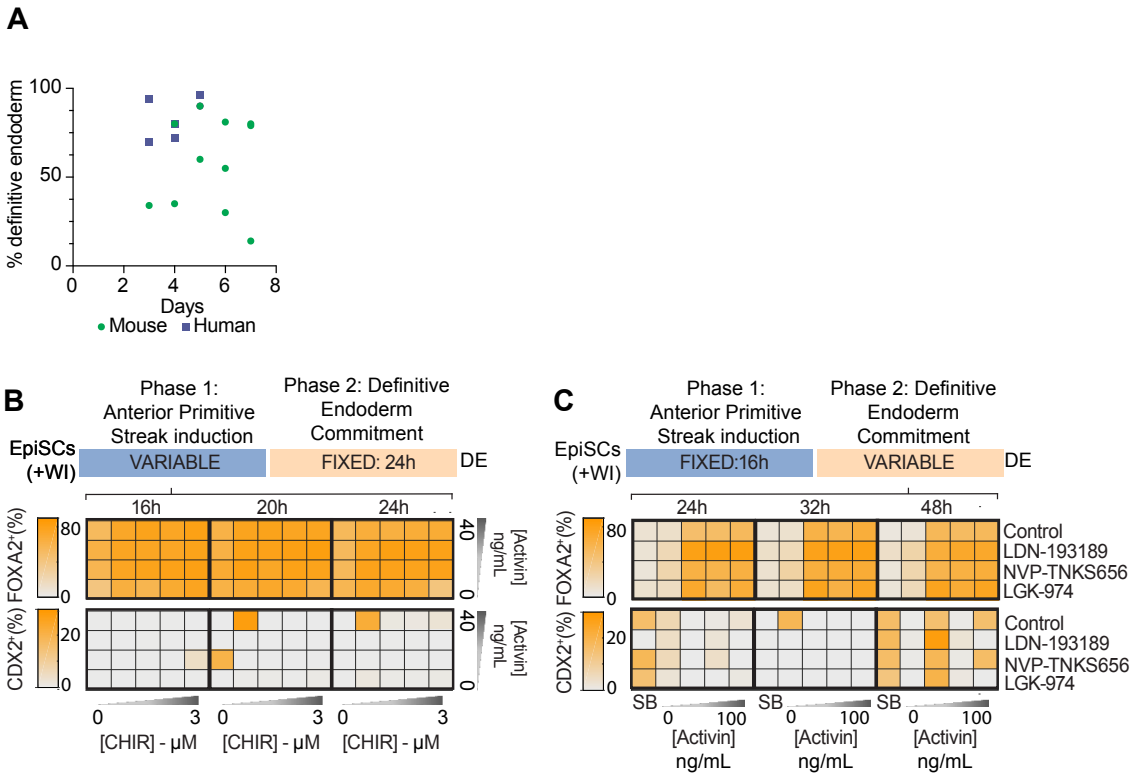

Fig. S1. Systematic optimization of conditions for EpiSC-DE differentiation. (**A**) Overview of state-of-the-art differentiation protocols for human (purple) and mouse (green) PSCs. Further details of each study are provided in **Supplementary Table 1**). (**B-C**) Results of DE protocol optimization experiments. For each condition, immunofluorescence staining was performed following 40 h of differentiation (end of Stage 2). Immunofluorescence images for the indicated antibodies were quantified using CellProfiler. Markers of DE (FOXA2) and mesoderm (CDX2) are shown. (**B**) Summary of results from anterior primitive streak (Stage 1) optimization experiments (n=2 technical replicates). After the indicated conditions for Stage 1, all conditions were exposed to the same Stage 2 conditions, and then quantified. (**C**) Summary of results for optimization of DE commitment (Stage 2) conditions (n=2 technical replicates). For Stage 1, the optimal conditions identified in (**B**) were used, and then cells were switched into the indicated conditions for Stage 2.

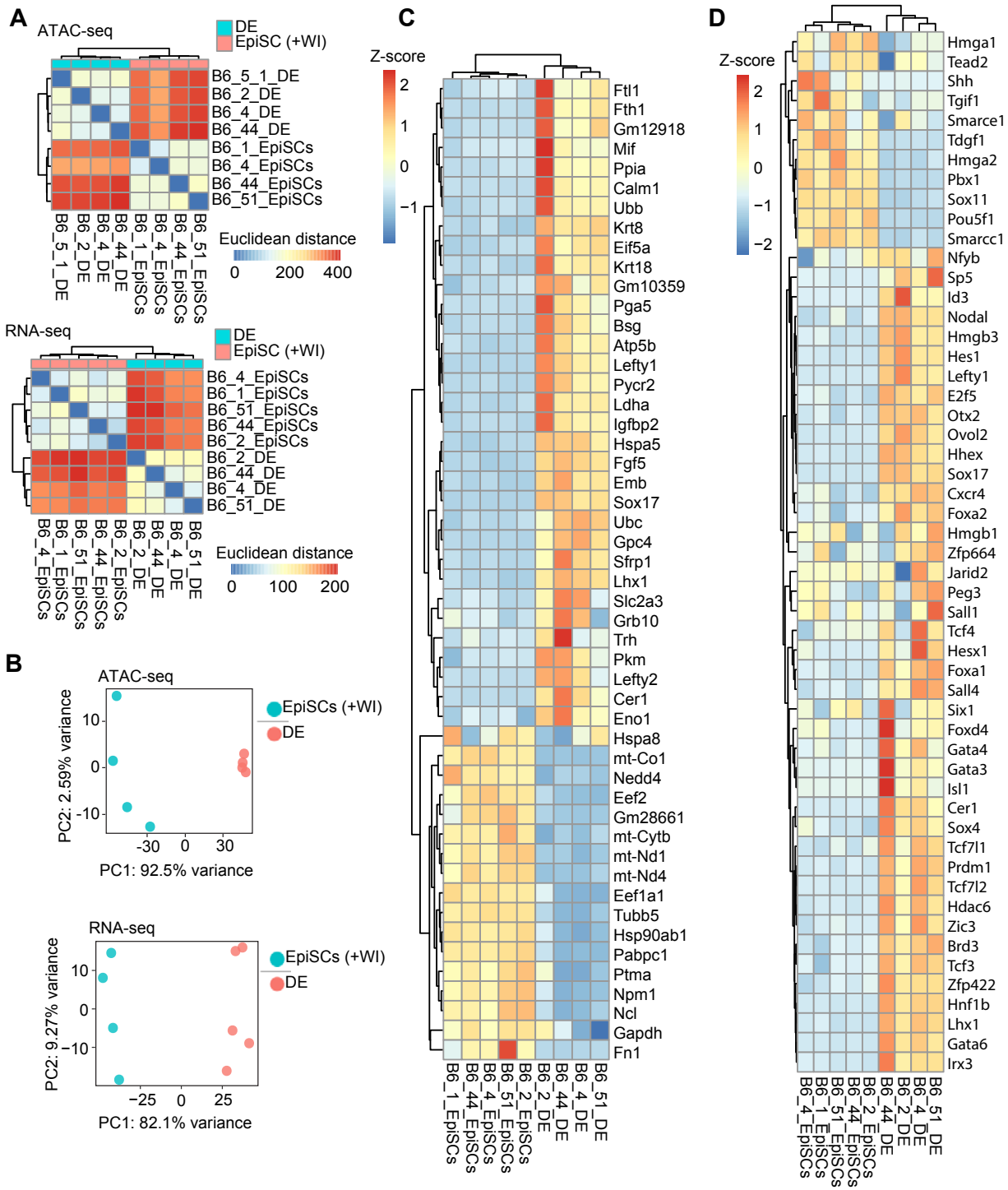

Fig. S2. Extended characterization of EpiSC-derived definitive endoderm. (**A**) Euclidean distance between samples based on ATAC-seq (n=4 per condition, left) and RNA-seq (n=5 for EpiSCs and n=4 for MACs-sorted DE samples, right). (**B**) PCA plot of bulk chromatin accessibility (left) and gene expression (right) of the same C57Bl/6J EpiSC and DE samples as (**A**). (**C**) Unbiased clustered heatmap of the top variable genes as detected by RNA-seq. (**D**) Expression of genes previously identified as DE markers in single cell gene expression studies of hPSC-derived DE and DE isolated from E7.0 embryos (Genga et al., 2019; Nowotschin et al., 2019).

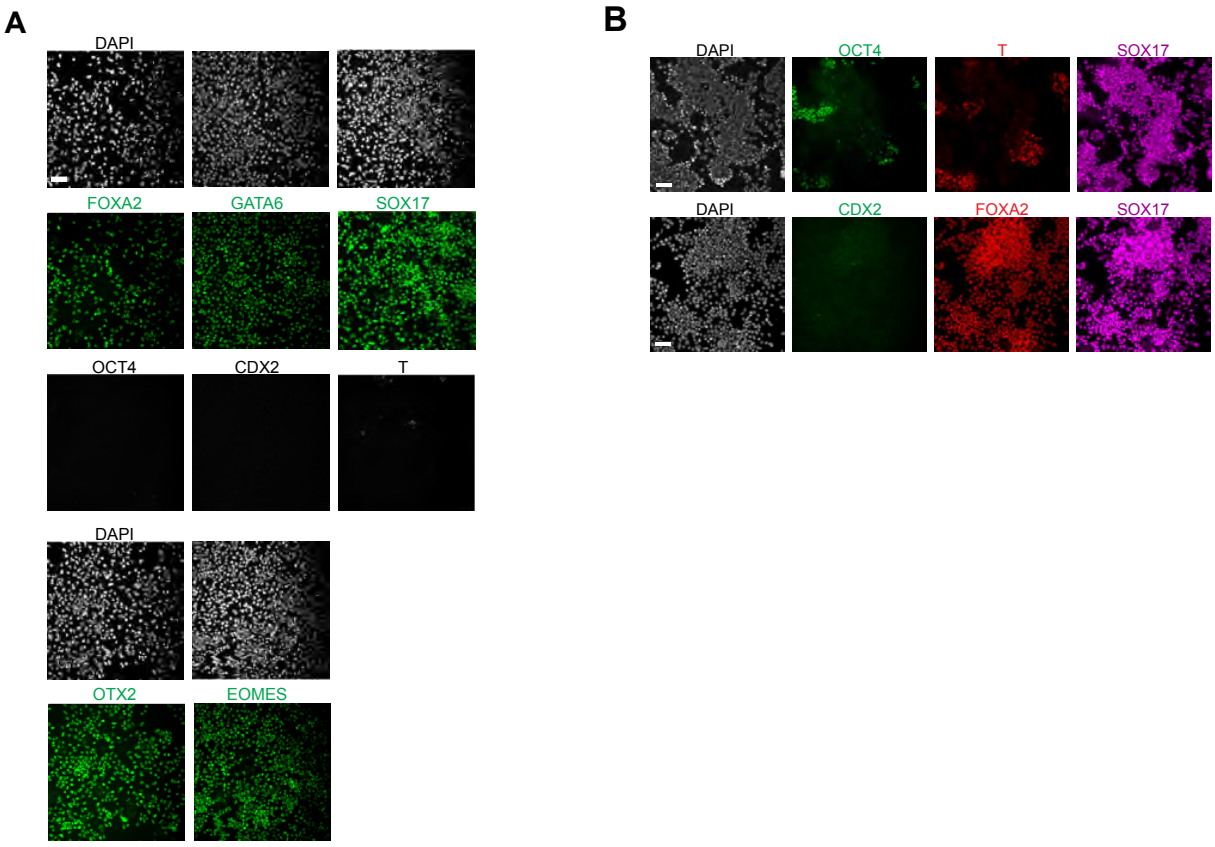

Fig. S3. Immunostainings of EpiSC-derived definitive endoderm. (**A**) Representative immunofluorescence images from DE differentiations for a panel of DE markers (FOXA2, GATA6, SOX17, OTX2, EOMES), pluripotency markers (OCT4), and primitive streak/mesoderm markers (T, CDX2). (**B**) Immunofluorescence images from feeder-free derived DE for SOX17, FOXA2, T, OCT4 and CDX2). All images represent the average results after 4 or more experiments, with at least 3 biological replicates each. Scale bar = 50 μm.

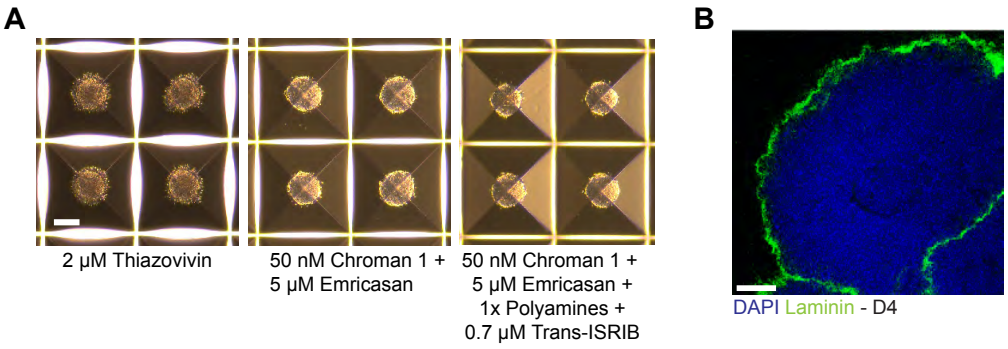

Fig. S4. Optimization of conditions for forebrain organoid generation from mouse EpiSCs. (**A**) Brightfield images of d1 organoids in Aggrewell wells. EBs were formed in the presence of Thiazovivin or chroman 1 + emricasan (CE), or the recently published CEPT cocktail (chroman 1, emricasan, polyamine mix, trans-ISRIB) (Chen et al., 2021). Scale bar = 100 µm. (**B**) Confocal immunofluorescence image of a day 4 EB/organoid. Scale bar = 25 µm.

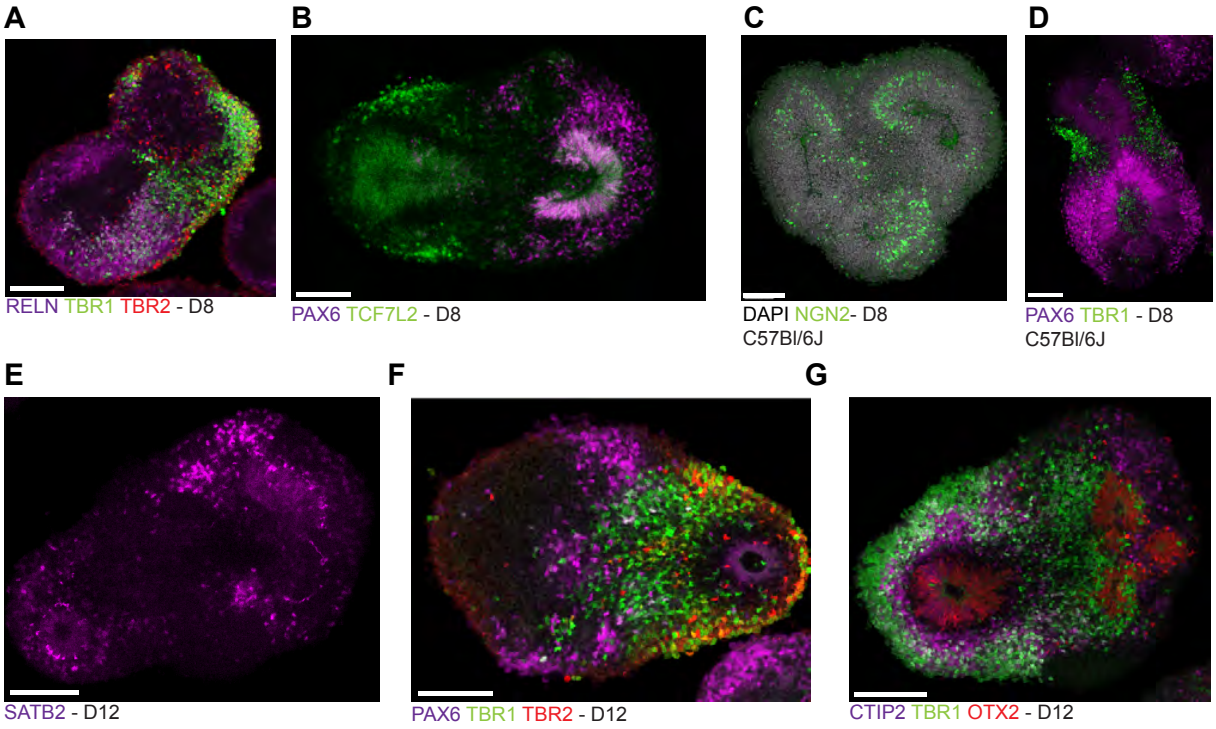

Fig. S5. EpiSC-derived brain organoids generate prethalamic and cortical-like neuronal populations. (**A,B**) Confocal immunofluorescence images of d8 organoids stained with antibodies against classical cortical markers (TBR1, TBR2, RELN and PAX6), which are also found in other regions of the brain such as the hippocampus, the cortical hem and the prethalamus, and thalamic markers (TCF7L2). Scale bar = 100 μm. (**C-D**) Confocal immunofluorescence of d8 organoids from C57Bl/6J background. Scale bar = 100 μm. (**E**) Confocal immunofluorescence image of a d12 organoid stained using antibodies against the classical upper-layer cortical marker SATB2. Scale bar = 100 μm. (**F-G**) Confocal immunofluorescence images of d12 organoids. Scale bar = 100 μm.

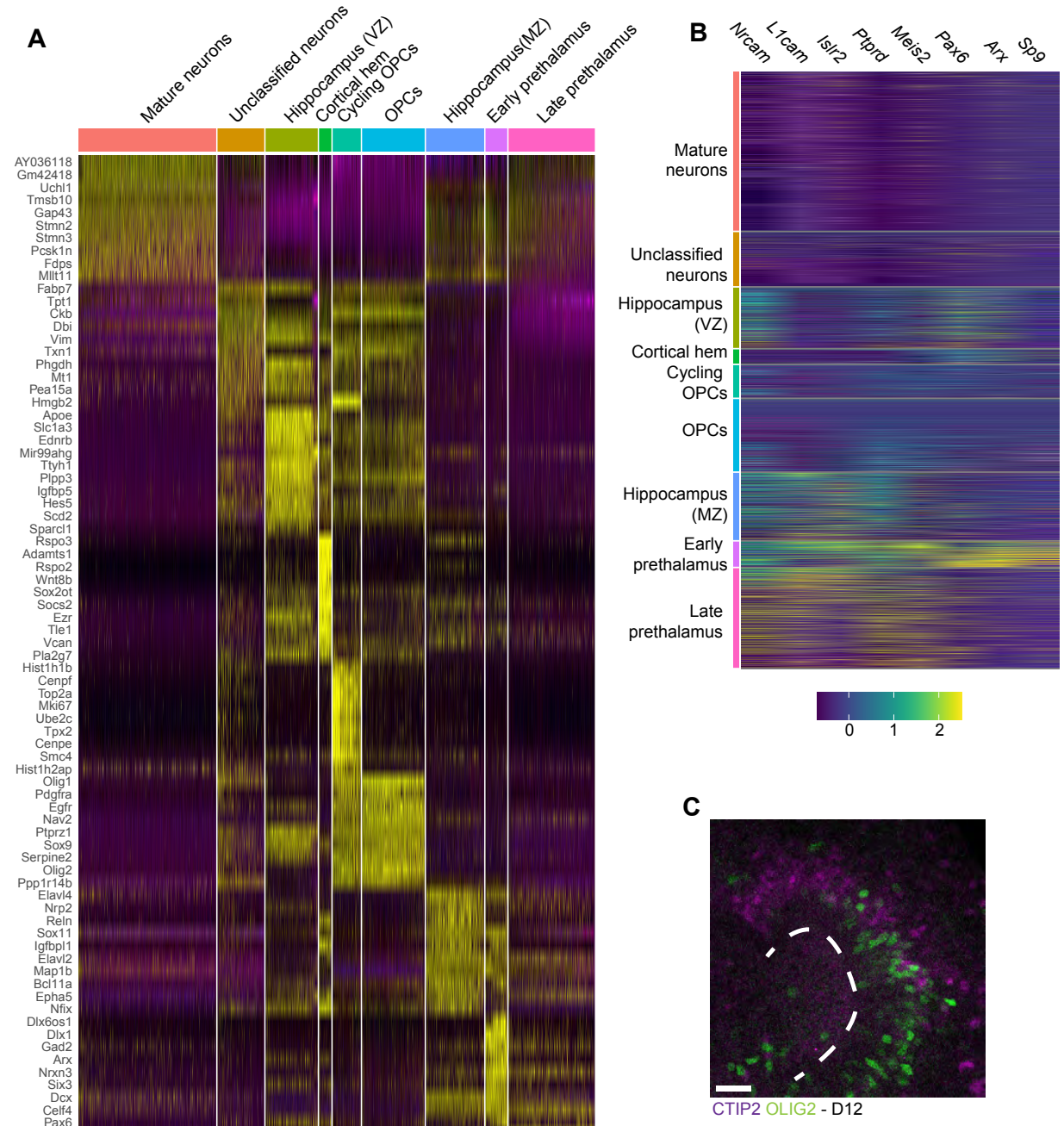

Fig. S6. scRNA-seq analyses on day 12 organoids reveals three main cell types. (**A**) Heatmap of the top 10 genes that define each cluster. Abbreviations: VZ = ventricular zone, MZ = mantle zone. (**B**) Expression profile, across clusters, of several prethalamic (*Sp9, Arx, Pax6, Meis2, Ptprd, Islr2*) and axonal (*L1cam, Nrcam*) markers. (**C**) Confocal immunofluorescence image of a day 12 organoid. Scale bar = 30 µm.

Table S1. Summary of previous mESC, mEpiLC, and hPSC directed differentiation protocols (related to Figure 2). References used to generate the plot in Fig. 2A (Borowiak et al., 2009; Chen et al., 2013; D'Amour et al., 2005; Diekmann et al., 2019; Green et al., 2011; Kinoshita et al., 2020; Korostylev et al., 2017; Li et al., 2011; Loh et al., 2014; Mfopou et al., 2014; Morrison et al., 2016; Morrison et al., 2008; Mou et al., 2012; Mulas et al., 2017; Ortmann et al., 2020; Sherwood et al., 2011; Shi et al., 2017).

PMID	Organism	Days	Efficiency	Journal	Published year
26675138	Mouse	7	80	The Embo journal	2016
33271069	Mouse	3	FS cells: 34%, EpiSCs 4%	Cell Stem Cell	2021
28669603	Mouse	5-6	60%	Stem Cell Reports	2017
24239964	Mouse	6	54.92	Stem cell research	2014
19341624	Mouse	6	81	Cell stem cell	2009
23293299	Mouse	7	79	Development	2013
28702321	Mouse	4	35	Molecular metabolism	2017
32795399	Mouse	6	30	Cell stem cell	2020
18940732	Mouse	7	14	Cell stem cell	2008
21400570	Mouse	4	80	Cellular Biochemistry	2011
22482504	Mouse	5	>90%	Cell Stem Cell	2012
21854845	Mouse	5	>90%	Mechanisms of Development	2011
24412311	Human	3	94	Cell stem cell	2014
28196600	Human	4	72	Cell stem cell	2017
16258519	Human	4	80	Nature biotechnology	2005
30700818	Human	3	70	nature scientific reports	2019
21358635	Human	5	96	Nature biotechnology	2011

Table S2. List of antibodies used.

Antibody	Concentration	Manufacturer	Cat.No.
Alexa Fluor 488 Anti-Human SOX17 conjugated antibody	5uL/10^6 cells	R&D Systems, Inc.	614013
Alexa Fluor 647 Anti-mouse CD184 conjugated antibody	0.5ug/10^6 cells	BioLegend	146504
Anti-CDX2	1/250	Abcam	Ab157524
Anti-CTIP2	1/200	Abcam	Ab18465
Anti-FOXA2	1/500	Abcam	Ab108422
Anti-GATA4	1/200	Santa Cruz	sc-25310
Anti-GATA6	1/500	Cell signaling technology	5851S
Anti-GFAP	1/1000	Invitrogen	13-0300
Anti-Human SOX17	1/200	R&D Systems	AF1924
Anti-Human/Mouse BRACHYURY antibody	1/200	R&D systems	AF2085
Anti-LAMININ	1/1000	Sigma	L9393
Anti-NESTIN	1/500	Aves	NES
Anti-NEUROGENIN-2	1/200	R&D Systems	MAB3314-SP
Anti-OCT4	1/500	Invitrogen	701756
Anti-OLIG2	1/500	Abcam	Ab109186
Anti-OTX1+OTX2	1/500	Abcam	Ab21990
Anti-OTX2	1/500	R&D Systems	AF1979
Anti-PAX6	1/200	BD Biosciences	561462
Anti-PDX1	1/100	Abcam	Ab47308
Anti-PH3	1/500	Cell Signaling	9706S
Anti-REELIN	1/200	Millipore	MAB5366
Anti-SATB2	1/200	Abcam	Ab51502
Anti-SOX1	1/200	R&D Systems	AF3369
Anti-SOX2	1/500	Sigma	AB5603
Anti-TBR1	1/500	Abcam	Ab31940
Anti-TBR2 (for brain organoids)	1/500	Millipore	AB15894

Anti-TBR2/ EOMES (for 2D staining)	1/500	Abcam	Ab23345
Anti-TCF7L2	1/200	Cell Signaling	2569
Anti-TUJ1	1/1000	BioLegend	801213
Anti-ZO-1	1/500	Thermo	617300
Live/dead zombie UV staining	1uL/10^6 cells	Invitrogen	L34962
DAPI	300nM (ICC) 1uM (organoid)	Invitrogen	D1306
Donkey anti Rabbit IgG Secondary Antibody, Alexa Fluor 488	1/500	Invitrogen	A-21206
Donkey anti-Goat highly cross-adsorbed secondary antibody, Alexa Fluor Plus 488	1/500	Invitrogen	A-32814
Donkey anti Rat IgG Highly Cross Adsorbed Secondary Antibody, Alex Fluor 488	1/500	Invitrogen	A-21208
Donkey anti Mouse IgG Highly Cross Adsorbed Secondary Antibody, Alexa Fluor 488	1/500	Invitrogen	A-21202
Goat anti-Chicken IgY Secondary Antibody, Alexa Fluor 555	1/500	Invitrogen	A-21437
Donkey anti Mouse IgG Secondary Antibody, Alexa Fluor 555	1/500	Invitrogen	A-31570
Donkey anti Rabbit IgG Secondary Antibody, Alexa Fluor 555	1/500	Invitrogen	A-31572
Donkey anti Goat IgG Cross Adsorbed Secondary Antibody Alexa Fluor 555	1/500	Invitrogen	A-21432
Chicken anti-Rat IgG Cross Adsorbed Secondary Antibody, Alexa Fluor 647	1/500	Invitrogen	A-21472

Chicken ant Goat IgG Secondary Antibody, Alexa Fluor 647	1/500	Invitrogen	A-21469
Donkey anti Mouse IgG Secondary Antibody, Alexa Fluor 647	1/500	Invitrogen	A-31571
Donkey anti Rabbit IgG Highly Cross Adsorbed Secondary Antibody, Alexa Fluor 647	1/500	Invitrogen	A-31573

Table S3. List of reagents used.

Reagent	Manufacturer	Reference #
2-mercaptoethanol	Gibco	21985023
Accutase	Gibco	A1110501
Activin A	Peprotech	120-14P
Aggrewell plate	STEMCELL	34415
Anti-Rat IgG Microbeads	Miltenyi Biotec	130-048-502
Apo-transferrin	InVitra	777TRF029
B27 supplement	ThermoScientific	17504044
B27 supplement (without vitamin A)	Gibco	12587010
BDNF	PeproTech	450-02
BenchMark Fetal bovine serum	Gemini	100-106
bFGF	Gibco	12587010
BMP-7	PeproTech	120-03P
Bovine Serum Albumin	Sigma	A2153
Cell recovery solution	Corning	354253
Chemically Defined Lipid Concentrate	Gibco	11905031
CHIR99201	Tocris Bioscience	252917-06-9
Chroman 1	MedChem Express	HY-15392
Chromium Next GEM Chip G Single Cell Kit, 48 rxns	10X genomics	1000120
Chromium Next GEM Single Cell 3' Kit v3.1, 16 rxns	10X genomics	1000268
CytoTune emGFP Sendai fluorescence reporter	ThermoScientific	A16519
Collagenase Type IV	Gibco	17104019
DAPI	Thermo Scientific	D1306
DeepClear	Celexplorer	DC-201
Digitonin	Sigma	D-141
DMEM with glutamax	Gibco	10564029
DMEM/F12	Gibco	11320082
Dual Index Kit TT Set A 96 rxns	10x genomics	1000215
eBioscience Fixation/Permeabilization Concentrate	Invitrogen	00-5123

eBioscience Fixation/Permeabilization Dilent	Invitrogen	00-5223-56
eBioscience Permeabiliation buffer (10X)	Invitrogen	00-8333
EDTA (0.5 M), pH 8.0, RNase-free	Invitrogen	AM9261
Emricasan	Selleckchem	S7775
ESGRO LIF	Sigma	ESG1107
F12 with GlutaMAX	Gibco	31765035
Fetal bovine serum	Gemini	100-106
Fgf-8b protein, CF	R&D Systems	423-F8-025/CF
Fibronectin	Sigma	FC010
Fixation/permeabilization concentrate	Invitrogen	00-5223-43
Fixation/permeabilization diluent	Invitrogen	00-5223
Flowmi cell strainer	Bel-Art	136800040
GDNF	PeproTech	450-10
Glutamax	Gibco	35050061
Heat stable recombinant human bFGF	Gibco	PHG0360
Hyclone fetal bovine serum	Cytiva	SH3007003
IMDM	Gibco	12440053
Insulin	Sigma	91077C
KAPA Hyper Prep Kit	Kapa Biosystems	KK8504
KingFisher Flex Magnetic Particle Processor	Thermo Scientific	5400630
Knockout serum replacement	Gibco	10828028
Laminin from Engelbreth-Holm-Swarm murine sarcoma basement membrane	Sigma	L2020
LDN-193189	Stemgent	04-0074
LGK-974	Selleck Chemicals	S7143
LY294002	Selleckchem	S1105
MACS multistand	Miltenyi Biotech	130-042-303
MagMAX *mir*Vana Total RNA Isolation Kit	Thermo Scientific	A27828
Matrigel	Corning	354230
Monothioglycerol	Sigma	M6145
MS column	Miltenyi Biotech	130-122-727
N2 supplement	Gibco	17502048

NEBNext® High-Fidelity 2X PCR Master Mix	NEB	M0541L
Neurobasal Media	Gibco	21103049
Non-adherent 6 well plate	Corning	3471
Non-essential amino acids	Gibco	11140050
NP-40 detergent	Sigma	74385
NVP-TNKS656	Selleck Chemicals	S7238
OctoMACS separator	Miltenyi Biotech	130-042-109
PD0325901	Tocris	4192
PD173074	STEMCELL Technologies	72164
Penicllin/streptomycin (100X)	Gibco	15140122
Permeabilization buffer	Invitrogen	00-8333
PiK-90	Sigma Aldrich	528117
Polyvinyl Alcohol	Sigma	341584
Putrescine	Sigma	P5780
rhLaminin-521	Gibco	A29249
SB-431542	Tocris	1614
SMART-Seq v4 Ultra Low Input RNA Kit	Clonetech	63488
Sodium pyruvate	Gibco	11360070
Spermidine	Sigma	S2626
Spermine	Sigma	S4264
16% Formaldehyde (w/v), Methanol-free	Thermo Scientific	28908
Thiazovivin	Sigma	SML1045
Tn5 enzyme and tagmentation buffer	Illumina	20034198
Trans-isrib	Tocris	5284
Tri Reagent	Sigma	T9424
TruSeq Stranded mRNA LT Kit	Illumina	RS-122-2102
TrypLE	Thermo Scientific	12605028
Triton X-100	Sigma-Aldrich	9002-93-1
Tween-20	Boston Bioproducts	P-934

Name	B6.129_17	B6.129_9	B6.129_4	DBA/2J_55	C57Bl/6J_44	C57Bl/6J_51	C57Bl/6J_1	C57Bl/6J_4	C57Bl/6J_2	PWK/PhJ_AC705	PWK/PhJ_AC698	PWK/PhJ_AC695	PWK/PhJ_AC699
Background	B6129SF1/J	B6129SF1/J	B6129SF1/J	DBA/2J	C57Bl/6J	C57Bl/6J	C57Bl/6J	C57Bl/6J	C57Bl/6J	PWK/PhJ	PWK/PhJ	PWK/PhJ	PWK/PhJ
Received from	Matthias Stadtfeld, PhD - Weill Cornell			Christopher L. Baker, Ph.D. - The Jackson Laboratory			inhouse, through IVF			Laura Reinholdt, Ph.D. - The Jackson Laboratory			
Culture conditions (mESCs)	On gelatin-coated dishes with irradiated mouse embryonic fibroblast feeder cells												
Media composition (mESCs)	Serum/LIF media: DMEM with glutamax, 1% nonessential amino acids, 1% sodium pyruvate, 1% penicillin-streptomycin, 0.1% 2-mercaptoethanol, 10% fetal bovine serum and 1% ESGRO LIF.			Serum/LIF media: DMEM with glutamax, 1% nonessential amino acids, 1% sodium pyruvate, 1% penicillin-streptomycin, 0.1% 2-mercaptoethanol, 10% fetal bovine serum, 1% ESGRO LIF, 3 uM CHIR99201 and 1 uM PD0325901.									
Culture conditions (mEpiSCs)	On gelatin-coated dishes with irradiated mouse embryonic fibroblast feeder cells												
Media composition (mEpiSCs)	N2B27 media: 50% DMEM-F12, 50% Neurobasal, 0.5% N2 supplement, 1% B27 supplement without vitamin A, 2 mM glutamax, 1% penicillin-streptomycin, 0.1% 2-mercaptoethanol, 20 ng/ml activin A, 12.5 ng/ml heat stable bFGF and 175 nM NVP-TNKS656												
Passage at EpiLC-to-EpiSC conversion	P5-10	P5-10	P5-10	P10	P5	P14	P6	P6	P11	P14	P10	P10	P8
Passage at experimental time	P5-10	P5-10	P5-10	P17	P13	P20	P12	P12	P18	P21	P17	P17	P15
Mycoplasma results	Negative	Negative	Negative	Negative	Negative	Negative	Negative	Negative	Negative	Negative	Negative	Negative	Negative
Karyotyped by LC-WGS		Yes - Normal			Yes - Normal	Yes - Normal					Yes - Normal		Yes - Normal

Table S4. Mouse embryonic stem cell lines

Development: doi:10.1242/dev.200561: Supplementary information

Table S5. EpiSC lines used in brain organoid experiments.

Genetic background	Biological replicates	Technical replicates
B6129SF1/J	3	>10
C57Bl/6J	1	2
C57Bl/6J X CAST/EiJ	1	2

Fig. S7. Complete UMAPs, related to figure 6.

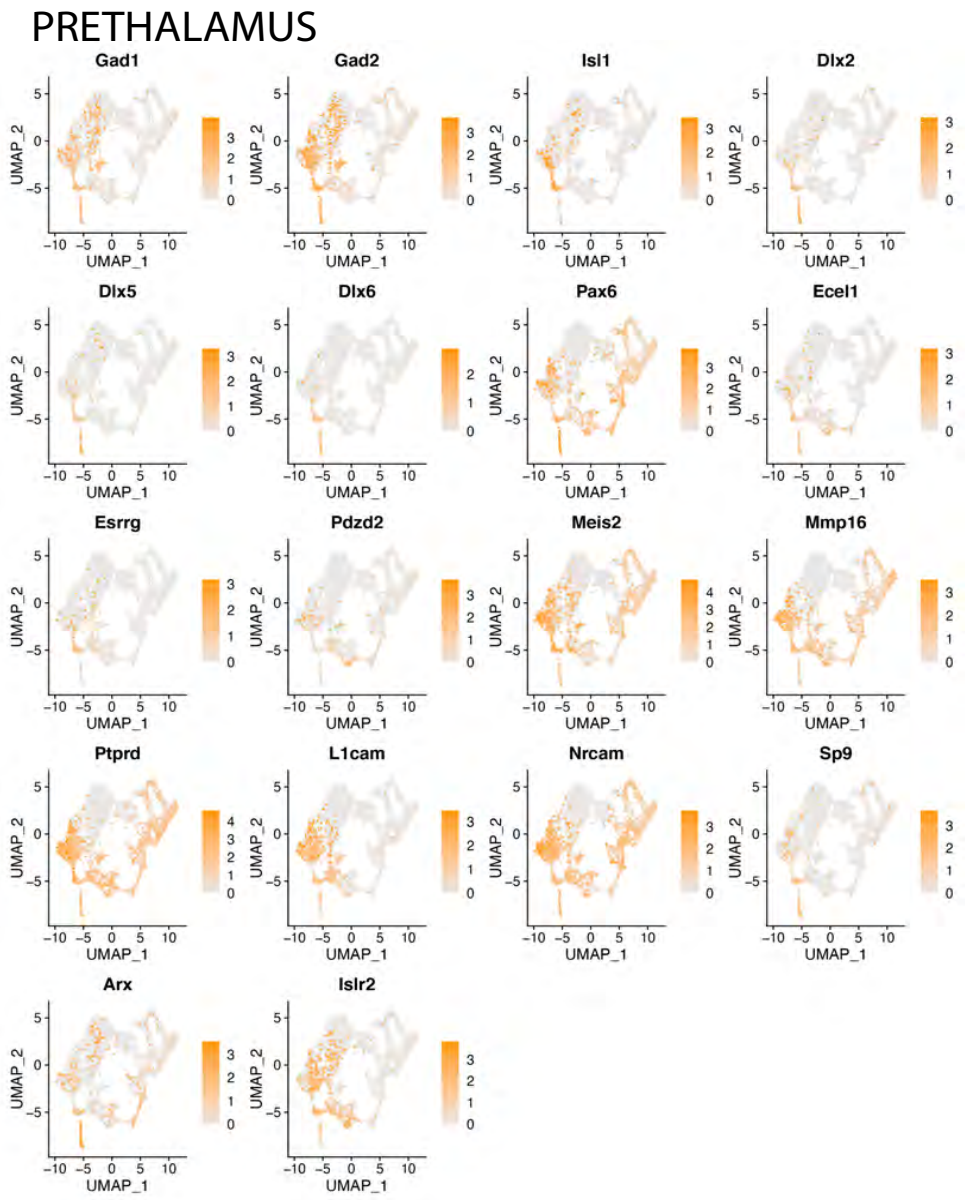

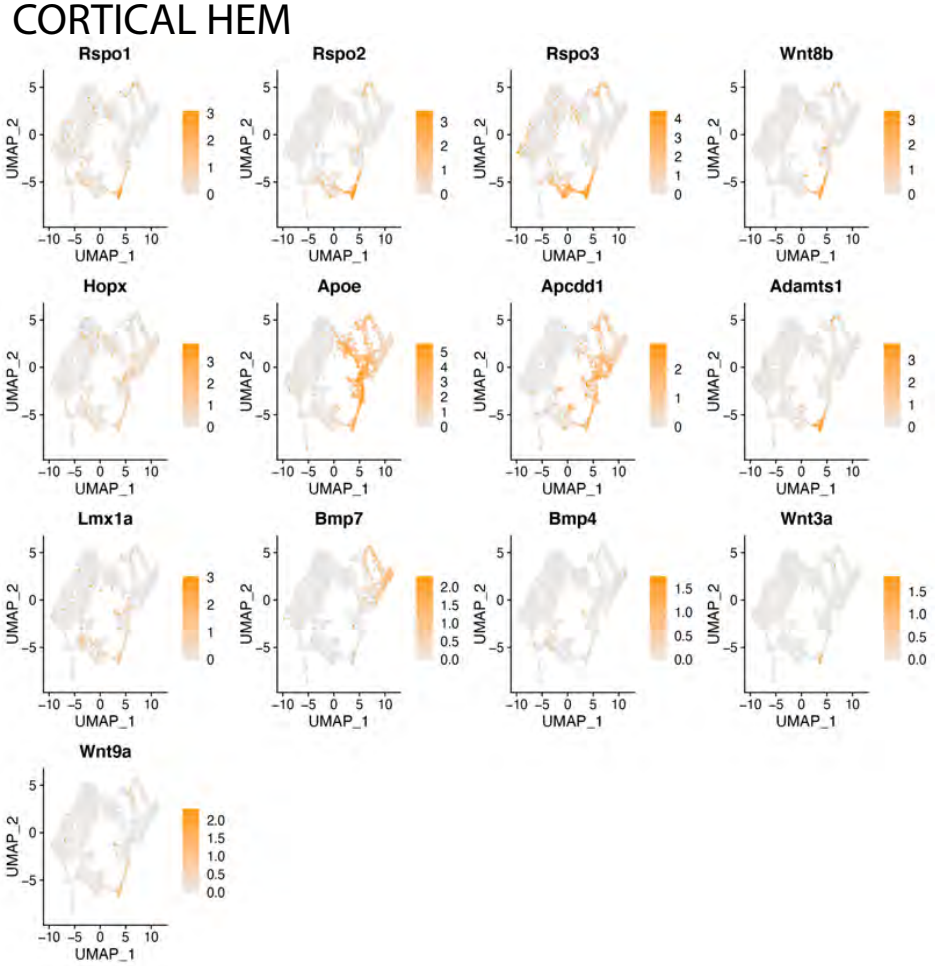

HIPPOCAMPUS

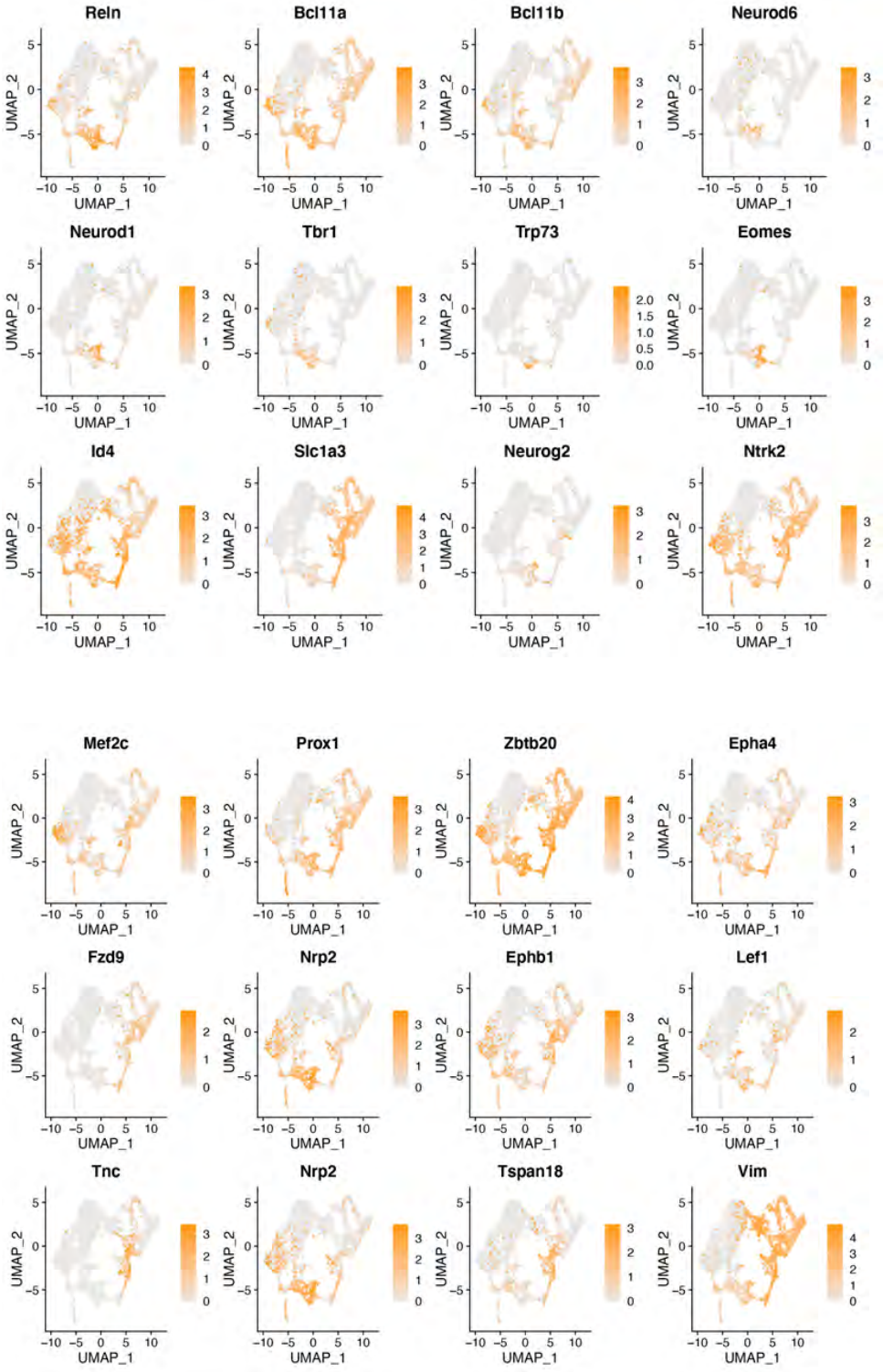

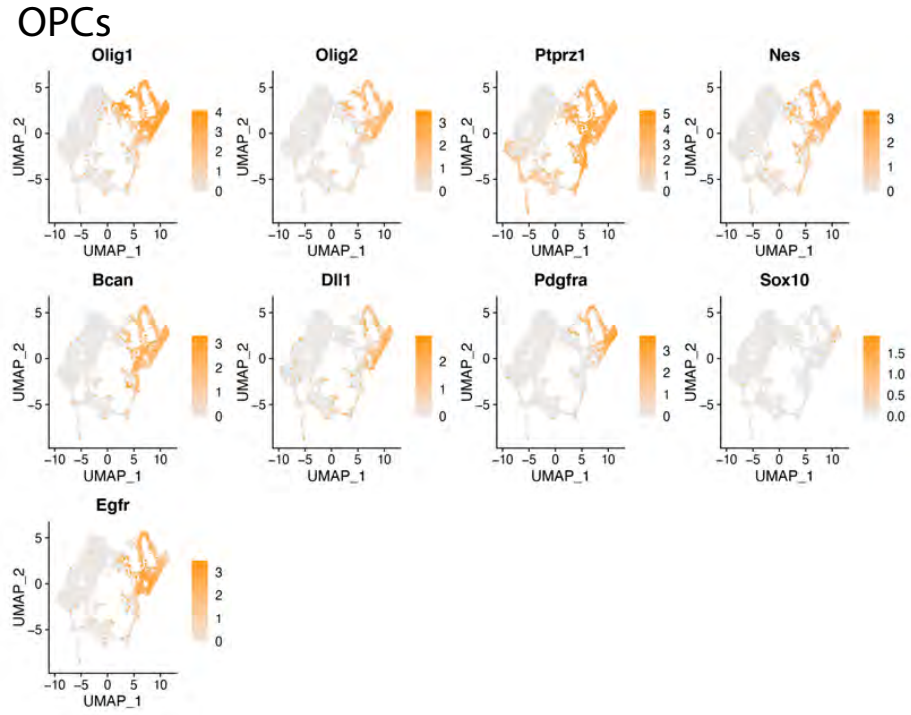

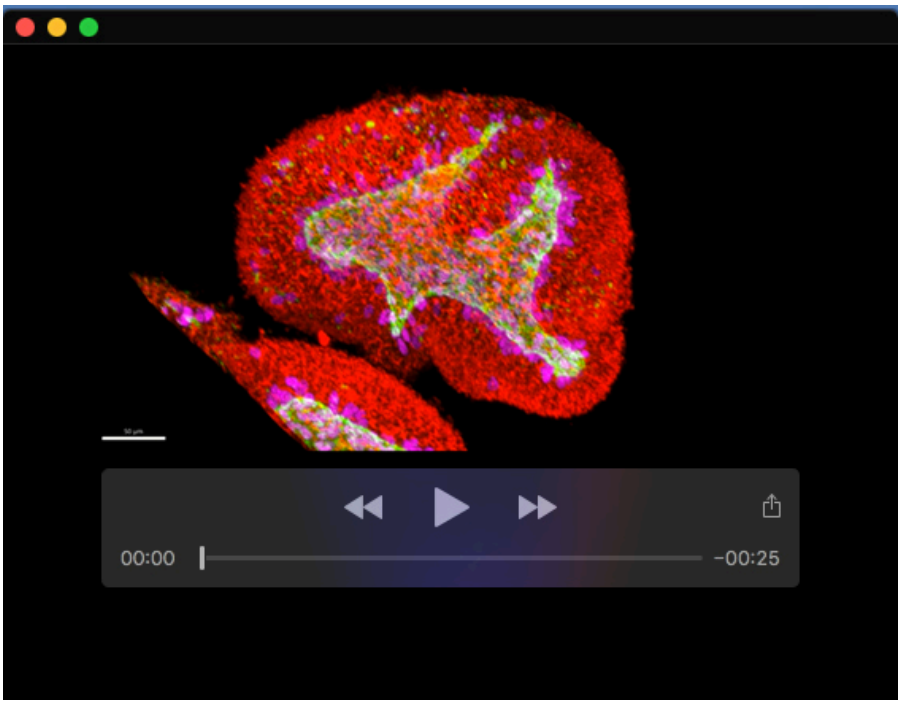

Movie 1. Day 4 forebrain organoid stained with antibodies against ZO-1 (green), phospho-histone H3 (purple) and Nestin (red).

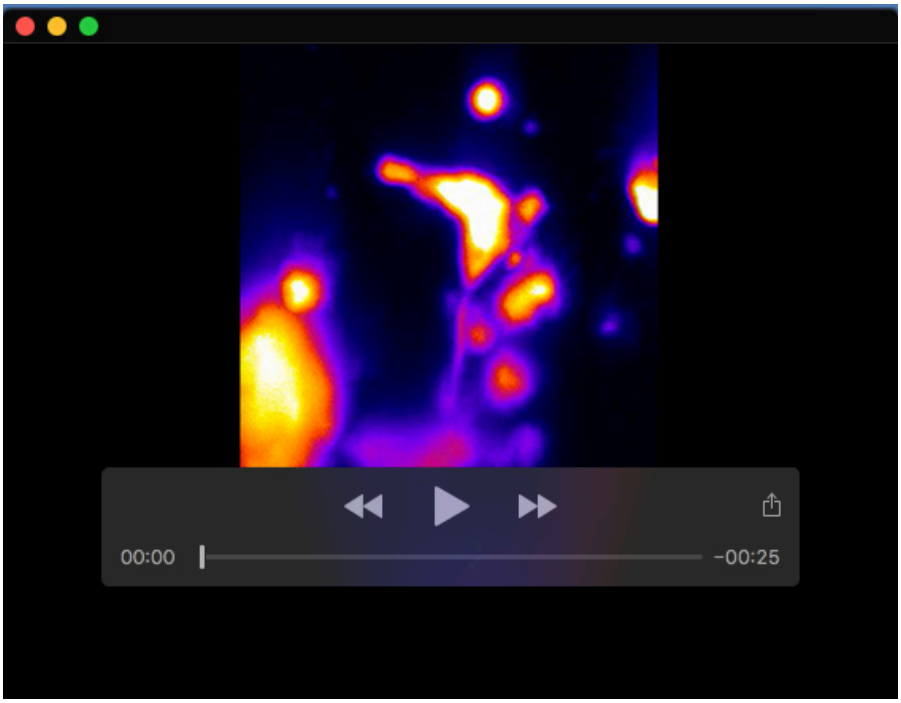

Movie 2. Live imaging of radial glial-like cells in a d3 organoid. emGFP Sendai virus was added to the EB formation media during the EB formation period to sparsely label developing neuroepithelial progenitor cells. The organoid was then embedded in Matrigel and imaged with a light sheet microscope from day 3 to day 4. The apical membrane is at the bottom of the video and the basal lamina on top.

Supplementary Materials and Methods

Protocol: Mouse ESC to EpiSC conversion and EpiSC culture

Notes before starting:

- Before use, all media should be warmed to 37 °C using a water or bead bath.
- All steps should be performed in a sterile BSC using rigorous aseptic technique.

Thawing ESCs

1. Remove cryovial of ESCs from liquid nitrogen storage and thaw rapidly with warmed media.
2. Once thawed, transfer into 15 mL falcon containing 5 mL Serum/Lif media (Table S7) to dilute the DMSO in the freezing media.
3. Centrifuge at 200 g for 3 minutes.
4. Aspirate media and resuspend cell pellet in appropriate volume of Serum/Lif media (Table S6).
5. Remove pre-plated feeders from the incubator and aspirate MEF media.
6. Add single cell suspension of ESCs to feeders and gently shake the plate left-to-right and up-and-down 3 times each to ensure cells are evenly distributed throughout.

Maintaining ESCs

Important notes

- Change media daily and passage cells upon 70% confluence at a 1:6 ratio.
- Feeders plated on gelatin should be prepared at least 8 hours in advance.

Passaging ESCs

1. Aspirate media and wash cells twice with PBS without calcium and magnesium ($PBS^{-/-}$).
2. Add warmed Accutase to wells for 2-3 minutes to dissociate the cells from the plate.
    a. *To speed up the dissociation process, place the plate with Accutase at 37 ℃ for 1-2 minutes.*
3. Gently tap the sides of the tissue culture plate to enhance cell dissociation.
4. Once all cells are lifted, collect Accutase and cells in a 15 mL centrifuge tube and dilute with equal amounts of $PBS^{-/-}$.
5. Centrifuge at 200 g for 3 minutes.
6. Aspirate supernatant and resuspend cell pellet in Serum/Lif media.
7. Remove MEF media from feeders and add the appropriate amount of ESC suspension to the plate for a 1:6 dilution.
8. If passaging long-term as ESCs, use collagenase to lift cells and accutase to bring to a single cell suspension to avoid accumulation of feeders. See "Passaging as EpiSCs" below.

ESC to EpiLC Conversion

Prepare plate

1. Coat the desired tissue culture plate with fibronectin diluted to 16.7 uL/mL in $PBS^{-/-}$. Rest plate at room temperature for ≥30 minutes.
2. Wash the coated plate twice with $PBS^{-/-}$.
3. Add additional $PBS^{-/-}$ to the plate until ready to add the cells to prevent desiccation. The plate can be stored with $PBS^{-/-}$ at 37 degrees for up to 4 hours.

Create single cell suspension and plate

1. Confirm ESC quality using a phase contrast microscope.
2. Aspirate ESC media from plate.
3. Use a serological pipette to wash each well twice with $PBS^{-/-}$.
4. Remove $PBS^{-/-}$ from the plate and apply pre-warmed Collagenase IV to each well to preferentially dissociate EpiSC colonies without feeder contamination.
    a. *Optional: place the plate with collagenase back in the incubator to increase the speed of dissociation.*
    b. *Gently tap the sides of the tissue culture plate to encourage colony lifting.*
    c. *Do not leave collagenase on wells for over 25-30 minutes as this will cause feeder cells to dissociate.*
5. Once the ESC colonies are lifted, gently collect colonies using serological pipette and transfer to a 15 mL centrifuge tube.
    a. *Optional: wash each well with HBSS++ to collect any remaining colonies and combine with the collagenase in the 15 mL tube.*
6. Centrifuge cells at 125 g for 4 minutes to pellet the ESC colonies and aspirate the supernatant.
7. Using a serological pipette, resuspend the pellet with 1 mL Accutase to break colonies into a single cell suspension. Leave the cell suspension under the hood for 2-4 minutes to ensure single cell suspension.
    a. *Optional: remove one drop of the suspension (~10 uL) and place on microscope slide. Observe with the microscope for residual colonies.*
8. Once the colonies are completely dissociated, add 5-10 mL $PBS^{-/-}$ to dilute the Accutase.
9. Centrifuge the solution at 200 g for 3 minutes to pellet single cells.
10. Aspirate supernatant and resuspend the pellet in EpiLC media (Table S7).
11. Count cells and plate at a density of 17,500 cells/cm^2.
12. Change the media 24 hours after plating. Cells should be cultured in EpiLC media for 48 hours before being converted to EpiSCs.

Conversion and Maintenance of EpiSCs

Important notes

- Change media daily and passage cells at 70% confluence, generally every other day
- Feeders plated on gelatin should be at least 8 hours before.

Converting EpiLCs to EpiSCs

1. After 48 hours of culture in EpiLC conditions, wash cells twice with $PBS^{-/-}$.
2. Add warmed Accutase to wells and collect in 15ml falcon tube once cells are lifted. Break the cells into small clumps of 5-10 cells (approx. 2-4 mins). Add equal volume of $PBS^{-/-}$ to dilute Accutase.
3. Centrifuge at 200 g for 3 minutes to pellet cells.
4. Resuspend in pre-warmed EpiSC media (Table S7).
5. Wash feeders twice with $PBS^{-/-}$. Aspirate the final PBS wash and plate 50,000-100,000 EpiLCs/cm^2 onto the feeders.
    a. *Note: Roughly, 1 well of a 12-well plate of EpiLCs can be seeded to 1 well of a 6-well plate for EpiSC culture.*

Passaging EpiSCs

1. Aspirate EpiSC media.
2. Use a serological pipette to wash each well twice with $PBS^{-/-}$.
3. Add pre-warmed Collagenase IV to each well to preferentially dissociate EpiSC colonies without feeder contamination.
    a. *Optional: place the plate with collagenase in the incubator to increase the speed of dissociation.*
    b. *Gently tap the sides of the tissue culture plate to encourage colony lifting.*
    c. *Do not leave collagenase on wells for over 25-30 minutes as this will cause feeder cells to dissociate.*
4. Once EpiSC colonies are lifted, gently collect colonies using serological pipette and transfer to a 15 mL centrifuge tube.
    a. *Optional: wash each well with HBSS++ to collect any remaining colonies and combine with collagenase in the 15 mL tube.*
5. Centrifuge cells at 125 g for 4 minutes to pellet EpiSC colonies and aspirate supernatant.
6. Using a serological pipette, resuspend the pellet with 1 mL Accutase to break colonies into clumps of 3-8 cells. Leave the cell suspension in hood for 1-2 minutes to ensure dissociation.
    a. *Optional: remove one drop of the suspension (~10uL) and place it on microscope slide. Observe colony size under the microscope.*
7. Once cells are dissociated, add 5-10 mL $PBS^{-/-}$ to dilute Accutase.
8. Centrifuge the solution at 200 g for 3 minutes to pellet cells.
9. Gently resuspend in EpiSC media to avoid additional dissociation.
10. Wash pre-plated feeders twice with $PBS^{-/-}$ to remove all MEF media and any traces of serum.
11. Plate EpiSCs on washed feeders with appropriate volume of media (Table S6) and place in incubator.
    a. *Optional: Check the size of the cell clumps after plating to ensure small colonies of 3-8 cells.*

12. EpiSCs grow very rapidly and therefore require daily media changes and are generally passaged every 48 hours.

Freezing EpiSCs

1. Aspirate media from each well of the plate and wash two times with $PBS^{-/-}$.
2. Add appropriate amount of accutase to each well (Table S6) and place in the incubator until the colonies are lifted.
3. Collect the mixture with a serological pipette and transfer to a 15 mL centrifuge tube.
4. Dilute Accutase with $PBS^{-/-}$.
5. Centrifuge cell solution at 200 g for 3 minutes.
6. Aspirate the supernatant.
7. Gently resuspend in EpiSC media with 10% DMSO, add to a cryotube and freeze.

Thawing EpiSCs

1. Remove EpiSCs from liquid nitrogen tank and thaw rapidly with warmed media.
2. Once thawed, add to a 15 mL falcon with 4 mL of N2B27 to dilute the DMSO.
3. Centrifuge at 200 g for 3 minutes to pellet cells.
4. Aspirate supernatant and gently resuspend the cells with EpiSC media.
5. Wash overnight feeders 2x with $PBS^{-/-}$ and plate cells directly onto feeders.

Frequent questions and concerns

Minimizing EpiSC differentiation (Figure S8B)

- Once there are many spontaneously differentiating colonies within the culture, it can be difficult to bring the line back to pluripotency. Prevention by culturing carefully is the best method to avoid spontaneous differentiation.
- Passage frequently, preferentially every other day, with no longer than 3 days on the same plate of feeders.
- Use collagenase to passage, as this will avoid propagation of differentiated cells.

Protocol: Directed differentiation of mouse EpiSCs into definitive endoderm

Notes before starting:

- Before use, all media should be warmed to 37 °C using a water or bead bath.
- All steps should be performed in a sterile BSC using rigorous aseptic technique.

Preparing the laminin coated cell culture dish

1. Dilute laminin-521 in PBS with calcium and magnesium to a final concentration of 10 ug/mL. Optionally, laminin from EHS murine sarcoma basement membrane (Sigma, L2020) can be used as a replacement at 20 ug/mL.

2. Once combined, use a serological pipette to dispense the diluted laminin into each well of a tissue culture plate (see Table S8 for volume recommendations). Shake plate to ensure that the entire surface is covered.
3. Place the laminin-coated tissue culture plate(s) in cell culture incubator at 37°C for 2 hours or O/N at 4°C.

Preparing and plating EpiSCs

1. Confirm EpiSC quality using a phase contrast microscope (Figure S8A).
2. Aspirate EpiSC media from plate.
3. Use a serological pipette to wash each well twice with $PBS^{-/-}$.
4. Remove the $PBS^{-/-}$ from the plate and apply pre-warmed Collagenase IV to each well to preferentially dissociate EpiSC colonies without feeder contamination.
    a. *Optional: place the plate with collagenase back in the incubator to increase the speed of dissociation.*
    b. *Gently tap the sides of the tissue culture plate to encourage colony lifting.*
    c. *Do not leave collagenase on wells for over 25-30 minutes as this will cause feeder cells to dissociate as well and should be avoided.*
5. Once the EpiSC colonies are lifted, gently collect colonies using serological pipette and transfer to a 15 ml centrifuge tube.
    a. *Optional: wash each gently with HBSS++ to collect any remaining colonies and combine with collagenase in the 15 mL tube.*
6. Centrifuge cells at 125 g for 4 minutes to pellet EpiSC colonies and aspirate the supernatant.
7. Using a serological pipette, resuspend the pellet with 1 mL Accutase to break colonies into a single cell suspension. Leave the cell suspension in hood for 2-4 minutes to ensure single cell suspension
    a. *Optional: remove one drop of the suspension (~10 uL) and place on microscope slide. Observe under the microscope for residual colonies.*
8. Once cells are completely dissociated, add 5-10 mL $PBS^{-/-}$ to dilute Accutase.
9. Centrifuge the solution at 200 g for 3 minutes to pellet single cells.
10. Aspirate the supernatant, resuspend in plating media (Table S9) and count the number of cells.
11. Calculate the appropriate volume of media and number of cells to seed the desired plate, then prepare master solution with 110,000 cells/cm^2 (Table S8).
12. Remove the laminin coated plate from incubator and aspirate laminin solution. Do not allow plate to dry—the cell suspension must be added immediately.
13. Homogenize the cell solution and immediately add the cell suspension to the plate.
14. Place the plate in the incubator for 5-6 hours. During this time cells will attach to the plate.

Changing media

1. After 5-6 hours, gently remove the plate from the incubator and check under microscope to confirm that most cells have attached. At this stage, the cells can be easily washed off if media is added too vigorously.
2. Slowly aspirate media off all wells at a 45-degree angle to the BSC surface. Gently add $PBS^{-/-}$ to wash off any residual media.
    a. *IMPORTANT: Use one hand to tilt the tissue culture plate towards you at a 45° angle and maintain this angle while gently removing and dispensing media into the side of the well (slow ejection speed on the pipettor). This will ensure minimal loss of cells.*
3. Using same technique, add appropriate amount of Differentiation Media 1 (Table S9).
4. Place the tissue culture dish in the incubator and allow to sit for 16 more hours.
5. After 16 hours, aspirate Differentiation Media 1.
6. While resting serological pipette tip on bottom wall of well, gently add $PBS^{-/-}$ to dilute any residual media.
7. Using same technique as $PBS^{-/-}$ application, add appropriate amount of Differentiation Media 2 (Table S9).
8. Return the tissue culture dish to the incubator for 24 hours.
9. After 24 hours in Differentiation Media 2, the cells should have reached the definitive endoderm stage. Examine all wells to confirm appropriate density and morphology.

Fixing and immunostaining

1. To fix cells, wash each well two times with $PBS^{-/-}$.
2. Add 4% PFA to each well and allow to rest at room temperature for 15 minutes.
3. After 15 minutes, aspirate the PFA and wash twice with $PBS^{-/-}$.
4. Add $PBS^{-/-}$ to each well and refrigerate at 4 °C until staining.

Frequent questions and concerns

Low cell density after plating

- Ensure the laminin was diluted and left for specified amount of time (2 hours). Do not rinse culture plates after laminin coating.
- Some cell lines have weak attachment. If this is a recurring issue for specific lines, increase the starting density when plating.

Cell loss during media changes

- Use one hand to tilt the tissue culture plate towards you at a 45° angle and maintain this angle while gently removing and dispensing media into the side of the well (slow ejection speed on the pipettor). This will ensure minimal loss of cells.
- Increase the size of the wells you are using. Cell loss is more common on smaller sized wells.
- Wait a longer period of time (6-8 hours) before changing plating media.

Low efficiency of differentiation

- It is important to begin with high quality EpiSCs with minimal spontaneous differentiation. At the beginning of the directed differentiation protocol, EpiSCs colonies should number ~50-200 and the plate should be no more than 70-80% confluent.
- This protocol was optimized on EpiSCs passaged no more than 18 passages as EpiSCs and it is unknown how high passage lines may respond to the differentiation protocol. In general, it is best to begin with low-passage ESCs to convert to EpiSCs and avoid prolonged culture.

Timing

- The timing of each media change was optimized to produce the highest Sox17 and FoxA2 expression at 40 hours of culture. Changing the timing of Step 1 and Step 2 can lead to reduced efficiency.

Protocol: Generation of forebrain organoids from mouse EpiSCs

Notes before starting:

- Before use, all media should be warmed to 37 °C using a water or bead bath.
- All steps should be performed in a sterile BSC using rigorous aseptic technique.

Formation of EBs

1. Confirm EpiSC quality using a phase contrast microscope (Figure S8A).
2. Aspirate EpiSC media from plate.
3. Use a serological pipette to wash each well twice with $PBS^{-/-}$.
4. Remove the $PBS^{-/-}$ from the plate and apply pre-warmed Collagenase IV to each well to preferentially dissociate EpiSC colonies without feeder contamination.

- *Optional: place the plate with collagenase back in the incubator to increase the speed of dissociation.*
- *Gently tap the sides of the tissue culture plate to encourage colony lifting.*
- *Do not leave collagenase on wells for over 25-30 minutes as this will cause feeder cells to dissociate as well and should be avoided.*

5. Once the EpiSC colonies are lifted, gently collect colonies using serological pipette and transfer to a 15 mL centrifuge tube.

- *Optional: wash each gently with HBSS++ to collect any remaining colonies and combine with collagenase in the 15 mL tube.*

6. Centrifuge cells at 125 g for 4 minutes to pellet EpiSC colonies and aspirate the supernatant.
7. Using a serological pipette, resuspend the pellet with 1 mL Accutase to break colonies into a single cell suspension. Leave the cell suspension in the hood for 2-4 minutes to ensure single cell suspension.

- *Optional: remove one drop of the suspension (~10 uL) and place on microscope slide. Observe under the microscope for residual colonies.*

8. Once cells are completely dissociated, add 5-10 mL $PBS^{-/-}$ to dilute Accutase.
9. Centrifuge the solution at 200 g for 3 minutes to pellet single cells.
10. Aspirate the supernatant, resuspend in EB formation media (Table S10) and count cells.
11. Calculate the appropriate volume of media and number of cells to seed the desired number of wells, then prepare master solution with 1,200,000 cells/well of Aggrewell, with each well containing a total of 2 mL media.
12. Using a serological pipette, disperse cell solution into well(s) of Aggrewell.
13. Using a P1000 pipette, gently pipet up and down to equally distribute the cells within the well(s).
14. Centrifuge the Aggrewell plate at 100 g for 3 minutes. Confirm cells are evenly distributed using microscope.
15. Place Aggrewell in incubator for 24 hours to form EBs. Avoid moving plate during the EB formation phase.

Collection and embedding of organoids

Important note:

- Matrigel should be thawed overnight on ice at 4°C (or for at least 3-4h)

1. Following 24 hours in EB formation media, Aggrewell should contain uniform, well-formed developing organoids. Using a P1000 pipette, gently remove as much media as possible from the Aggrewell without disturbing organoids.
2. Using a P1000, add 1 mL of Neural Induction media (Table S10) to Aggrewell and, using a wide orifice pipette tip, gently resuspend the developing organoids.
3. Transfer organoids to a 6 cm Petri dish containing 5 mL Neural Induction media and swirl briefly to dilute EB formation media. Transfer organoids to a 10 cm Petri dish containing 10 mL Neural induction media.
   a. *Note: washing with $PBS^{-/-}$ should be avoided as this may cause organoids to adhere to the plate.*
4. Determine the total number of organoids desired and how many wells of a low-adherence 6 well plate are needed.
   a. *Note: Each well of the plate should contain 20-50 organoids.*
5. Then, carefully gather 20-50 organoids in 67 uL of Neural Induction media and mix with 100 uL of Matrigel. Carefully dispense the mix of Matrigel, media, and organoids in the center of a well, being sure to avoid the walls of the well (Derived from Qian et al., 2018).
6. Repeat for desired number of wells then place the plate in the incubator for 30 minutes to solidify the Matrigel.
7. Following the 30-minute incubation, carefully remove the plate from the incubator and gently add 3 mL of Neural Induction media to each well. Return to incubator for 24 hours.
   a. *Note: when adding the media, Matrigel domes may float off plate. This does not affect organoid quality.*

Maintenance and patterning of organoids

1. Following 24 hours in Neural Induction media, gently remove as much media as possible from the well without disturbing Matrigel domes.
2. Add 3 mL of Neuroepithelial Expansion media (Table S10) to each well. Place plate in incubator for 48 hours.
3. After 48 hours in Neuroepithelial Expansion media, gently remove media and wash twice with $PBS^{-/-}$.
    a. *Note: Wash and media change should be performed under a dissection microscope to avoid organoid loss.*
4. After removing second $PBS^{-/-}$ wash, add 2mL Corning Cell Recovery Solution to each well of the 6 well plate. Gently swirl plate and place in incubator for 30 minutes to remove Matrigel from organoids.
    a. *Optional: To improve recovery, gently swirl plate every 5-10 min while in incubator.*
5. Following Matrigel removal, gently add 2 mL of Neuronal media (Table S10) to each well of the 6 well plate to dilute solution.
6. Using a wide orifice pipette tip, transfer the organoids to a freshly prepared low adherence 6 well plate containing 2 mL Neuronal media per well.
7. Using a wide orifice pipette tip, transfer the organoids to an additional freshly prepared low adherence 6 well plate containing 2 mL Neuronal media per well to ensure maximum dilution of Corning Cell Recovery solution.
8. Finally, using a wide orifice pipette tip, transfer organoids to a 10 cm Petri dish containing 12.5mL of Neuronal media and place on shaker.
    a. *Note: speed of shake will depend on the specific shaker being used. For Celltron benchtop shaker, 65 rpm was sufficient in preventing organoid merging while minimizing impact.*
9. Change media using fresh Neuronal media every other day until collection day.

Protocol: Immunostaining of mouse EpiSC-derived forebrain organoids (method derived from Dekkers et al., 2019)

Fixation and immunostaining of organoids

1. Coat a 15 mL falcon tube with 1% BSA to avoid organoid attachment and place on ice.
2. While on ice, gently add organoids to the pre-coated falcon tube and wash three times with 4°C $PBS^{-/-}$.
    a. *Note: Organoids at day 4 or earlier should be centrifuged at 70 g for 3 minutes at 4 ℃ for each wash step. Organoids later than day 4 will naturally settle to the bottom of the tube due to their size.*
3. To fix organoids, add 4% PFA to 15 mL falcon tube until organoids are completely submerged. Place on ice for 45 minutes and gently resuspend halfway through incubation to ensure proper fixation.
4. Following fixation, wash three times with $PBS^{-/-}$ containing 0.1% Triton-X (PBST) to remove any remaining PFA.

5. To permeabilize organoids, add PBS$^{-/-}$ containing 0.5% Triton-X until organoids are completely submerged and incubate for 15 minutes at 4°C.
6. Following 15-minute incubation, remove permeabilization buffer and block organoids for 15 minutes in organoid washing buffer (OWB) containing 0.2% Triton-X, 0.02% SDS and 0.2% BSA in PBS$^{-/-}$. Calculate appropriate volume of OWB by determining number of staining conditions (200 uL OWB per staining condition).
7. Equally distribute the organoids in a low-adhesion 24-well plate with a total of 200 uL OWB and desired number of organoids in each well. Each well will represent a single staining condition.
8. Following 15-minute blocking, directly add primary antibodies of interest prediluted in 200 uL OWB to each well for a total volume of 400 uL per well.
9. Place plate on shaker and incubate in primary antibodies overnight at 4°C.
10. Following overnight incubation, add 800 uL of OWB directly to each well and place on shaker at room temperature for 5 minutes.
11. Next, remove 1 mL of solution, replace with a fresh 1mL of OWB, and place on shaker for two hours at room temperature to wash organoids.
12. Repeat this wash step two additional times, for a total of 6 hours of washing.
13. After 6 hours of washing, remove 1 mL of OWB from each well and directly add 200 uL of prediluted secondary antibodies and DAPI (final concentration of 1 µM) in OWB, for a total volume of 400 uL per well.
14. Place on shaker and incubate overnight at 4°C.
15. Following overnight secondary antibody incubation, remove from 4°C, and add 800 uL of OWB with 1 µM DAPI per well. Place on shaker at room temperature and allow to shake for 5 minutes.
16. Next, remove 1 mL of OWB from each well and replace with a fresh 1 mL of OWB with 1 µM DAPI. Place on shaker at room temperature for 2 hours to wash organoids.
17. Repeat this wash step twice more, for a total of 6 hours of washing.

Preparation of slide for imaging

1. Using a standard hole puncher, punch a hole (0.5cm Ø) into a sticky silicone pad (20x20x1 mm).
2. Place sticky pad on imaging slide. (Figure S9)

Mounting of organoids for imaging

1. Using a wide orifice pipette tip, Transfer the organoids to a 1.5 mL Eppendorf.
2. Remove as much supernatant as possible without disturbing the organoids
    a. *Note: If the organoids at day 4 or less, centrifuge at 70 g for 3 minutes to pellet.*
3. Using a wide orifice pipette tip, add 35 uL of DeepClear solution, gently resuspend organoids, and transfer to prepared slide. Add a coverslip and image.

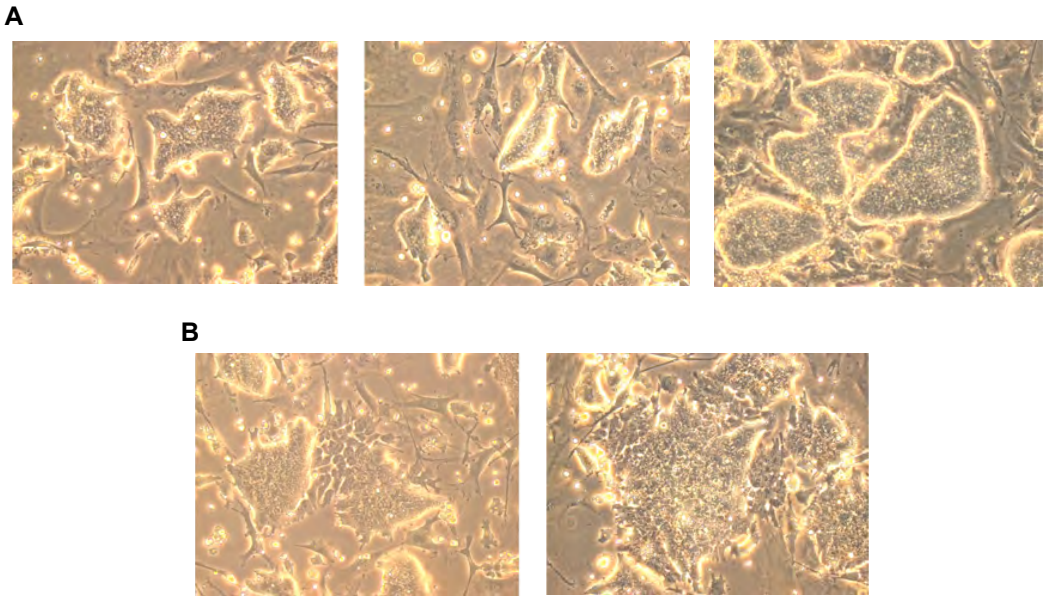

Fig. S8. EpiSCs in culture. (A) Standard culture of EpiSCs. (B) Spontaneous differentiation in EpiSC culture.

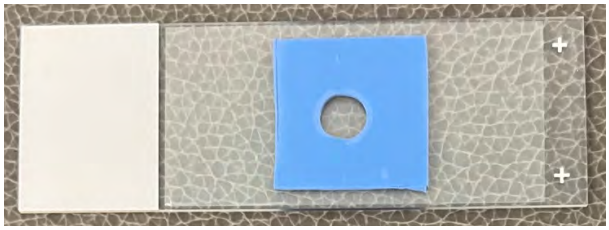

Fig. S9. Slide for organoid imaging.

Table S6. Plate sizes and suggested volumes for stem cell culture

Plate size	Surface area (cm^2)	Volume of collagenase, $PBS^{-/-}$ and Accutase (mL)	Media Volume (mL)
96 well	0.32	0.1	0.2
48 well	1.1	0.3	0.6
24 well	1.9	0.4	0.8
12 well	3.5	0.5	2
6 well	9.6	1	5
10cm dish	56.7	5	15

Table S7. Media composition for stem cell culture

MEF	ESC	EpiLC	EpiSC
MEF media	S/L media	N2B27	N2B27
	3uM CHIR99021*	12.5 ng/ml Heat stable recombinant human bFGF	12.5 ng/ml Heat stable recombinant human bFGF
	1uM PD0325901*	20 ng/ml Activin A	20 ng/ml Activin A
		1% KOSR	175 nM NVP-TNKS656

*Optional components to create 2i/SL culture conditions

Table S8. Plate sizes and suggested volumes for DE differentiation

Plate size	Surface area (cm^2)	Volume of laminin, collagenase, PBS (ml)	Media Volume (ml)	Number of cells per well
96 well	0.32	0.1	0.2	35,000
48 well	1.1	0.3	0.6	120,000
24 well	1.9	0.4	0.8	208,000
12 well	3.5	0.5	2	382,000
6 well	9.6	1	5	1,050,000
10cm dish	56.7	5	15	6,200,000

Table S9. DE differentiation media composition

Plating Media	Differentiation media 1	Differentiation media 2
CDM + 0.7 µg/ml insulin	CDM + 0.7 µg/ml insulin	CDM + 0.7 µg/ml insulin
12.5 ng/ml FGF	3 µM CHIR99021	100 ng/ml Activin A
20 ng/ml Activin	40 ng/ml Activin A	100 nM LDN-193189 (BMP inhibitor)
175 nM NVP-TNKS656		
1% Knockout Serum Replacement		
2 µM Thiazovivin		

Table S10. Media composition for neural organoids

EB Formation media	Neural induction media	Neuroepithelial expansion media	Neuronal media
N2B27 (B27 without vitamin A)	N2B27 (B27 without vitamin A)	N2B27 (B27 without vitamin A)	N2B27 (B27 with vitamin A)
50 nM chroman-1	100 nM LDN	100ng/ml Fgf8b	20ng/mL BDNF
5 µM emricasan	10 µM SB431542		20ng/mL GDNF
100 nM LDN	100 nM PD173074		
10 µM SB431542	4 nM LGK974		
100 nM PD173074			
4 nM LGK974			

MEF MEDIA: [**For 500ml**] Sterile filter and store at 4˚C

Solution (stock concentration)	Volume	Final concentration
DMEM w/ glutamine (1x)	445 mL	2 mM (L-glutamine)
Penicillin-streptomycin (100x)	5 mL	100 ug/mL
FCS (Hyclone)	50 mL	10%

SERUM/LIF MEDIA: [**For 500ml**] Sterile filter and store at 4˚C

Solution (stock concentration)	Volume	Final concentration
DMEM w/ glutamine (1x)	430ml	2mM (L-glutamine)
NEAA (100x)	5ml	0.1mM
Sodium pyruvate (100x)	5ml	1mM
Penicillin-streptomycin (100x)	5ml	100ug/ml
2-mercaptoethanol (1000x)	500ul	0.1mM
FCS (Hyclone)	50ml	10%
ESGRO LIF (100x)	5ml	1000U/ml

N2B27 MEDIA: [**For 500ml**] Sterile filter and store at 4˚C

Solution (stock concentration)	Volume	Final concentration
DMEM- F12	241ml	
Neurobasal medium	241ml	
N2 supplement	2.5ml	1:200
B27 supplement	5ml	1:100
GlutaMax	1.875ml	2mM
Penicillin-streptomycin (100x)	5ml	100ug/ml
2-mercaptoethanol (1000x)	500ul	0.1mM

CHEMICALLY DEFINED MEDIA (CDM): [**For 500ml**] Sterile filter and store at 4°C

Solution (stock concentration)	Volume	Final Concentration
IMDM (1x)	243 ml	50%
F12 with GlutaMAX (1x)	243 ml	50%
Chemically Defined Lipid Concentrate (100x)	5 ml	1x
Monothioglycerol (11.5 M)	19.3 µL	450 µM
Polyvinyl Alcohol (100 mg/mL)	5 ml	1 mg/mL
Apo transferrin (10 mg/mL)	750 µL	15 ug/mL
Glutamax (100x)	2.5 ml	100x
Insulin (10 mg/mL)	35 µL	0.7 µg/ml

Preparation of stock solutions

Activin A: Peprotech (120-14P)

- Reconstitute lyophilized protein to 100ug/ml in sterile H_2O with 0.1% BSA (5,000X solution)
- Aliquot and store at -80 C for up to 3 months.

Heat-stable bFGF2: Gibco (PHG0360)

- Reconstitute FGF to 1 g/L in sterile diH2O.
- Add sterile PBS + 0.1% BSA to dilute solution to 25 ug/ml (2,000X stock for a working concentration of 12.5 ng/mL).
- Store at -20 for up to 12 months.

NVP-TNKS656: Selleck chemicals (S7238)

- Dilute powder with DMSO to make a 35 mM solution (for 10 mg, add 577 µL DMSO)
- Dilute 35 mM stock further to 350 uM
- Aliquot 350uM stock (2,000X) and store at -80 C for up to 2 years.

Collagenase Type IV: Gibco (17104109)

- Add 10 ml of HBSS++ directly to the vial of collagenase.
- Vortex to complete dissolution.
- Determine final volume of HBSS++ required to bring collagenase solution to 5 u/µL (10X) & vortex.

- Filter to sterilize stock solution with a low protein binding filtration unit (PES Membrane, 0.2 µm).
- Aliquot and store at -20C for up to 24 months.
- Add HBSS++ to bring concentration to 5X before use.

Thiazovivin: Sigma (SML1045)

- Resuspend in DMSO to make 2mM stock (for 5 mg, 8.030 mL DMSO for a 1,000X solution).
- Aliquot and store at -20C for up to 6 months.

CHIR99021: Tocris Bioscience (252917-06-9)

- Resuspend in DMSO to make 5mM stock (for 10mg, 4.2979 mL DMSO for a 5,000X working solution).
- Aliquot and store at -20C.

Apo-transferrin: InVitra (777TRF029)

- Resuspend 1g in 100 mL diH2O, mix until complete homogenization and filter.
- This will give a 666 X stock solution. Aliquot and store at -80C.

Lif: Sigma (ESG1107)

- Each vial contains 10^7 units/mL. Dilute it 100 times in sterile tissue culture media to make a 100x solution, which is stored at 4C until use.

Insulin: Sigma (91077C)

- Take 250 mg, add 25 mL diH2O, leading to a cloudy solution.
- Add HCl until a pH=3.0 is achieved.
- Filter and store at 4C.

LDN-193189: Stemgent (04-0074)

- Dilute the powder (2 mg) with 22.75 mL DMSO to make a 200 µM solution (2,000X).
- Aliquot and store at -20C for up to 6 months.

PD0325901: Tocris (4192)

- Add 830 µL of DMSO to 10mg powder to make a 25 mM stock solution.
- Aliquot and store at -20C.

Polyvinyl alcohol (PVA): Sigma (341584)

- Within a clean, autoclaved bottle (around 2 L capacity), add 20 g of PVA and 200 mL diH2O (100 mg/mL stock, 100X).
- Autoclave (wet settings) with the cap slightly opened for 1-2h until the powder fully dissolves.
- Store at 4C and use it within the next 3 months.

Chroman 1: MedChem Express (HY-15392)

- Dilute the powder (5 mg) with 11.4548 mL DMSO to make a 1 mM solution (20,000X).
- Aliquot and store at -80C for up to 6 months.

Emricasan: Selleckchem (S7775)

- Dilute the powder (25 mg) with 877 µL of DMSO to make a 50mM solution (10,000X).
- Aliquot and store at -80C for up to 2 years.

SB-431542: Tocris (1614)

- Dilute the powder (10 mg) with 2.6 mL 100% ethanol to make a 200 µM solution (1,000X).
- Aliquot and store at -20C for up to 1 month.

PD-173074: STEMCELL technologies (72164)

- Dilute the powder (10 mg) with 19.09 mL of DMSO to make a 1 mM solution (10,000X).
- Aliquot and store at -80C for up to 2 years.

LGK-974: Selleck Chemicals (S7143)

- Dilute the powder (1 mg) with 63.06 mL DMSO, warmed at 50C in a water bath if needed to fully dissolve, to make a 40 µM solution (10.000X) .
- Aliquot and store at -80C for up to 2 years.

FGF8b: R&D systems (423-F8-025/CF)

- Dilute the powder (25 µg) in 250 uL PBS-/- to make a 1,000X solution, store at 4C for up to 3 months.

BDNF: Peprotech (450-02)

- Resuspend the powder (50 µg) in 2.5 mL PBS-/- with 0.1% BSA to make a 1.000X solution.
- Aliquot and store at -20C for up to a year.

GDNF: Peprotech (450-10)

- Resuspend the powder (50 µg) in 2.5 mL PBS-/- with 0.1% BSA to make a 1.000X solution.
- Aliquot and store at -20C for up to a year.

REFERENCES

Dekkers, J.F., Alieva, M., Wellens, L.M., Ariese, H.C.R., Jamieson, P.R., Vonk, A.M., Amatngalim, G.D., Hu, H., Oost, K.C., Snippert, H.J.G., et al. (2019). High-resolution 3D imaging of fixed and cleared organoids. Nat Protoc 14, 1756-1771.

Qian, X., Jacob, F., Song, M.M., Nguyen, H.N., Song, H., and Ming, G.L. (2018). Generation of human brain region-specific organoids using a miniaturized spinning bioreactor. Nat Protoc 13, 565-580.